SMOS L1 Processor Algorithm Theoretical Baseline Definition

Code : SO-DS-DME-L1PP-0011
Issue : 2.10
Date : 29/10/10

	Name	Function	Signature
Prepared by	A. Gutiérrez	Project Engineer	
Checked by	J. Barbosa	Quality A. Manager	
Approved by	J. Barbosa	Project Manager	

DEIMOS Engenharia
Av. D. João II, Lote 1.17, Torre Zen, 10º,
1998-023 Lisboa, PORTUGAL
Tel: +351 21 893 3013
Fax: +351 21 896 9099
E-mail: mailto:deimos@deimos.com.pt

This page intentionally left blank

Document Information

Contract Data	Classification
Contract Number: 4000101241/10/I-AM	Internal ☐ Public ☐ Industry ☐ Confidential ☑
Contract Issuer: ESA	

Internal Distribution		
Name	Unit	Copies

External Distribution		
Name	Organisation	Copies
Jean-Claude Debruyn	ESA	1
Steven Delwart	ESA	1

Archiving	
Word Processor:	MS Word 2000
File Name:	SO-DS-DME-L1PP-0011-Algorithm_Theoretical_Baseline.doc
Archive Code:	SO-DS-DME-L1PP-0011

Document Status Log

Issue	Change description	Date	Approved
1.0	Delivered to ESA	2004-01-19	
1.1	Updated to comments from Final Presentation	2004-01-30	
2.0	Update for Phase 2 CDR	2005-06-30	
2.1	Updates after CDR RIDs	2005-08-31	
2.2	Introduction of FTT and NIR calibration	2005-11-04	
2.3	Revision after L1PP implementation	2006-04-07	
2.4	Final delivery for Phase 2 activities	2006-06-07	
2.5	Updates for L1PP V2R	2006-11-15	
2.6	Reviewed by CASA and ESA	2006-11-24	
2.7	V3R Delivery	2007-04-09	
2.8	V3.5 Delivery	2007-07-15	
2.9	V4 Delivery	2007-11-16	
2.10	Updated after review for the Maintenance Phase and for L1PP v3.5.0	2010-10-29	

Table of Contents

List of Figures

List of Tables

1. INTRODUCTION

1.1. Purpose and Scope

This document describes the SMOS L1 Algorithms Theoretical Baseline, explaining in depth all the mathematical and processing operations needed to successfully transform the SMOS L0 Data into all the L1 output.

1.2. Acronyms and Abbreviations

AOCS	Attitude and Orbital Control Subsystem
BT	Brightness Temperature
CAS	Calibration System
CIP	Correlated Noise Input Plane
DICOS	Digital Correlation System
DLR	Deutschen Zentrum für Luft und Raumfahrt
FEP	Front End Processor
FFT	Fast Fourier Transform
FOV	Field of View
FTT	Flat Target Transformation
FWF	Fringe Washing Function
GSL	GNU Scientific Library
I-HKTM	Instrument Housekeeping Telemetry
MIRAS	Microwave Imaging Radiometer by Aperture Synthesis
NDN	Noise Distribution Network
NIR	Noise Injection Radiometer
PMS	Power Measurement System
PVT	Position-Velocity-Time (orbital vector)
RMSE	Root Mean-Square Error
SC-HKTM	Satellite Housekeeping Telemetry
SEPS	SMOS Performance Simulator
TBH	Temperature Brightness at Horizontal polarisation
TBV	Temperature Brightness at Vertical polarisation
TEC	Total Electron Content

TM	Telemetry
TOA	Temperature Of Antenna
UPC	Universidad Politécnica de Cataluña
VTEC	Vertical Total Electron Content

1.3. Applicable and Reference Documents

1.3.1. Applicable Documents

Ref.	Code	Title	Issue
AD.1	SO-SOW-CASA-PLM-0380	Level 1 Processor Prototype Development Phase 2 and Support Activities. Statement of Work	01
AD.2	SO-RS-ESA-PLM-0003	SMOS System Requirements Document	3.0
AD.3	SMOS-DME-L1PP-0014	SMOS L1 Processor Input Output Data Definition	2.3
AD.4	SO-TN-CASA-PLM-0017	SMOS Payload Technical Description	2
AD.5	SO-TN-UPC-PLM-01	IN-ORBIT CALIBRATION PLAN	3.3
AD.6	SO-TN-UPC-PLM-0019	SMOS In Orbit Calibration Plan Phase C-D	1.5
AD.7	ECSS-E-40B	ECSS E-40 Software Engineering Standards	
AD.8	SO-TN-CASA-PLM-0279	SMOS PLM Command and Control	2.4
AD.9	SO-PL-CASA-PLM-0022	Definition of coordinate system / reference frame & units nomenclature	2.0

Table 1: Applicable Documents

1.3.2. Reference Documents

Ref.	Code/Author	Title	Issue
RD.1	EE-MA-DMS-GS-0001-1-5_090313	Earth Explorer Mission CFI Software MISSION CONVENTIONS DOCUMENT	1.5
RD.2	PE-TN-ESA-GS-0001	Earth Explorer Ground Segment File Format Standard	1.3
RD.3	EE-MA-DMS-GS-0002-3-7-2_080731	Earth Explorer Mission CFI Software GENERAL SOFTWARE USER MANUAL	2.0
RD.4	SO-IS-DME-L1PP-0014	SMOS L1 Processor Input/Output Definition Document	2.3
RD.5	SO-IS-DME-L1PP-0002	SMOS L1 Product Format Specification	2.3

Ref.	Code/Author	Title	Issue
RD.6	SO-IS-DME-L1PP-0003	SMOS L1 Auxiliary Product Format	**2.3**
RD.7	R. Butora, M. Martín-Neira, A.L. Rivada	*"Fringe-Washing Function Calibration in Aperture Synthesis Microwave Radiometry"*, Radio Science, Volume 38, Issue 2, pp. 15-1	2003
RD.8	David M. Le Vine & Saji Abraham	*"Faraday rotation and passive microwave remote sensing of soil moisture from space"*, Microwave Radiometer Remote Sensing Earth's Surf. Atmos., P. Pampaloni and S. Paloscia, Eds., VSP BV, The Netherlands, 89-96.	2000
RD.9	SO-DS-DME-L1PP-0006	SMOS L1 System Concept	**2.9**
RD.10	SO-TN-DME-L1PP-0024	SMOS L1 Full Polarisation Data Processing	**1.6**
RD.11	IEEE Trans. Geosc. and Remote Sensing, Vol. 42, No.8, 2004.	E. Anterrieu *"A resolving matrix approach to synthetic aperture imaging radiometers."*,	2004
RD.12	A. Camps, M. Vall-llossera, N. Duffo, M. Zapata, I. Corbella, F. Torres, V. Barrena	*"Sun Effects In 2D Aperture Synthesis Radiometry Imaging And Their Cancellation"*, IEEE Transactions on Geoscience and Remote Sensing, 42 (6): 1161-1167. ISSN: 0196-2892	2004
RD.13	A. Camps, M. Vall-llossera, N. Reul, F. Torres, N. Duffo, I. Corbella.	*"Impact and Compensation of Diffuse Sun Scattering in 2D Aperture Synthesis Radiometers Imagery"*, IGARSS, Seoul, Korea, July 25-29, 2005	2005
RD.14	P. Waldteufel, G. Caudal,	*"About Off-Axis Radiometric Polarimetric Measurements"*, IEEE Transactions on Geoscience and Remote Sensing	2002
RD.15	SMOS-DMS-TN-5100	Adaptive Apodisation Function Development Technical Note	**1.2**
RD.16	SO-TS-HUT-NIR-0005	NIR Calibration and Characterisation Plan	**5E**
RD.17	SO-TN-UPC-PLM-0010	Distributed Amplitude Calibration by the Two-Level Approach	**1.0**
RD.18	SPS-TN-GMV-PL-0003	SMOS End-to-End Performance Simulator (SEPS) Architectural and Detailed Design Document	**4.1**
RD.19	A. Camps, I. Corbella, F. Torres, M. Vall-llossera, N. Duffo,	*"Polarimetric Formulation Of The Visibility Function Equation Including Co- And Cross-Polar Antenna Patterns"*, IEEE Geoscience and Remote Sensing Letters Vol.2 No. 3. pp 292 - 295	2006

Ref.	Code/Author	Title	Issue
RD.20	A. Camps, F. Torres, I. Corbella, N. Duffo, M. Vall-llossera, M. Martín-Neira,	*"The impact of Antenna Pattern Frequency Dependence in Aperture Synthesis Microwave Radiometers"*, IEEE Transactions on Geoscience and Remote Sensing Vol. 43 No. 10 pp 2218-2224	2006
RD.21	I. Corbella, F. Torres, A. Camps, J. Bará, N. Duffo, M. Vall-llossera,	*"L-band Aperture Synthesis radiometry: Hardware Requirements and System Performance"*, IGARSS '00; Proceedings of the IGARSS '00, Hawaii, USA	July 2000
RD.22	A. Camps, J. Bará, I. Corbella, F. Torres,	*"The Processing of Hexagonally Sampled Signals with Standard Rectangular Techniques: Application to 2D Large Aperture Synthesis Interferometric Radiometers"*, IEEE Transactions on Geoscience and Remote Sensing, GRS-35, pp. 183-190	January 1997
RD.23	Corbella, et al,	"*The visibility function in interferometric aperture synthesis radiometry*", IEEE Trans. Geoscience and Remote Sensing, Vol. 42, No. 8, pp. 1677-1682.	2004
RD.24	Coliander, et al,	"*MIRAS reference radiometer: A fully polarimetric NIR*", IEEE Transactions on Geoscience and remote sensing, Vol. 43. No. 5.	2005
RD.25	Campbell, S. L. and Meyer, C. D. Jr.	*"Generalized Inverses of Linear Transformations"* New York: Dover	1991
RD.26	SO-TN-UPC-PLM-0048	MIRAS EM tests at INTA facilities	***2.6***
RD. 27	SO-RS-CASA-PLM-0050	CCU Requirements Specification	***3.3***
RD. 28	SO-TN-UPC-PLM-0054	In Orbit LICEF and CAS receiver temperature calibration	***2.1***
RD.29	M. Zundo, B.Duesmann SO-TN-ESA-GS-5873	*On-ground BT Frame of Reference TN*	***3.3***

Table 2: Reference Documents

1.4. Naming and Mathematical Conventions

Throughout this document, polarisations H and V are used to refer to the *antenna reference frame*. Other documentation within the project use only H and V to refer to the *ground reference frame*, and reserve X and Y for the antenna reference frame.

It should be taken into account when reading the current document that all data produced with the presented equations using H and V parameters shall be expressed in the ***antenna reference frame***, unless otherwise indicated.

For each pixel in L1c, the information of Brightness Temperatures is retrieved along chosen polarisations (e.g. TX and TY polarisation directions are parallel to Za and Ya directions on the Antenna Reference frame), but for the scope of simplicity on the current document, from now on these measurements are referred only as "Brightness Temperature values".

Throughout the document, whenever the superscript * is used, it denotes the complex conjugate of the value to which it is applied. Indexes in the S-Parameters definitions also denote specific components, unless otherwise noted: *k* represents receiver positions, *s* represents noise sources and numerical values represent the NIRs. LICEF channel modes are indicated as superscripts with H for horizontal polarization, V for vertical polarization , U for uncorrelated noise injection and C for correlated noise injection, representing the switch from which the signal being correlated is coming..

2. INSTRUMENT OPERATION MODES

This chapter shows briefly the instrument possible operation modes as taken from section 6 of the [AD.5] where the in-orbit modes are described. These operation modes are also reflected in the APID of the L0 instrument source packets containing the information transmitted.

There are two main observation modes, and 4 calibration modes, although in all of them the output format is the same. In one integration time, each receiver's signal is correlated against the other receivers in an arrangement shown in Figure 5.

2.1.1. Measurement modes

There are two instrument polarisation modes, dual and full polarisation. In dual polarisation, all arms are in the same polarisation mode. In full polarisation, one arm is in a cross-polarisation mode for 1/3 of the integration time. The cross-polarized arm is rotated in a clockwise fashion. Schematically:

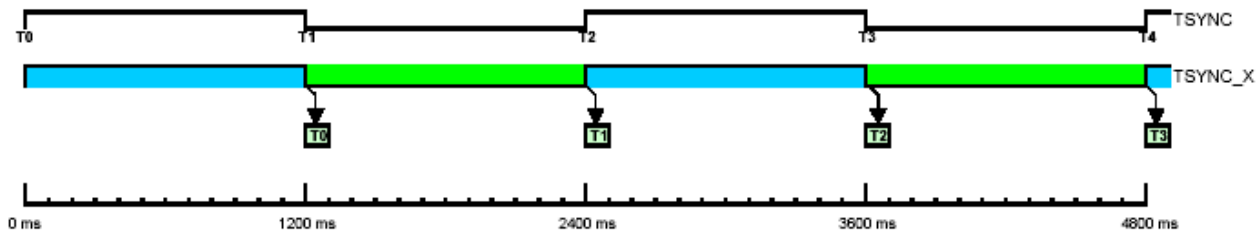

Figure 1: Time sequence for dual polarisation mode

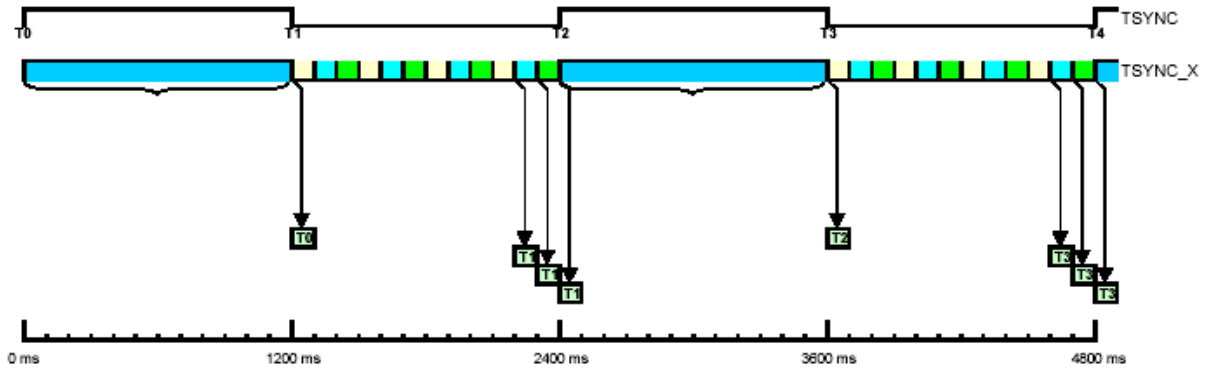

Figure 2: Time sequence for full polarisation mode

This means that, in four consecutive integration intervals, the instrument will measure two dual polarisation brightness temperature, HH and VV, and two cross-polarized brightness temperatures, VH and HV. In fact, as can be seen from the previous figure, the arms in full-polarisation mode rotate polarisations four times, each mode producing one set of visibilities corresponding to a third of the integration time.

2.1.1.1. Dual Polarisation Mode

In dual polarisation mode, each scene will be a complete HH or VV mode measurement, with the upper triangle of the correlator matrix containing the *iq* raw correlations and the lower triangle containing the *ii* raw correlations. Therefore, each scene can be calibrated and processed individually. The complete array of visibilities in the star domain can be obtained by taking the complex conjugates of the opposite elements in the correlations matrix.

2.1.1.2. Full Polarisation Mode

In the case of full polarisation mode, however, data within each scene will contain information about different cross-polarisation measurements. This is depicted in the following picture:

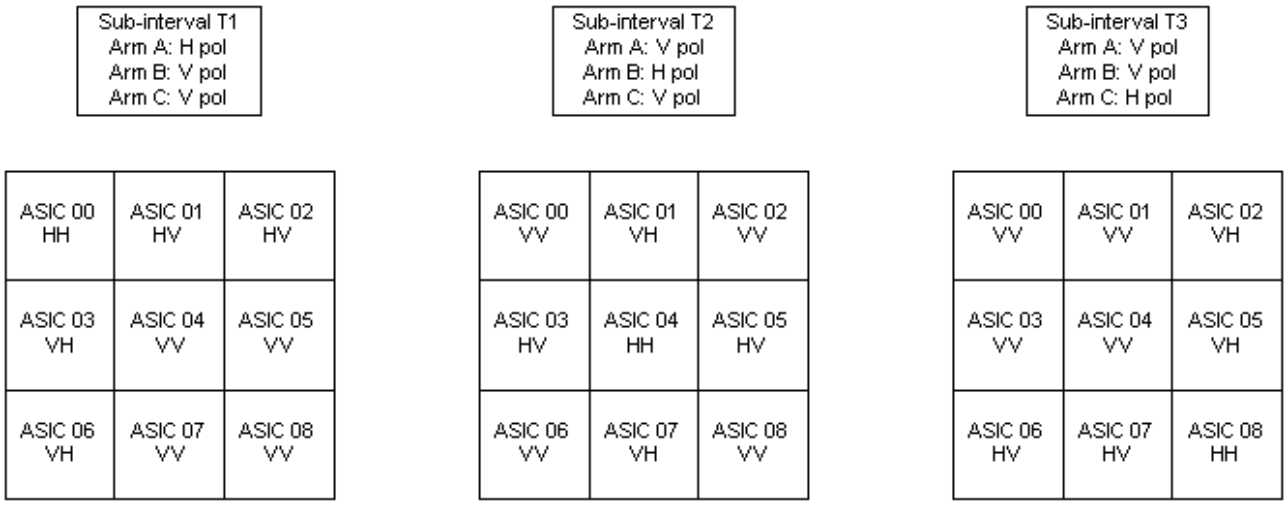

Figure 3: Full polarisation scene output

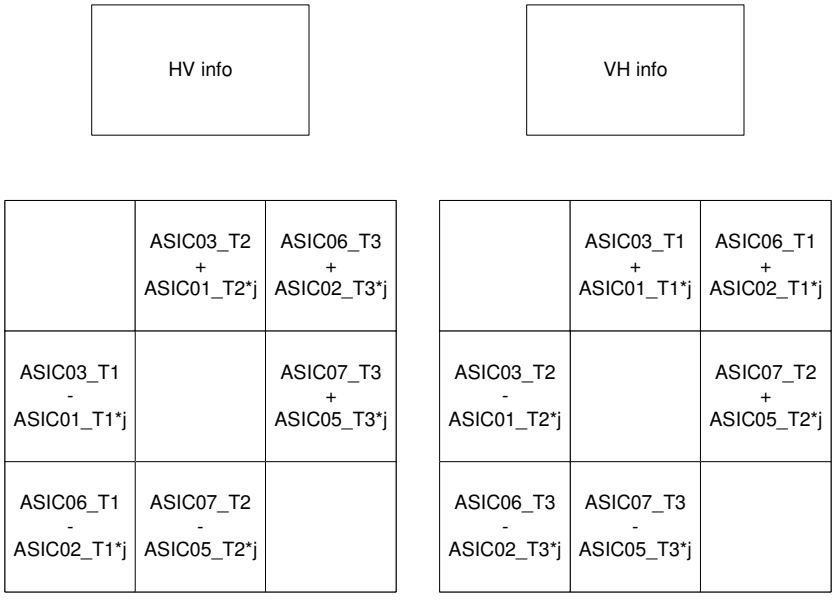

Figure 4: Full polarisation L0 data reordering

In order to process the full polarisation data, the ASIC data in the three top scenes (as they are received in L0), must be rearranged in order to retrieve same cross-polarisation brightness temperatures. It has been decided that this reorganization will only be done after L1a data has been produced, namely in the Image Reconstruction module. In fact, each scene for full polarisation measurements is self-contained calibration wise. What this means is that each scene, even if it has information about different cross-polarized modes, has all the necessary information to be amplitude and phase calibrated. For more information on this subject [RD.10] can be consulted.

2.1.2. Internal Calibration modes

These operation modes are switched on demand in order to inject noise in the radiometers and measure calibration coefficients for several elements. The procedures are described in detail in [AD.5] and [AD.6].

2.1.2.1. Uncorrelated Noise Injection

Uncorrelated Noise is generated locally at each LICEF, with the purpose of detecting any offset that may happen in the correlators.

2.1.2.2. Correlated Noise Injection

Correlated Noise is injected through the Noise Sources following a certain strategy described in the [AD.5] and [AD.6]. Additionally, attenuators may be activated on the PMS elements and delays introduced in the path of the correlated signals.

Not only the APID is used to determine the processing strategy, but also additional parameters in the ancillary packet, like the CMN Last Executed Command and FWF delay, are needed in order to properly identify and process the calibration data.

2.1.2.3. External Calibration modes

These operation modes are switched on demand in order to calibrate the NIR elements, PMS gains and offsets and also to image sky or moon scenes that may be used for the Flat Target Transformation or G-Matrix calibration in orbit. The APID is commanded to change to APID_EXC_DUAL, APID_EXC_FULL, depending on the polarisation mode, or APID_EXC_C and APID_EXC_U for noise injection calibration while measuring external targets.

However, not all packets with the previous APIDs are used for NIR calibration; it also depends on the status of other processing flags. The procedures are also described in detail in [AD.5].

2.1.2.4. Test mode

This operation mode is not described in [AD.5] or [AD.6], as it is a built-in test mode with a fixed output in all correlators. It is described in section 10.3.3 of [AD.4]. The APID APID_TEST shall identify it.

3. ALGORITHM STEPS

In the next part, a description of the processing steps needed to complete the transition from one product to the next is provided. This document shall describe the processing methodology and how to extract information, but it shall not attempt to group activities into "processing modules". This task is performed in the System Concept document [RD.9] and in the respective Detailed Processing Model documents.

3.1. Level 0 to Level1a

This processing step extracts calibration parameters and offsets from calibration data, and applies them appropriately to the measurement data. It is responsible for decoding the original packetised science and ancillary data, and converting it into engineering units.

Most of the calibration procedures presented in this section have been gathered from [AD.5] and [AD.6]

3.1.1. L0 data structure

Input Data at this level is the Digital Correlator System (DICOS) output, the PMS's output voltages and the NIR pulse length outputs as well as the instrument physical temperatures, attitude and orientation. All these quantities are directly retrieved from the L0 product, with each correlation encoded in 16bit.

PMS output voltage has to be transformed into system temperatures by means of manufacturer tables that specify the conversion formulae and characterisation approaches. These tables will have measurements throughout the temperature range. The in-flight measured temperatures will then be used to retrieve the correct parameters. The PMS parameters are also calibrated in-flight through correlated noise injection, to correct for changes in the response and allow for correct values of those parameters to be used.

The NIR pulse length output is transformed into the L-band antennae temperatures, using an algorithm provided by the NIR manufacturer. Final antenna temperature can be computed as the average temperature of the three NIR receivers, although it is also possible to use the three measurements independently.

The DICOS output consists of correlator counts, N_C, for each pair of receiver outputs in addition to correlator counts between each receiver outputs (quadrature and in-phase) and one of two constant channels (with "1" and "0" values respectively).

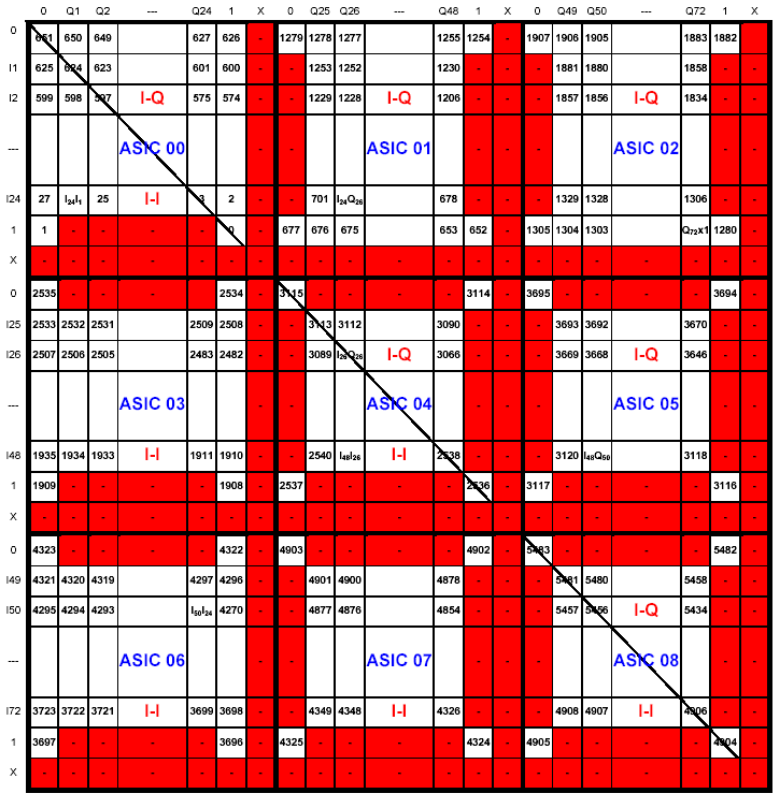

Figure 5: Logical organization of L0 data, nominal layer

$N_{C\max}$ is the maximum number of counts, which is a function of the sliding window of the DICOS and the integration time used. For dual polarisation mode, the value of $N_{C\max}$ is 65437 while for full polarisation mode it is 43625. In Fig.3, there is only the representation for the L0 nominal layer. In fact, there is a redundant layer of L0 data, which contains the Q-I correlations instead of I-Q correlations (and QQ instead of II). In the remainder of this document we will only address the processing of the nominal layer data, being the redundant layer processing essentially the same. Whenever there are differences in the equations for each layer, they will be explicitly presented.

The following figure depicts the counting schema of the LICEF and LICEF-NIR receivers for each arm. As can be see, the elements in the hub can be assigned to each arm by extending the arm direction into the hub as far as the hub centre. For those elements in the hub in a region between arms, the arm the naming convention [AD.9] incorporates the labelling for the two adjacent arms. For example, the elements between arms A and B are labelled AB.

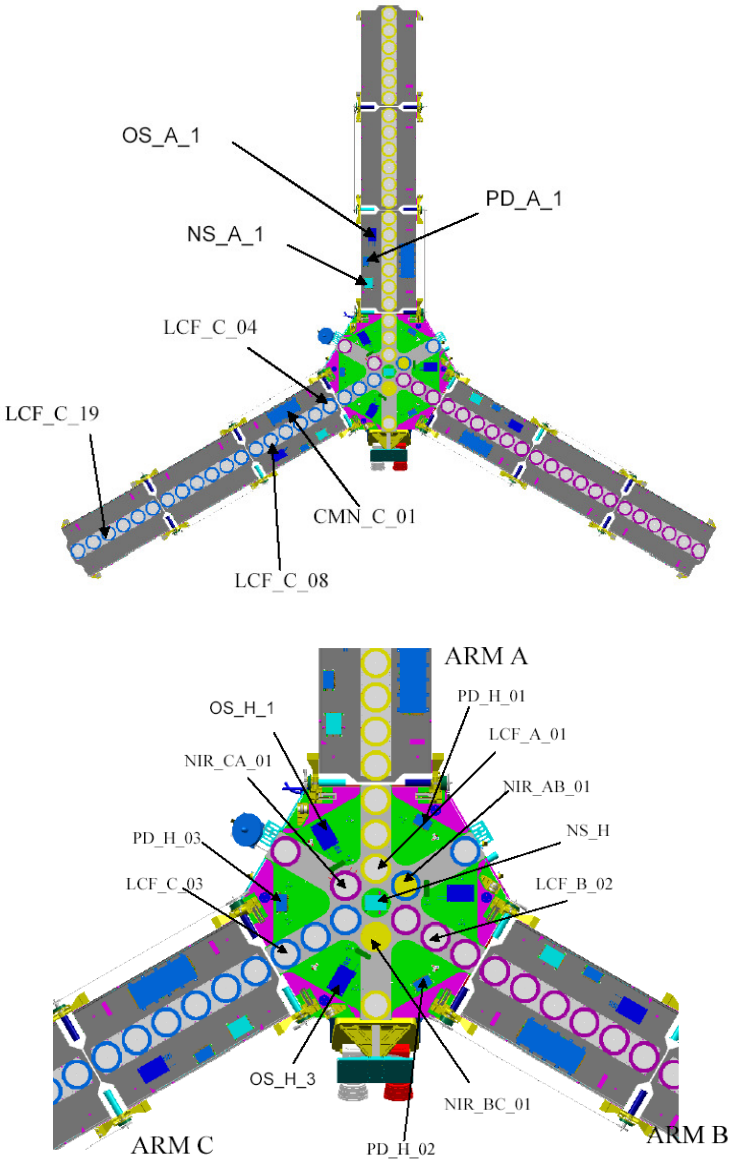

Figure 6: Antenna indexing in the SMOS instrument

Using this nomenclature, it is possible to clarify the data organization in the L0 format (Figure 7). Note that the output starts with the elements in the hub – LCF_AB_03 in the case of arm A- followed by the two separate outputs from the LICEF-NIR, in horizontal and vertical mode - NIR_AB_01_H and NIR_AB_01_V, in the case of arm A – and only then we have the arm receivers outputs' – LCF_A_01 to LCF_A_21.

The L0 data also contains correlation data between each antenna and a stable signal of "0" or "1". In Fig. 5, these correlations are colour coded in red, and are stored in between the cross-correlations data. Finally, the diagonal of the logical data matrix contains the autocorrelations between the quadrature and in-phase outputs for each antenna. Above the diagonal, for nominal layer L0 data, the cross-correlations are between in-phase (I) and quadrature (Q) outputs for each of the antennas, while below the diagonal the cross-correlations are the between the in-phase outputs of both antennas. For more information on the L0 data structure, refer to documents [RD.27] and [RD.5].

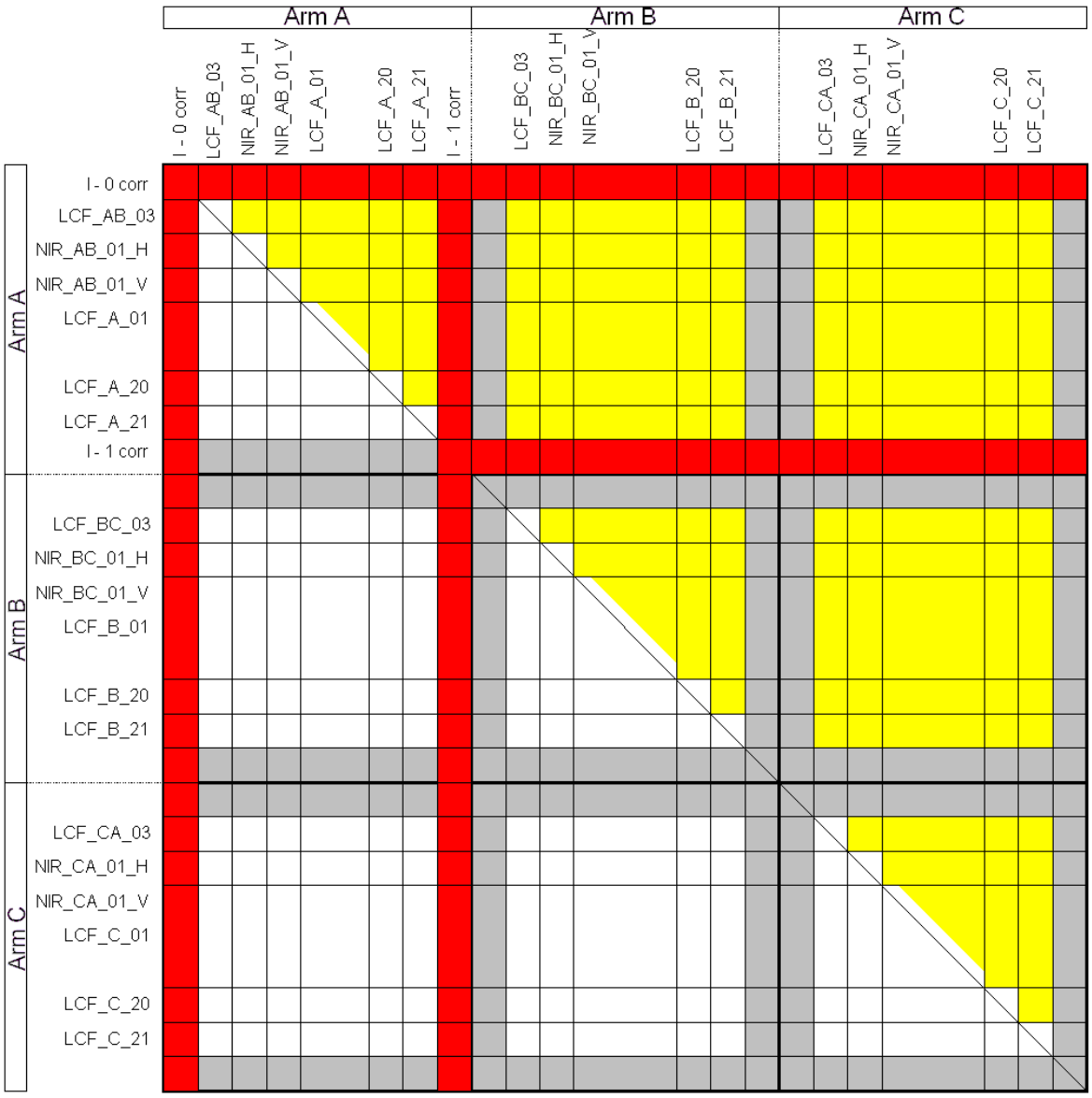

Figure 7: Correlations ordering in L0 nominal data packets

Therefore, the data accessible on the nominal correlations layer according to [AD.8] consists of:

- 2556 correlations between I channels of different receivers ($N_C = (I_k, I_j)$)
- 2556 correlations between I and Q channels of different receivers ($N_C = (I_k, Q_j)$)
- 72 correlations between I and Q channels of same receiver ($N_C = (I_k, Q_k)$)
- 72 correlations between I and 0 channels ($N_C = (I_k, 0)$)
- 72 correlations between Q and 0 channels ($N_C = (Q_k, 0)$)
- 72 correlations between I and 1 channels ($N_C = (I_k, 1)$)

- 48 correlations between Q and 1 channels ($N_C = (Q_k, 1)$)
- 36 control correlations between 1 and 0 channels (4 for each ASIC)

Since each LICEF-NIR has two separate output channels, one for each polarisation mode, only 69 signals from the receivers will be used at a time when doing the image reconstruction of the scene. In H-polarisation measurement mode, for example, the horizontal outputs of the LICEF-NIR will be used and the vertical polarisation outputs will be discarded. However, the data calibrated from L0 to L1a are the complete 72 signals from all receivers.

For correlations between antennae and stable signal, it should be noted that the total information for correlations between the Q channels and the "1" channel is missing. Their values, however, are easily retrieved from the I-0 and Q-0 correlations due to the fact that I-0 and I-1 values, as well as Q-0 and Q-1 values, are complementary ($N_C(I_k, 0) + N_C(I_k, 1) = N_{C\max}$, for example).

So, at any given integration time where all receivers are configured in a unique polarisation (H or V), only the following data shall be useful, as the rest of the data shall be in the opposite polarisation:

- 2346 correlations between I channels of different receivers ($N_C = (I_k, I_j)$)
- 2346 correlations between I and Q channels of different receivers ($N_C = (I_k, Q_j)$)
- 69 correlations between I and Q channels of same receiver ($N_C = (I_k, Q_k)$)
- 69 correlations between I and 0 channels ($N_C = (I_k, 0)$)
- 69 correlations between Q and 0 channels ($N_C = (Q_k, 0)$)

The Error Correction module will nevertheless process all L0 data in the same processing step, using the 72 signals for each antenna (66 LICEF + 2*3 LICEF-NIR). An even more simplified logical organization of the useful data in a scene is depicted in the following diagram:

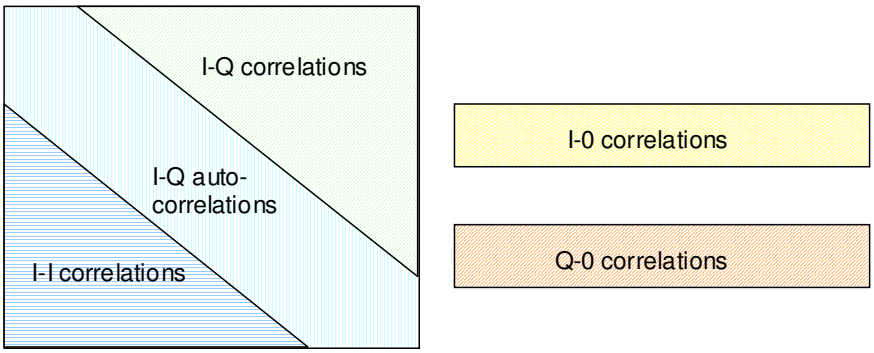

Figure 8: Simplified organization of L0 nominal layer science data

The composite matrix will be used to define two symmetric matrices, the μ_{kj}^{ii} correlations full matrix containing the real components, and the μ_{kj}^{iq} correlations full matrix containing the imaginary components. For the dual-pol case, after the raw normalized correlations are computed (Eq. 2), the full μ_{kj}^{ii} correlations matrix can be simply built by transposing the elements measured below the

diagonal, and the full μ_{kj}^{iq} correlations matrix must be built using the complex conjugate when transposing elements. For full-pol mode, the L0 data must be previously re-arranged, as described in Section 2.1.1.2. .

The main diagonal values are only used for the quadrature correction since they do not define any baseline (each element corresponds to an auto-correlation).

3.1.2. L0 decoding and fundamental calibration equations

To obtain the digital correlations, $c_{kj}^{ii,iq}$, from the correlator counts, the following transformation is used:

$$c_{kj}^{ii,iq} = \frac{N_C}{N_{C\max}} \qquad \textit{Eq. 1}$$

where $N_{C\max}$ is the maximum number of counts. N_C is an integer from 0 to $N_{C\max}$, the digital correlations (or raw normalised correlations), $c_{kj}^{ii,iq}$, range from 0 to 1.

The raw normalised correlations between antennas k and j and, for each polarisation and cross-polarisations, the in-phase and quadrature values (ii and iq) [1] are converted into normalised correlations $\mu_{kj}^{ii,iq}$ by solving the non-linear equation proposed in:

$$c_{kj}^{ii,iq} = \frac{1}{2} + \frac{1}{\pi}\sin^{-1}\mu_{kj}^{ii,iq} - \frac{1}{\sqrt{1-\left(\mu_{kj}^{ii,iq}\right)^2}}\left(\mu_{kj}^{ii,iq}\left(X_k^{i,q}\right)^2 + \mu_{kj}^{ii,iq}\left(X_j^{i,q}\right)^2 - 2X_k^{i,q}X_j^{i,q}\right)$$

with

$$\frac{\partial c_{kj}^{ii,iq}}{\partial \mu_{kj}^{ii,iq}} = -\frac{1}{\pi}\frac{1}{\sqrt{1-\left(\mu_{kj}^{ii,iq}\right)^2}} + \left(\frac{\left(X_k^{i,q}\right)^2 + \left(X_j^{i,q}\right)^2}{\sqrt{1-\left(\mu_{kj}^{ii,iq}\right)^2}} + \frac{\left(\mu_{kj}^{ii,iq}\right)^2\left(X_k^{i,q}\right)^2 + \left(\mu_{kj}^{ii,iq}\right)^2\left(X_j^{i,q}\right)^2 - 2X_k^{i,q}X_j^{i,q}\mu_{kj}^{ii,iq}}{\left(\sqrt{1-\left(\mu_{kj}^{ii,iq}\right)^2}\right)^3}\right) \qquad \textit{Eq. 2}$$

Where the values of $X_{k,j}^{i,q}$ are built using the correlations of I and Q channels with constant 1 and 0 channels, using the following expressions, in which x_{k0}^{i} is the correlation of I channels to all zeros (first vertical red line in Fig. 5) and x_{k1}^{q} is the correlation of the I or Q channels to all ones:

$$X_k^i = \frac{1}{2}\left(x_{k0}^i - x_{k1}^i\right), X_k^q = \frac{1}{2}\left(x_{k0}^q - x_{k1}^q\right), X_j^i = \frac{1}{2}\left(x_{j0}^i - x_{j1}^i\right), X_j^q = \frac{1}{2}\left(x_{j0}^q - x_{j1}^q\right)$$

Equation 2 has to be solved iteratively, using as first solution $\mu_{kj}^{ii,iq} = \sin\left(\frac{\pi}{2}\left(2c_{kj}^{ii,iq} - 1\right)\right)$.

[1] Note that in [AD.6] the equations are written based on II and QI correlations. This document approach is not inconsistent with that formulation (see Section 9 of [AD.6]), only the equations are based on the nominal layer data (II and IQ correlations).

After computing the digital correlations, complex normalised correlation of baseline *kj* can be written, for the L0 nominal layer and any time delay, as:

$$\mu_{kj}^{N} \equiv \mu_{kj}^{ii} + j\mu_{jk}^{qi} = \mu_{kj}^{ii} - j\mu_{kj}^{iq}$$
$$\mu_{kj}^{N}(\tau) \equiv \mu_{jk}^{ii}(-\tau) - j\mu_{kj}^{iq}(\tau) \qquad \textbf{Eq. 3}$$

and, for the redundant layer, as:

$$\mu_{kj}^{R} \equiv \mu_{kj}^{qq} - j\mu_{jk}^{iq} = \mu_{kj}^{qq} + j\mu_{kj}^{qi}$$
$$\mu_{kj}^{R}(\tau) \equiv \mu_{jk}^{qq}(-\tau) + j\mu_{kj}^{qi}(\tau) \qquad \textbf{Eq. 4}$$

The redundant data will only be used in the case of failure of the nominal layer. Please note that Eqs. 3 and 4 account for the only difference in the processing of nominal or redundant data. The processing of time delays is only important for the FWF shape computation but it should be noted that the real parts of the delayed signals must be switched to build the complex correlations.

After computing μ_{kj} all the subsequent processing is unchanged. The complex correlations are theoretically related to the calibrated visibilities through the equation:

$$\mu_{kj} = \frac{1}{\sqrt{T_{sys_k} T_{sys_j}}}\left(\mathrm{Re}\left[\tilde{r}_{kj}^{ii}(0)\hat{V}_{kj}\right] + j\,\mathrm{Im}\left[\tilde{r}_{kj}^{qi}(0)\hat{V}_{kj}\right]\right) \qquad \textbf{Eq. 5}$$

where $\tilde{r}_{kj}^{ii,qi}$ is the fringe washing function at the origin for the corresponding pair of filters indicated by the sub and superscripts and $\hat{V}_{kj}$ are the calibrated visibilities. The system temperatures are the sum of the antenna temperature and the receiver noise temperature referred to the theoretical antenna phase centre and including antenna ohmic losses. The objective of the calibration procedures is to compute the system temperatures and the FWF values at the origin to recover the calibrated visibilities.

The final calibrated visibilities are computed as [AD.6]:

$$\hat{V}_{kj}^{V,H} = \frac{V_{kj}^{VV,HH} - V_{kj}^{UV,UH}}{g_{kj}^{V,H}}$$
$$V_{kj}^{VV,HH} = \sqrt{T_{sys_k}^{VV,HH} T_{sys_j}^{VV,HH}}\, M_{kj}^{V,H} \qquad \textbf{Eq. 6}$$
$$V_{kj}^{UV,UH} = \sqrt{T_{sys_k}^{UV,UH} T_{sys_j}^{UV,UH}}\, M_{kj}^{U}$$

where M_{kj} is defined as:

$$M_{kj}^{q} = \frac{1}{\cos\theta_{qj}}\left(\mathrm{Re}\left[M_{1kj}\mu_{kj}^{N}\right] + j\,\mathrm{Im}\left[M_{2kj}^{*}\mu_{kj}^{N}\right]\right)\text{(for Nominal layer)}$$
$$M_{kj}^{q} = \frac{1}{\cos\theta_{qj}}\left(\mathrm{Re}\left[M_{1kj}^{*}\mu_{kj}^{R}\right] + j\,\mathrm{Im}\left[M_{2kj}\mu_{kj}^{R}\right]\right)\text{(for Redundant layer)} \qquad \textbf{Eq. 7}$$

with index q=H, V or U, and T_{sys} are the system temperatures during measurement. The parameter g_{kj}, in Eq. 6, is the value of the fringe washing function at the origin. M_{kj} is the quadrature-corrected normalised correlation and in turn has the following parameters:

$$M_{1kj} = \cos\left(\frac{\theta_{qj}}{2} + \frac{\theta_{qk}}{2}\right) + j\sin\left(\frac{\theta_{qj}}{2} - \frac{\theta_{qk}}{2}\right)$$
$$M_{2kj} = \cos\left(\frac{\theta_{qj}}{2} - \frac{\theta_{qk}}{2}\right) + j\sin\left(\frac{\theta_{qj}}{2} + \frac{\theta_{qk}}{2}\right) \quad \textit{Eq. 8}$$

The terms in these equations, other than the complex correlations, are computed during three calibration procedures - quadrature, phase/amplitude and offset.

3.1.3. Quadrature Error Correction

The quadrature correction is computed for all instrument modes' outputs and applied before any other processing is done. This approach obtains the θ_{qk} term, which is directly estimated from the measured normalised auto-correlation between an antenna in-phase and quadrature outputs [AD.6]:

$$\theta_{qk} = -\arcsin\left(\mu_{kk}^{qi}\right) \quad \textit{Eq. 9}$$

After knowing θ_{qk}, and defining

$$Q_{kj} = \frac{\theta_{qj}}{2} - \frac{\theta_{qk}}{2}$$
$$Q_{kj}^{'} = \frac{\theta_{qj}}{2} + \frac{\theta_{qk}}{2} \quad \textit{Eq. 10}$$

Eq. 8 transforms into

$$M_1 = \cos Q_{kj}^{'} + j\sin Q_{kj}$$
$$M_2 = \cos Q_{kj} + j\sin Q_{kj}^{'} \quad \textit{Eq. 11}$$

M_1 and M_2 are easily computed and M_{kj}, the quadrature corrected correlations, are computed through Eq. 7. Since it is obtained directly from the instrument's own output, the quadrature-corrected correlation M_{kj} can be considered as instrument output.

3.1.4. Amplitude and In-Phase Error Correction

The correction parameters for amplitude and in-phase errors are computed from MIRAS output while in correlated noise injection mode. The outputs of these computations are then used in conjunction with the system temperatures measured in observation mode to calibrate the visibilities.

3.1.4.1. Power Measurement System calibration

The four-point measurement technique is based on a linear model of the PMS. A measured PMS voltage at receiver k (v_k) depends on the system temperature T_{sysk} as [AD.6]:

$$\begin{aligned} T_{sysk} &= T_{extk} + T_{rk} \\ v_k &= v_{offk} + G_k T_{sys} + a_k T_{sys}^2 \end{aligned} \qquad \textit{Eq. 12}$$

where T_{rk} is the system noise temperature, T_{extk} is the external temperature, v_{offk} is the PMS offset, G_k is the PMS gain and a_k is the PMS 2nd order linearity correction (although this parameter is not used, and instead the deflection C_k from Eq.36 is used instead).

It should be noted that in case the linearity correction is enabled, Eq.36 should be applied to all input PMS voltages before using them in the remaining equations.

If two external noise temperatures are used, T_{C1} (WARM) and T_{C2} (HOT), and if an attenuator is used to switch the system gain between two values, G and G/L, we have four possible PMS measurements:

$$\begin{aligned} v_{1k} &= v_{offk} + G_k (T_{C1k} + T_r) \\ v_{2k} &= v_{offk} + G_k (T_{C2k} + T_r) \\ v_{3k} &= v_{offk} + \frac{G_k}{L} (T_{C1k} + T_r) \\ v_{4k} &= v_{offk} + \frac{G_k}{L} (T_{C2k} + T_r) \end{aligned} \qquad \textit{Eq. 13}$$

The estimated calibration parameters are obtained as

$$\begin{aligned} v_{offk} &= \frac{v_{2k} v_{3k} - v_{1k} v_{4k}}{(v_{2k} - v_{4k}) - (v_{1k} - v_{3k})} \\ G_k &= \frac{v_{2k} - v_{1k}}{T_{C2k} - T_{C1k}} \end{aligned} \qquad \textit{Eq. 14}$$

and the estimated system temperatures, with the calibrated PMS data, will then be

$$T_{sysk} = \frac{v_k - v_{offk}}{G_k} = \frac{v_k - v_{offk}}{v_{2k} - v_{1k}} (T_{C2k} - T_{C1k}) \qquad \textit{Eq. 15}$$

As can be seen from Eq 14, only a differential knowledge of the calibration temperatures is needed. The attenuator value is not needed.

In the case of relative amplitude calibration, a single noise source is used, delivering two calibration temperatures, T_{S1} (WARM) and T_{S2} (HOT), to port 0 of the NDN. The NIR will measure two

temperatures, T_{NS1} and T_{NS2} at the port 1 of the NDN – the calibration external temperatures. As there are three NIRs in the MIRAS instrument, the values T_{NS1} and T_{NS2} will be the average of the noise temperatures measured by each NIR (each NIR has two outputs, H and V and will in fact provide two measurement of the noise temperature in NIR-R mode, which will also be averaged). This averaging of the NIR signals reduces the noise and possible systematic errors. The equivalent system temperatures at the LICEF receivers (port k and j) of the NDN are T_{CS2k}, T_{CS2j}, T_{CS1k} and T_{CS1j}. For example [AD.6]:

$$T_{CS2k} = T_{S2}\left|S_{ks}\right|^2 + \Delta T_{[S],T_{ph}}$$
$$T_{NS2} = T_{S2}\left|S_{1s}\right|^2 + \Delta T'_{[S],T_{ph}} \qquad \textit{Eq. 16}$$

where ΔT and ΔT' are the noise contributions from the NDN due to its physical temperature. S_{ks} is the S-Parameter of the path connecting receiver k with a noise source s, while S_{ls} is the S-parameters of the path connecting the NIR with the same noise source.

Rearranging Eq. 16 and inserting into Eq. 15, the system temperature can be written as

$$T_{sysk} = \frac{v_k - v_{offk}}{v_{2k} - v_{1k}}(T_{C2k} - T_{C1k}) = \frac{v_k - v_{offk}}{v_{2k} - v_{1k}}\frac{\left|S_{ks}\right|^2}{\left|S_{1s}\right|^2}(T_{NS2} - T_{NS1}) \qquad \textit{Eq. 17}$$

3.1.4.2. Fringe Washing Function Estimation

The estimated values of the fringe washing function at the origin are used as a parameter to correct amplitude and in-phase errors. Together with the values at two different time delays it will also be used later during the image reconstruction process. The fringe washing function needs to be estimated for all possible pairs of receivers, without repetition. This gives a total of $N_{Receivers}(N_{Receivers}-1)/2$ pairs to be computed.

The amplitude of the FWF is computed using data from the relative amplitude calibration approach, using the system temperatures computed during calibration with correlated noise injection. Three different measurements are made at the three different time delays needed.

Special care has to be taken in the computation of the M_{kj} terms for the two time delays (-t_s and +t_s). The baseline for the time delay is given from a Local Oscillator at 55.84 MHz, and the value shall be retrieved from the PLM ADF. As mentioned in [RD.26], Equations 3, 4 and 7 must be adjusted for the effect of the time delay. The net effect is that the real part of $\mu_{kj}(-t_s)$ has to be computed from the correlations at time delay $+t_s$ and viceversa.

Additionally, the quadrature error correction computed in Eq.9 θ_{qk} has to be taken from the zero delay self-correlations, as otherwise the quadrature error is badly estimated.

The resulting equations for the fringe wash amplitude term g_{kj} at the hub, at time delays $\tau = -t_s, 0, +t_s$ are [AD.6]:

$$g_{kj}^{C}(\tau)=\frac{M_{kj}^{C2}(\tau)\sqrt{\left(v_{2k}-v_{offk}\right)\left(v_{2j}-v_{offj}\right)}-M_{kj}^{C1}(\tau)\sqrt{\left(v_{1k}-v_{offk}\right)\left(v_{1j}-v_{offj}\right)}}{\sqrt{\left(v_{2k}-v_{1k}\right)}\sqrt{\left(v_{2j}-v_{1j}\right)}}\frac{\left|S_{k0}\right|\left|S_{j0}\right|}{S_{k0}S_{j0}^{*}}$$

$$\begin{cases}\overline{g}_{kj}^{C}(-\tau)=\dfrac{g_{kj}^{C}(-\tau)}{g_{kj}^{C}(0)}e^{j2\pi f_{if}\tau}\\ \overline{g}_{kj}^{C}(-\tau)=1\\ \overline{g}_{kj}^{C}(\tau)=\dfrac{g_{kj}^{C}(\tau)}{g_{kj}^{C}(0)}e^{-j2\pi f_{if}\tau}\end{cases}$$

Eq. 18

where $\left|S_{k,j0}\right|$ are the modulus of the S-parameters relating the k receiver with the noise source (dependent on physical temperature). The term M_{kj}^{C2} will be measured with HOT noise temperature while the term M_{kj}^{C1} is measured with WARM noise temperature. The normalised values at time delays shall be used to estimate the FWF shape coefficients, as it is described in [RD.16] The value of fIF is the intermediate frequency computed as the central frequency minus the local oscillator frequency (both values are contained in the PLM ADF.

The FWF estimated values at the origin are then computed in the antenna polarisation reference planes by:

$$g_{kj}^{H,V}(0)=g_{kj}^{C}(0)\frac{\overline{S}_{LH,Vk}\overline{S}_{LH,Vj}^{*}}{\overline{S}_{LCk}\overline{S}_{LCj}^{*}}e^{j(\phi_{H,Vk}-\phi_{H,Vj})}$$

Eq. 19

Where $\overline{S}_{LCk}$ and $\overline{S}_{LH,Vk}$ are the phases of the switch S-parameters relating port C and H (or V) with port L in the k receiver (dependent on physical temperature) and $\phi_{H,Vk}$ are the antenna patterns absolute phases. Only the FWF at the origin needs to be translated to the antenna plane, the shape values (FWF at time delays) will be a function of $g_{kj}(0)$. The g_{kj} values are complex and will be used to correct amplitude and in-phase errors.

The values shown in Eq. 19 can only be computed for pairs of receivers that share the same Noise Source, as correlated noise can only be injected through the same Noise source. This means that the total number of elements that can be measured is 1296 (see next figure), and for the rest of the pairs, the values should be estimated based on these measurements.

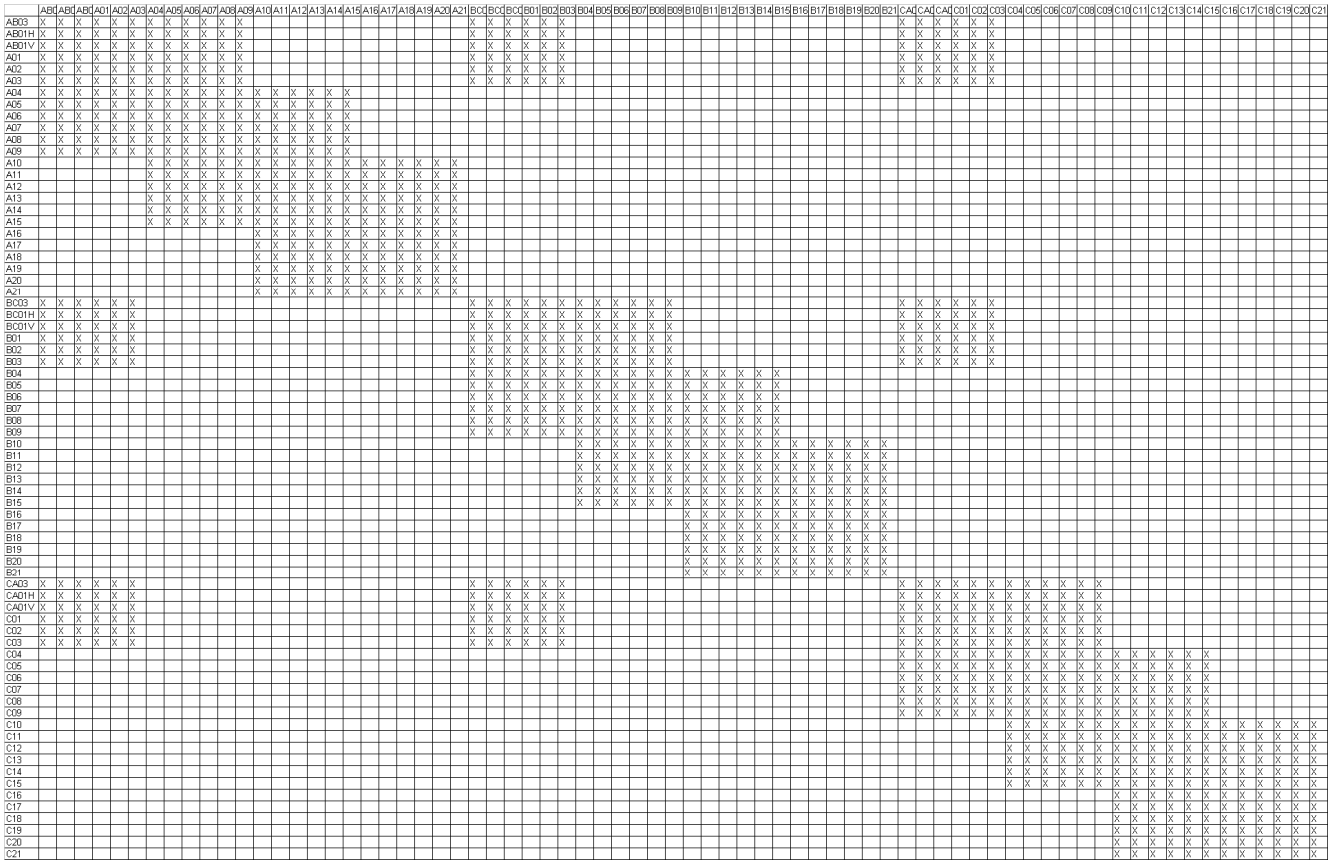

Figure 9 - Baselines covered by the same Noise Sources (Even and Odd)

Amplitude and phase estimations need to be done at CIP (Calibration Input Plane) plane, and they are achieved by using the closure relationships method proposed in RD.7. In this method the value of the FWF for pairs of receivers not connected to the same noise source, *k* and *j*, can be computed by using the following relationship between the Fourier transforms of FWF values for pairs of receivers that use the same noise source, *kl* , *mj*, and *lm*:

$$F\left[g_{kj}(t_s)\right] = \frac{F\left[g_{kl}(t_s)\right] F\left[g_{mj}(t_s)\right]}{\left(F\left[g_{lm}(t_s)\right]\right)^*} \qquad \textit{Eq. 20}$$

Not all of these closures can be made with the direct measurements from Fig. 9. As such, a series of closures will be found consecutively, trying to use as many direct measurements as possible. In the following figure, the number of closures to compute the FWF for each pair of receivers is displayed.

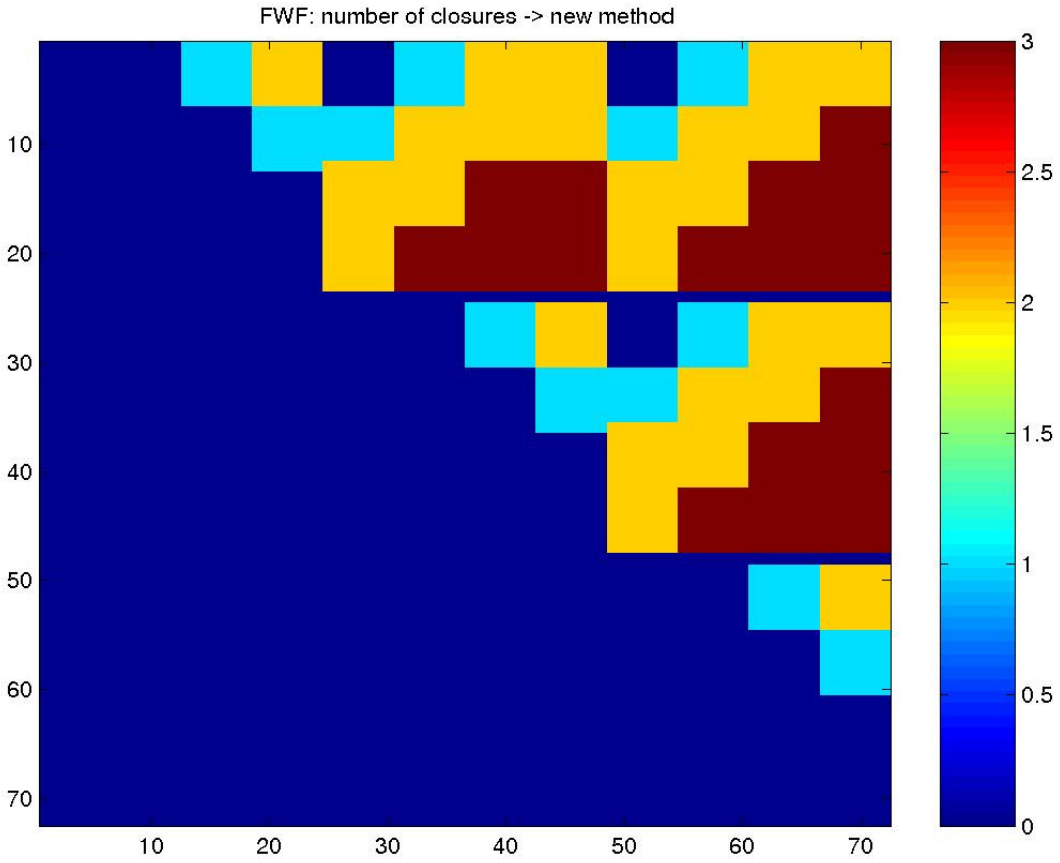

Figure 10 - Number of closures needed to compute the FWF for each pair of receivers

There are, however, a number of baselines that do not have any possible closure for the estimation of the FWF, namely the ones between receiver LICEF_A21 and all the receivers in arms B and C and the ones between the receiver LICEF_B21 and all the receivers in arm C, amounting to a total of 72 baselines. For these remaining pairs of receivers, the FWF will have to estimated by computing the average amplitude value at CIP plane of the measured elements, and assigning it to the baselines that were not measured.

Phase estimation for these remaining pairs of receivers is achieved by first solving the system of equations determined by:

$$\alpha_{kj} = \theta_j - \theta_k - \theta_{kj} \qquad \textit{Eq. 21}$$

Where α_{kj} is the FWF phase of the baseline k-j at CIP plane, θ_j, θ_k are the phase of receivers j and k, respectively, and θ_{kj} is the non-separable error.

The system is solved initially by assuming that the non-separable errors are negligible. The system is over-determined, as there are 1296 equations and only 72 unknowns. As a reference phase is required, the phase of receiver LICEF A01 shall be taken as 0º.

Once the best solution is found for each receiver phase, the non-separable error can be estimated for those baselines that are not covered by any closure, by computing the average value of the error between the measured FWF phase and the solutions of the receivers' phases, as per the next equation:

$$\bar{\theta} = mean\left(\theta_j - \theta_k - \alpha_{kj}\right) \qquad \textbf{Eq. 22}$$

The FWF phase is then estimated by using a modified version of equation 21:

$$\alpha_{kj} = \theta_j - \theta_k - \bar{\theta} \qquad \textbf{Eq. 23}$$

3.1.5. System Temperatures Computation

In measurement mode, the visibilities must be amplitude and phase corrected with the parameters computed in calibration mode. While the quadrature, offset and in-phase corrections are straightforward to apply, since the coefficients have been computed during the noise injection modes, the de-normalisation of the calibrated visibilities will rely on the computation of the system temperatures in the reference planes at the time of each measurement.

First, the correct PMS parameters must be retrieved from auxiliary or previous calibration data, indexed by physical temperature. The correct parameters will be the ones computed ate the closest physical temperature to the one at measurement time. If the temperature change between calibration and observation times is

$$\Delta T_{phy} = T_{phyL1k} - T_{phyL0k} \qquad \textbf{Eq. 24}$$

the gain and offset of the PMSs during observation is computed using ΔT_{phy} and the PMS sensitivity to physical temperature:

$$\begin{aligned} G_k^C &= G_k\left(1 + S_{T_{phy}}^G \frac{1}{100}\Delta T_{phy}\right) \\ v_{offk}^C &= v_{offk} + S_{T_{phy}}^{v_{off}} \Delta T_{phy} \end{aligned} \qquad \textbf{Eq. 25}$$

The sensitivity terms, $S_{T_{phy}}^G$ and $S_{T_{phy}}^{v_{off}}$, will be characterized on ground as well as in-orbit during the calibration procedures.

3.1.5.1. Hub system temperatures

Using Eq. 15, one can express the calibration temperature at the receiver *k* and the system temperature at the antenna plane as

$$\begin{aligned} T_{sys_k}^{HC,VC} &= \frac{v_k - v_{off}}{G_k} \\ T_{sys_k}^{HH,VV} &= T_{sys_k}^{HC,VC} \frac{\left|S_{LCk}\right|^2}{\left|S_{LH,Vk}\right|^2 \eta_{H,Vk}} \end{aligned} \qquad \textbf{Eq. 26}$$

where $|S_{LCk}|$ and $|S_{LH,Vk}|$ are the modulus of the switch S-parameters relating port C and H (or V) with port L in the *k* receiver (dependent on physical temperature), $\eta_{H,Vk}$ is the ohmic efficiency of the antenna *k* in H (or V) mode, v_k are the PMS voltages for the antenna *k* measured while the visibilities are retrieved, v_{offk} are the PMS calibrated offsets and G_k are the PMS calibrated gains(also dependent on physical temperature).

A further correction to PMS 2nd order linearity needs to be applied before the plane transition, as is explained in Eq. 36 in the next section.

3.1.5.2. Arm system temperatures

The MIRAS/SMOS configuration uses a distributed approach to inject noise in the three arms of the instrument. Each arm is divided in three sections, with 6 receivers each, denominated quite simply segments 1, 2 and 3. The following assumptions were made:

- 2 EVEN noise sources: 0 and β placed at ports 0 and β of the NDN
- 2 ODD noise sources: α and γ placed at ports α and γ of the NDN
- 18 PMS *k* placed at the HUB
- 3 NIR placed at port 1 of the HUB
- 6 PMS *l* placed at first segment of each arm
- 6 PMS *m* placed at second segment of each arm
- 6 PMS *n* placed at third segment of each arm

The hub PMS calibration method of section 3.1.4.1 can be extended and applied to the PMS in the arms. Two sets of PMS voltage readings can be obtained, from EVEN and ODD noise sources. In the first segment, the PMS can be calibrated using the NIR at port 1 of the HUB when driven by the common ODD noise source α. Due to the symmetry of the temperature at port C of each of the 6 PMS *l* receivers, we can calculate [RD.17]:

$$T_{sys_l}^{C} = \frac{1}{4}\sum_{h=1}^{4}\frac{|S_{l\alpha}|^2}{|S_{h\alpha}|^2}\frac{v_l - v_{offl}}{v_{2l}^{\alpha} - v_{1l}^{\alpha}}\frac{|S_{l0}|^2}{|S_{h0}|^2}\frac{v_{2h}^{\alpha} - v_{1h}^{\alpha}}{v_{2h}^{0} - v_{1h}^{0}}(T_{NS2}^{0} - T_{NS1}^{0}) \qquad \textbf{Eq. 27}$$

where the noise source temperatures are averaged from the measurements of the receivers in the hub, excluding the NIR channels. Since the offset term can be calculated from both sources, EVEN and ODD, it can be written as

$$v_{offl} = \frac{1}{2}(v_{offl}^{0} + v_{offl}^{\alpha}) \qquad \textbf{Eq. 28}$$

where

$$v_{offl}^{0} = \frac{v_{2l}^{0} v_{3l}^{0} - v_{1l}^{0} v_{4l}^{0}}{v_{2l}^{0} - v_{4l}^{0} - v_{1l}^{0} + v_{3l}^{0}}$$
$$v_{offl}^{\alpha} = \frac{v_{2l}^{\alpha} v_{3l}^{\alpha} - v_{1l}^{\alpha} v_{4l}^{\alpha}}{v_{2l}^{\alpha} - v_{4l}^{\alpha} - v_{1l}^{\alpha} + v_{3l}^{\alpha}}$$

Eq. 29

Please note that for the last segment in each arm, Eq. 27 is not used, since there is only one noise source available.

While this averaging can be done for the offsets, the same can not be done for the gains, since these depend on the S-Parameters of the paths connecting the LICEFS with each Noise Source. Making use of the same symmetry, the calibration temperature for receivers *m* in the second segment can be calibrated with

$$T_{sys_m}^{C} = \frac{v_m - v_{offm}}{v_{2m}^{\beta} - v_{1m}^{\beta}} \frac{\left|S_{m\beta}\right|^2}{\left|S_{l\beta}\right|^2} (T_{sys_l}^{\beta C2} - T_{sys_l}^{\beta C1})$$

Eq. 30

since any PMS *l* in the first segment can play the role of NIR when both segments are driven by the common noise source β. Since the PMS *l* have been calibrated already, we have

$$T_{sys_l}^{\beta C2} = \frac{1}{4}\sum_{h=1}^{4} \frac{\left|S_{l\alpha}\right|^2}{\left|S_{h\alpha}\right|^2} \frac{v_{2l} - v_{offl}}{v_{2l}^{\alpha} - v_{1l}^{\alpha}} \frac{\left|S_{l0}\right|^2}{\left|S_{h0}\right|^2} \frac{v_{2h}^{\alpha} - v_{1h}^{\alpha}}{v_{2h}^{0} - v_{1h}^{0}} (T_{NS2}^{0} - T_{NS1}^{0}) = \frac{v_{2l} - v_{offl}}{v_{2l}^{\alpha} - v_{1l}^{\alpha}} \frac{\left|S_{l\alpha}\right|^2}{\left|S_{h\alpha}\right|^2} (T_{NS2}^{\alpha} - T_{NS1}^{\alpha})$$
$$T_{sys_l}^{\beta C1} = \frac{1}{4}\sum_{h=1}^{4} \frac{\left|S_{l\alpha}\right|^2}{\left|S_{h\alpha}\right|^2} \frac{v_{1l} - v_{offl}}{v_{2l}^{\alpha} - v_{1l}^{\alpha}} \frac{\left|S_{l0}\right|^2}{\left|S_{h0}\right|^2} \frac{v_{2h}^{\alpha} - v_{1h}^{\alpha}}{v_{2h}^{0} - v_{1h}^{0}} (T_{NS2}^{0} - T_{NS1}^{0}) = \frac{v_{2l} - v_{offl}}{v_{2l}^{\alpha} - v_{1l}^{\alpha}} \frac{\left|S_{l\alpha}\right|^2}{\left|S_{h\alpha}\right|^2} (T_{NS2}^{\alpha} - T_{NS1}^{\alpha})$$

Eq. 31

yielding

$$T_{sys_m}^{C} = \frac{v_m - v_{offm}}{v_{2m}^{\beta} - v_{1m}^{\beta}} \frac{\left|S_{m\beta}\right|^2}{\left|S_{l\beta}\right|^2} \frac{v_{2l}^{\beta} - v_{1l}^{\beta}}{v_{2l}^{\alpha} - v_{1l}^{\alpha}} \frac{\left|S_{l\alpha}\right|^2}{\left|S_{1\alpha}\right|^2} (T_{NS2}^{\alpha} - T_{NS1}^{\alpha})$$

Eq. 32

Moreover, the taking into account that each noise source drives 12 receivers, 6 PMS in each segment can be used as NIR and the results averaged in order to improve the results. The previous will then transform into:

$$T_{sys_m}^{C} = \frac{1}{6}\sum_{l=1}^{6} \frac{v_m - v_{offm}}{v_{2m}^{\beta} - v_{1m}^{\beta}} \frac{\left|S_{m\beta}\right|^2}{\left|S_{l\beta}\right|^2} \frac{v_{2l}^{\beta} - v_{1l}^{\beta}}{v_{2l}^{\alpha} - v_{1l}^{\alpha}} \frac{\left|S_{l\alpha}\right|^2}{\left|S_{1\alpha}\right|^2} (T_{NS2}^{\alpha} - T_{NS1}^{\alpha})$$

Eq. 33

Finally, the same procedure can be applied to the third segment, for the PMS *n*:

$$T_{sys_n}^{C} = \frac{v_n - v_{offn}}{v_{2n}^{\gamma} - v_{1n}^{\gamma}} \frac{\left|S_{n\gamma}\right|^2}{\left|S_{m\gamma}\right|^2} (T_{sysm}^{\gamma C2} - T_{sysl}^{\gamma C1})$$

Eq. 34

and again using the fact that the PMS *m* have already been calibrated and can be averaged, we have

$$T_{sys_n}^{C} = \frac{1}{36}\sum_{m=1}^{6}\sum_{l=1}^{6}\frac{v_n - v_{offn}}{v_{2n}^{\gamma} - v_{1n}^{\gamma}}\frac{\left|S_{n\gamma}\right|^2}{\left|S_{m\gamma}\right|^2}\frac{v_{2m}^{\gamma} - v_{1m}^{\gamma}}{v_{2m}^{\beta} - v_{1m}^{\beta}}\frac{\left|S_{m\beta}\right|^2}{\left|S_{l\beta}\right|^2}\frac{v_{2l}^{\beta} - v_{1l}^{\beta}}{v_{2l}^{\alpha} - v_{1l}^{\alpha}}\frac{\left|S_{l\alpha}\right|^2}{\left|S_{1\alpha}\right|^2}(T_{NS2}^{\alpha} - T_{NS1}^{\alpha}) \qquad \textit{Eq. 35}$$

After computing the system temperatures at CIP for all receivers $T_{sys_k}^{SC(1)}$, a further 2nd order linearity correction must be performed using the deflection parameter measured on ground C_k.

$$v_{ik}^{(2)} - v_{off_k} = C_k\sqrt{1 + \frac{2}{C_k}\left(v_{ik}^{(1)} - v_{off_k}\right)} - C_k \qquad \textit{Eq. 36}$$

The objective is to apply again the previous equations, but using these new voltages $v_{ik}^{(2)}$ as a starting point, in order to obtain a final system temperature $T_{sys_k}^{SC(2)}$ (i.e. computing again new offsets and gains with Eq. 27-35)

To extract the system temperature at the antenna phase centre the following plane translation, between calibration and antenna planes, is made (H mode exemplified):

$$T_{sys_{l,m,n}}^{H} = \frac{\left|S_{LCl,m,n}\right|^2}{\left|S_{LHl,m,n}\right|^2 \eta_{Hl,m,n}} T_{sys_{l,m,n}}^{C(2)} \qquad \textit{Eq. 37}$$

where $\left|S_{LCl,m,n}\right|$ and $\left|S_{LHl,m,n}\right|$ are the modulus of the switch S-parameters relating port C and H with port L for PMS *l,m,n* (dependent on physical temperature) and $\eta_{l,m,n}$ is the antenna efficiency in horizontal mode. The same procedure must be applied for the vertical measurement modes.

So, introducing the definition of PMS gain from Eq. 12, for each segment we have the values of system temperature in terms of PMS output $v_{l,m,n}$, gain $G_{l.m.n}^{\alpha,\beta,\gamma}$ and offset $v_{off_{l,m,n}}$:

$$\begin{aligned} T_{sys_l}^{H,V} &= \frac{\left|S_{LCl}\right|^2}{\left|S_{LH,Vl}\right|^2 \eta_{H,Vl}} \frac{v_l^{(2)} - v_{offl}^{(2)}}{G_l^{\alpha(2)}} \\ T_{sys_m}^{H,V} &= \frac{\left|S_{LCm}\right|^2}{\left|S_{LH,Vm}\right|^2 \eta_{H,Vm}} \frac{v_m^{(2)} - v_{offm}^{(2)}}{G_m^{\beta(2)}} \\ T_{sys_n}^{H,V} &= \frac{\left|S_{LCn}\right|^2}{\left|S_{LH,Vn}\right|^2 \eta_{H,Vn}} \frac{v_n^{(2)} - v_{offn}^{(2)}}{G_n^{\gamma(2)}} \end{aligned} \qquad \textit{Eq. 38}$$

3.1.5.3. NIR temperatures

This section was based on the description of NIR calibration procedures in [RD 16] and on the latest In Orbit Calibration Plan [AD 6]. For more information, please refer to those documents.

3.1.5.3.1. NIR brightness temperatures

3.1.5.3.1.1. Dual polarisation temperatures

In dual polarisation mode, the NIR brightness temperatures are computed from data retrieved in NIR-A mode, namely the NIR pulse length and the measured noise temperature:

$$T'_{A,v} = \left(A_{A,v} + \Delta A_{A,v}\right)\eta_v + \left(B_{A,v} + \Delta B_{A,v}\right)$$
$$T'_{A,h} = \left(A_{A,h} + \Delta A_{A,h}\right)\eta_h + \left(B_{A,h} + \Delta B_{A,h}\right)$$

with

$$\Delta A_{A,v} = a_v(T_{p7} - T_{p7,0}) \qquad \textit{Eq. 39}$$
$$\Delta A_{A,h} = a_h(T_{p7} - T_{p7,0})$$
$$\Delta B_{A,v} = b_v(T_{p7} - T_{p7,0})$$
$$\Delta B_{A,h} = b_h(T_{p7} - T_{p7,0})$$

where $\eta_{v,h}$ are the NIR pulse lengths in H and V polarisations, T_{p7} is the physical temperature of the antenna patch (subscript 0 indicates the temperature during calibration) and A_A and B_A are coefficients computed as is explained in the following paragraphs.

The coefficient A_A can be computed simply from

$$A_{A,v} = -L_{1v}L_{2v}T_{NA,v}$$
$$A_{A,h} = -L_{1h}L_{2h}T_{NA,h} \qquad \textit{Eq. 40}$$

where T_{NA} is the corrected noise injection temperature, computed from the noise injection level measured during calibration, T_{NA0} (see Section 3.1.9.1), by

$$T_{NA,v} = T_{NA0,v} + u_{Av}(T_{p1v} - T_{p1v,0})$$
$$T_{NA,h} = T_{NA0,h} + u_{Ah}(T_{p1h} - T_{p1h,0}) \qquad \textit{Eq. 41}$$

with the parameters defined as:

- $u_{Av,h}$ - Sensitivity to physical temperature gradient (please check [RD 16] - Section 5.3.3)
- T_{p1} - Is the physical temperature of the noise source
- $T_{p1h,v0}$ - Is the physical temperature of the noise source during calibration (see Section 3.1.9.1)
- L_1 - Attenuator between antenna plane and antenna intermediate layer computed as $L_{1h,v} = L^0_{1h,v} + \delta L_{1h,v} + \alpha_{h,v}(T_{p7,0} - T_{p7,ref}) + \beta_{h,v}(T_{p7} - T_{p7,ref})$ in which
  - $L^0_{1h,v}$ is the L1 attenuator value measured on-ground

- $\delta L_{1h,v}$ is a fixed L1 attenuator error characterised in-orbit using data from the first year
- $\alpha_{h,v}$ is the long term drift component of the L1 attenuator in-orbit using data from the first year
- $\beta_{h,v}$ is the short term drift component of the L1 attenuator in-orbit using data from the first year
- $T_{p7,ref}$ is the reference Tp7 at which the previous 3 coefficients were obtained
- T_{p7} is the physical temperature of the radiator of the antenna (antenna patch) during the current measurement
- $T_{p7,0}$ is the physical temperature of the radiator of the antenna (antenna patch) during the NIR calibration sequence

- L_2 - Attenuator between antenna intermediate layer and antenna input plane

As for the coefficient B_A, several intermediate temperatures must be computed. First, the thermal noise contributions are computed from

$$
\begin{aligned}
T_{t1v} &= \left(1-\frac{1}{L_{1v}}\right)\frac{T_{p7}}{L_{2v}}+\left(1-\frac{1}{L_{2v}}\right)T_{p6v} \\
T_{t1h} &= \left(1-\frac{1}{L_{1h}}\right)\frac{T_{p7}}{L_{2h}}+\left(1-\frac{1}{L_{2h}}\right)T_{p6h} \\
T_{t2v} &= \left(1-\frac{1}{L_{NCv}}\right)\frac{T_{p3v}}{L_{Av}L_{DAv}}+\left(1-\frac{1}{L_{Av}}\right)\frac{T_{Cabv}}{L_{DAv}}+\left(1-\frac{1}{L_{DAv}}\right)T_{pUv} \\
T_{t2h} &= \left(1-\frac{1}{L_{NCh}}\right)\frac{T_{p3h}}{L_{Ah}L_{DAh}}+\left(1-\frac{1}{L_{Ah}}\right)\frac{T_{Cabh}}{L_{DAh}}+\left(1-\frac{1}{L_{DAh}}\right)T_{pUh}
\end{aligned}
\qquad \textit{Eq. 42}
$$

where

- T_{p7} - Physical temperature of the radiator of the antenna (antenna patch)
- T_{p6} - Physical temperature of the intermediate layer of the antenna
- T_{p3} - Physical temperature of the attenuator in reference noise injection channel
- L_{NC} - Attenuator between antenna input plane and antenna output plane
- L_A - Attenuator between antenna output plane and LICEF input plane
- L_{DA} - Attenuator between antenna LICEF input plane in H or V port and LICEF output plane
- T_U - Physical temperature measured inside the LICEF (between U-Load and isolator)

- T_{pU} - U-load. Approximated by T_U
- T_{Cab} - Physical temperature between radiator output plane and LICEF input plane. Shall be approximated from T_{p3} and T_U as

$$T_{Cabv} = \frac{T_{p3v} + T_{Uv}}{2}$$
$$T_{Cabh} = \frac{T_{p3h} + T_{Uh}}{2} \qquad \textit{Eq. 43}$$

Finally, the coefficient B_A is computed as

$$B_{Av} = L_{1v}L_{2v}\left[L_{NCv}L_{Av}L_{DAv}\left(T_{Uv} - T_{t2v}\right) - T_{t1v}\right]$$
$$B_{Ah} = L_{1h}L_{2h}\left[L_{NCh}L_{Ah}L_{DAh}\left(T_{Uh} - T_{t2h}\right) - T_{t1h}\right] \qquad \textit{Eq. 44}$$

and Eq. 39 is applied. The resulting brightness temperature is further corrected by

$$\hat{T}_{A,v} = T'_{A,v} + c_{Av}\left(T'''_{A,v} - T'''_{A0,v}\right) + d_{Av}\left(T'''_{A,v} - T'''_{A0,v}\right)^2$$
$$\hat{T}_{A,h} = T'_{A,h} + c_{Ah}\left(T'''_{A,h} - T'''_{A0,h}\right) + d_{Ah}\left(T'''_{A,h} - T'''_{A0,h}\right)^2 \qquad \textit{Eq. 45}$$

where the parameters c_A and d_A are parameters measured on-ground and used to compensate the uncertainty in the front-end characterization (first and second order). $T'''_{A,v}$ and $T'''_{A0,v}$ are computed by:

$$T'''_{A,v} = \frac{T'_{A,v}}{L_{1,v}L_{2,v}} + T_{t1,v}$$
$$T'''_{A,h} = \frac{T'_{A,h}}{L_{1,h}L_{2,h}} + T_{t1,h} \qquad \textit{Eq. 46}$$

and T'''_{A0} is the antenna temperature during calibration (see Section 3.1.9), and stored with the NIR-A data (i.e. with physical temperatures measured at the time of calibration).

3.1.5.3.1.2. Full polarisation temperatures

In the case of the processing of full polarisation scenes, the NIR brightness temperatures are computed as in the dual polarisation case but the 3rd and 4th Stokes parameters, T_3 and T_4, have to be computed from NIR pulse lengths, the FWF(0) values and the phase corrected correlations.

The 3rd and 4th Stokes parameters are retrieved by using

$$\begin{bmatrix} T_3 \\ T_4 \end{bmatrix} = \begin{bmatrix} g'_S & 0 \\ 0 & g'_S \end{bmatrix} \begin{bmatrix} r_3 \\ r_4 \end{bmatrix} + \begin{bmatrix} f_{ii} \\ f_{qi} \end{bmatrix} \qquad \textit{Eq. 47}$$

The factors in the previous computation must be retrieved from a set of measurement and calibration data. The steps to obtain these are shown below. First, the correlations are used to compute the factor

$$\begin{bmatrix} r_3 \\ r_4 \end{bmatrix} = \begin{bmatrix} \arcsin(\mu_{ii}^{CIP}) \\ \arcsin(\mu_{qi}^{CIP}) \end{bmatrix} \qquad \textit{Eq. 48}$$

And the g'_S are gain parameters computed as

$$g'_S = \frac{1}{g_{kj_{NIR}}} \Lambda_{kj} \sqrt{T_{sys}^{HA} T_{sys}^{VA}} \qquad \textit{Eq. 49}$$

where $g_{kj_{NIR}}$ is the Fringe Wash Function at the origin applicable to the two LICEF correlation within a NIR, T_{sys}^{AA} are the system temperatures computed through Eq. 61 and $T''_{NA,hv}$ is the noise injection temperature from Eq. 41, converted to the antenna plane by

$$T''_{NA,vh} = L_{1,vh} L_{2,vh} T_{NA,vh} - L_{1,vh} T_{L2,vh} - T_{L1,vh} \qquad \textit{Eq. 50}$$

with $T_{L2,vh}$ and $T_{L1,vh}$ defined in the next section.

Additionally, parameter Λ_{kj} from Eq. 49 is dependant on the condition $\eta_h > \eta_v$, as shown in the following equation.

$$\eta_V > \eta_H :$$

$$\Lambda_{kj} = \left(n_1 \sqrt{\frac{T_{sys}^{HA} T_{sys}^{VA}}{\left(T_{sys}^{HA} + T''_{NA,h}\right)\left(T_{sys}^{VA} + T''_{NA,v}\right)}} + n_2 \sqrt{\frac{T_{sys}^{VA}}{\left(T_{sys}^{VA} + T''_{NA,v}\right)}} + n_3 \right)^{-1}$$

$$\eta_V < \eta_H :$$

$$\Lambda_{kj} = \left(n_1 \sqrt{\frac{T_{sys}^{HA} T_{sys}^{VA}}{\left(T_{sys}^{HA} + T''_{NA,h}\right)\left(T_{sys}^{VA} + T''_{NA,v}\right)}} + n_2 \sqrt{\frac{T_{sys}^{HA}}{\left(T_{sys}^{HA} + T''_{NA,h}\right)}} + n_3 \right)^{-1} \qquad \textit{Eq. 51}$$

Finally, the coefficients n_i are computed from the NIR pulse lengths by the following rules

$$n_1 = \frac{1}{2}\min\left(\eta_v, \eta_h\right)$$
$$n_2 = \frac{1}{2}\max\left(\eta_v, \eta_h\right) - \frac{1}{2}\min\left(\eta_v, \eta_h\right) \qquad \textit{Eq. 52}$$
$$n_3 = \frac{1}{2} - \frac{1}{2}\max\left(\eta_v, \eta_h\right)$$

By expanding all the coefficients of Eq. 48, the full equation for T_3 and T_4 is obtained:

$$T_3^V = \mathrm{Re}\left\{\frac{1}{g_{kj_{NIR}}}\Lambda_{kj}\sqrt{T_{sys}^{HA}T_{sys}^{VA}}M_{kj_{NIR}}\right\} + f_{ii}$$
$$T_4^V = \mathrm{Im}\left\{\frac{1}{g_{kj_{NIR}}}\Lambda_{kj}\sqrt{T_{sys}^{HA}T_{sys}^{VA}}M_{kj_{NIR}}\right\} + f_{qi} \qquad \textit{Eq. 53}$$

The terms f_{ii} and f_{qi} are the corrections for cross-coupling and leakage, computed during the NIR calibration process (Section 3.1.9.3). Moreover, Eq.53 has been further simplified from Eq.48 by using the definition of quadrature corrected correlations (Eq. 7).

The values are computed in VIP, since both NIR-LICEF are switched to the NIC (and subsequently to the antenna) using the VIP port. The procedure to transform the FWF(0) to the antenna plane is the same as described in Eq.19, but taking care to use the combination of H and V polarisation needed in this case, and noting that the final plane is still VIP for both polarisations.

3.1.5.3.2. NIR receiver noise temperatures

The receiver noise temperatures measured in LICEF-LC/LC2 mode ($T_{rec}^{LV-CIP,LH-CIP}$, see Section 3.1.8.2) are converted from the calibration plane to the H and V Input planes through:

$$T_{rec}^{LV-VIP} = \frac{L_{DAv}}{L_{DCv}}T_{rec}^{LV-CIP} + \left(\frac{L_{DAv}}{L_{DCv}} - 1\right)T_{pUv}$$
$$T_{rec}^{LH-HIP} = \frac{L_{DAh}}{L_{DCh}}T_{rec}^{LH-CIP} + \left(\frac{L_{DAh}}{L_{DCh}} - 1\right)T_{pUh} \qquad \textit{Eq. 54}$$

and then, into the antenna planes by:

$$T_{rec}^{VAP} = T_{L1v} + L_{1v}T_{L2v} + L_{1v}L_{2v}T_{LNCv} + L_{1v}L_{2v}L_{LNCv}T_{LAv} + L_{1v}L_{2v}L_{LNCv}L_{Av}T_{rec}^{LV-VIP}$$
$$T_{rec}^{HAP} = T_{L1h} + L_{1h}T_{L2h} + L_{1h}L_{2h}T_{LNCh} + L_{1h}L_{2h}L_{LNCh}T_{LAh} + L_{1h}L_{2h}L_{LNCh}L_{Ah}T_{rec}^{LH-HIP} \qquad \textit{Eq. 55}$$

Where $T_{rec}^{HAP,VAP}$ is the total receiver noise temperature at the antenna plane.

The coefficients present in the previous computation are found using the following relations. The receiver temperature between antenna patch input plane and antenna intermediate plane (H or V) is

$$T_{L1v,h} = (L_{1v,h} - 1)T_{p7v,h} \qquad \textit{Eq. 56}$$

The receiver temperature between the antenna intermediate plane and the input connector plane (H or V) is

$$T_{L2v,h} = (L_{2v,h} - 1)T_{p6v,h} \qquad \textit{Eq. 57}$$

The receiver temperature between the input connector plane and output connector plane is

$$T_{LNCv,h} = (L_{LNCv,h} - 1)T_{p3v,h} \qquad \textit{Eq. 58}$$

The receiver temperature between the output connector plane and LICEF input connector plane is

$$T_{LAv,h} = (L_{Av,h} - 1)T_{Cabv,h} \qquad \textit{Eq. 59}$$

The parameters used in the previous equations, measured on-ground, are

- T_{L1} - Receiver temperature between antenna plane and antenna intermediate layer
- T_{L2} - Receiver temperature between antenna intermediate layer and antenna input plane
- T_{LNC} - Receiver temperature between antenna input plane and antenna output plane
- T_{LA} - Receiver temperature between antenna output plane and LICEF input plane
- L_{DC} - Attenuator between antenna LICEF input plane in C port and LICEF output plane

3.1.5.3.3. LICEF-NIR baselines system temperatures

For LICEF-NIR baselines, while the LICEF system temperature can be computed in the usual way (Sections 3.1.5.1 and 3.1.5.2), the NIR system temperature needs to be computed in a different way, making use of the antenna temperature, the receiver temperature described above, the noise temperature in the antenna plane and a the NIR pulse length information.

The noise injection level $T''_{NA,hv}$, is translated to the antenna plane, through Eq. 50, and the NIR equivalent system temperature, T_{sys}^{VV,HH_b}, is defined as:

$$T_{sys}^{VV_b} = T_{sys}^{VA}\left[\frac{1}{2}\left(\eta_v\sqrt{\frac{T_{sys}^{VA}}{T_{sys}^{VA}+T''_{NA,v}}}+1-\eta_v+\frac{S_{LV}^{U-V}}{\sqrt{L_{FE,v}}}\sqrt{\frac{T_{sys}^{VA}}{T_{sys,v}^{UU}}}\right)\right]^{-2}$$
$$T_{sys}^{HH_b} = T_{sys}^{HA}\left[\frac{1}{2}\left(\eta_h\sqrt{\frac{T_{sys}^{HA}}{T_{sys}^{HA}+T''_{NA,h}}}+1-\eta_h+\frac{S_{LH}^{U-V}}{\sqrt{L_{FE,h}}}\sqrt{\frac{T_{sys}^{HA}}{T_{sys,h}^{UU}}}\right)\right]^{-2} \qquad \textit{Eq. 60}$$

where

$$
\begin{aligned}
T_{sys}^{VA} &= \hat{T}_{A,v} + T_{rec}^{VAP} \\
T_{sys}^{HA} &= \hat{T}_{A,h} + T_{rec}^{HAP} \\
T_{sys,v}^{UU} &\approx T_{rec}^{LV-CIP} + T_{ph,v} \\
T_{sys,h}^{UU} &\approx T_{rec}^{LH-CIP} + T_{ph,h}
\end{aligned}
\qquad \textbf{Eq. 61}
$$

with $S_{LH,V}^{U-V}$ as the complex Dicke Switch isolation, and $L_{FE} = L_1 L_2 L_{NC} L_A$, where the attenuator parameters have been used in Eqs. 56-59. It has to be remarked, that the Dicke Switch Isolation is provided in the NIR ADF, and that it must be interpolated to the corresponding temperature of the NIR unit $T_{ph,h-v}$.

3.1.5.4. Applying system temperatures to PMS calibration

After measuring the 4 voltages from each PMS, the calibration parameters for the hub are obtained through (Eqs. 14 and 16) [RD.17]:

$$
\begin{aligned}
v_{off_k} &= \frac{v_{2k} v_{3k} - v_{1k} v_{4k}}{(v_{2k} - v_{4k}) - (v_{1k} - v_{3k})} \\
G_k &= \frac{v_{2k} - v_{1k}}{\frac{|S_{k0}|^2}{|S_{N0}|^2} T_{S2} - T_{S1}}
\end{aligned}
\qquad \textbf{Eq. 62}
$$

and for the PMS *l,m,n* in each of the three arms, A, B and C through[2]:

$$
\begin{aligned}
v_{offl,m} &= \frac{1}{2}(v_{offl,m}^{odd} + v_{offl,m}^{even}) \\
v_{off_{l,m,n}} &= \frac{v_{2l,m,n} v_{3l,m,n} - v_{1l,m,n} v_{4l,m,n}}{(v_{2l,m,n} - v_{4l,m,n}) - (v_{1l,m,n} - v_{3l,m,n})} \\
G_{l,m,n}^{s} &= \frac{v_{2l,m,n} - v_{1l,m,n}}{(T_{C2} - T_{C1})_{l,m,n}}
\end{aligned}
\qquad \textbf{Eq. 63}
$$

where the system temperatures differential for each segment can be related to the measured one at the hub by:

[2] please note that, for the last segment on each arm, the offset is computed with the only noise source available and that there is no averaging

$$(T_{C2}-T_{C1})_l = \frac{1}{4}\sum_{h=1}^{4}\frac{|S_{l\alpha}|^2}{|S_{h\alpha}|^2}\frac{v_{2h}^{\alpha}-v_{1h}^{\alpha}}{v_{2h}^{0}-v_{1h}^{0}}\frac{|S_{l0}|^2}{|S_{h0}|^2}(T_{NS2}^{0}-T_{NS1}^{0})$$

$$(T_{C2}-T_{C1})_m = \frac{1}{24}\sum_{l=1}^{6}\frac{|S_{m\beta}|^2}{|S_{l\beta}|^2}\frac{v_{2l}^{\beta}-v_{1l}^{\beta}}{v_{2l}^{\alpha}-v_{1l}^{\alpha}}\frac{|S_{l\alpha}|^2}{|S_{N\alpha}|^2}\sum_{h=1}^{4}\frac{|S_{l\alpha}|^2}{|S_{h\alpha}|^2}\frac{v_{2h}^{\alpha}-v_{1h}^{\alpha}}{v_{2h}^{0}-v_{1h}^{0}}\frac{|S_{l0}|^2}{|S_{h0}|^2}(T_{NS2}^{0}-T_{NS1}^{0}) \qquad \textit{Eq. 64}$$

$$(T_{C2}-T_{C1})_n = \frac{1}{144}\sum_{m=1}^{6}\sum_{l=1}^{6}\frac{|S_{n\gamma}|^2}{|S_{m\gamma}|^2}\frac{v_{2m}^{\gamma}-v_{1m}^{\gamma}}{v_{2m}^{\beta}-v_{1m}^{\beta}}\frac{|S_{m\beta}|^2}{|S_{l\beta}|^2}\frac{v_{2l}^{\beta}-v_{1l}^{\beta}}{v_{2l}^{\alpha}-v_{1l}^{\alpha}}\sum_{h=1}^{4}\frac{|S_{l\alpha}|^2}{|S_{h\alpha}|^2}\frac{v_{2h}^{\alpha}-v_{1h}^{\alpha}}{v_{2h}^{0}-v_{1h}^{0}}\frac{|S_{l0}|^2}{|S_{h0}|^2}(T_{NS2}^{0}-T_{NS1}^{0})$$

It has to be taken into account, that in order to correct the PMS linearity term, this process must be done in two iterations, as indicated in Eq. 36, and only the second iteration PMS voltage $v_{ik}^{(2)}$ is used to compute the final PMS gain/offset and the System Temperatures.

3.1.6. Correlator Offset correction

All receivers from the same segment should have zero cross-correlation when connected to separate uncorrelated noise sources. In order to have this behaviour, the residual offset must be calibrated through periodic injection of uncorrelated noise in the receivers. The cross-correlations are quadrature corrected and de-normalised, yielding a set of visibilities. The measured visibilities are then stored in memory and subtracted from all subsequent visibilities measured in normal observation mode or during calibration.

Uncorrelated noise injection will be done at various points of the orbit and at various temperatures. More than one offset per visibility will be stored, as a function of the temperatures of the LICEFs involved in the generation of the visibility.

The subtractions are performed at the level of de-normalised visibilities, so the U-load temperatures during uncorrelated noise injection will be computed as Eq. 26.

$$T_{sys_k}^{UC} = \frac{v_k - v_{offk}}{G_k^U} \qquad \textit{Eq. 65}$$

The U-load system temperatures and Fringe Washing Function at the origin are then used together with the quadrature corrected correlations compute the visibilities offset:

$$\hat{V}_{kj}^{UC} = \frac{\sqrt{T_{sys_k}^{UC}T_{sys_j}^{UC}}M_{kj}^{UC}}{g_{kj}^{C}} \qquad \textit{Eq. 66}$$

3.1.7. Error Compensation

3.1.7.1. Visibilities Calibration

The final step for calibrating visibilities is to de-normalise them, with the system temperatures computed in the measurement mode calibration

$$V_{kj}^{H,V} = \sqrt{T_{sys_k}^{H,V} T_{sys_j}^{H,V}}\, M_{kj}^{H,V} \qquad \textit{Eq. 67}$$

and apply the in-phase and amplitude error corrections as well as removing the offsets computed previously.

The visibilities offsets are corrected with the switch S-parameters, retrieved using the physical temperature at calibration time:

$$V_{kj}^{UH,V} = V_{kj}^{UC} \frac{\left|S_{LCk}\right|\left|S_{LCj}\right|}{\left|S_{LH,Vk}\right|\left|S_{LH,Vj}\right|\sqrt{\eta_{H,Vk}\eta_{H,Vj}}} \qquad \textit{Eq. 68}$$

The final equation will thus be:

$$\hat{V}_{kj}^{H,V} = \frac{V_{kj}^{H,V}}{g_{kj}^{H,V}} - a_{kj}\hat{V}_{kj}^{UH,V} \qquad \textit{Eq. 69}$$

where a_{kj} is a coefficient to adjust the influence of the visibilities offsets in the final calibrated visibility. This coefficient is defined as an integer number (0, 1 or 2) indicating if offset correction is needed for baseline *kj*.

Additionally, as discovered by ESTEC during November 2007, the offset correction for baselines involving NIR-LICEF needs to be corrected with a factor 2, due to the different integration time in which the NIR-LICEF are providing correlations (the rest of the time it operates as a NIR).

During IVT campaign, it was seen that offset correction is only required for baselines sharing the same Local Oscillator, so for the current time there shall be three configurable processing options:

- ❑ No offset correction ($a_{kj} = 0$ for all baselines)
- ❑ Offset correction ($a_{kj} = 1$ for all LICEF baselines, and $a_{kj} = 2$ for all NIR-LICEF baselines)
- ❑ Local Oscillator Offset Correction ($a_{kj} = 1$ only for LICEF baselines sharing the same Local Oscillator, i.e. the LICEF for those baselines are linked to the same CMN, and $a_{kj} = 2$ only for NIR-LICEF baselines sharing the same Local Oscillator)

3.1.7.2. Redundant Space Calibration

This method is based on the fact that there are redundant baselines measured that should be measuring the same value, in case this is not true, it can be attributed to separable amplitude and phase errors associated to each receiving chain.

As this method is very sensitive to non-separable errors, in SEPS it has only been applied to calibrate non-normalised visibilities to correct for error terms associated to the path between the antenna and the input switch, that is, for all the antennae along the arms.

The set of equations for this purpose is expressed in phase and amplitude as [RD.18]:

$$\phi^{raw}_{k-1,k} = f_{k-1} - f_k + \phi_{k-1,k}$$
$$\left|V^{raw}_{k-1,k} = g_{k-1} g_k V_{k-1,k}\right| \Rightarrow \ln\left(\left|V^{raw}_{k-1,k}\right|\right) = \ln\left(g_{k-1}\right) + \ln\left(g_k\right) + \ln\left(\left|V_{k-1,k}\right|\right) \quad \textbf{Eq. 70}$$

Where *k* and *k-1* are the indexes of adjacent antennae in the same direction along the arms (spaced the minimum distance *d*). These baselines should measure the same correlations and any difference between measurements is attributed to the separable phase and amplitude errors. As a starting assumption, the phase of the first element in the first arm is set to 0, and its amplitude is set to unity. The set of equations is solved for $f_{k,1}$ and $g_{k,1}$.

This method amplifies the amplitude errors, so UPC recommends in [AD.5] that it be used only for phase calibration, and only after having made Noise Injection Calibration for calibrating the path after the switch, so that only the path antenna to switch is covered by RSC.

3.1.8. NIR calibration

By NIR calibration, two sets of different sets of measurements are defined. While in NIR-A mode, the NIR measures the brightness temperatures and acts in parallel as a LICEF, forming mixed baselines. In NIR-R mode, the NIR is measuring the CAS noise level, and the gain, offset and receiver temperature of the NIR channels. Therefore, the description of NIR-R measurements is included in this chapter since it is a NIR calibration procedure.

On the other hand, the NIR-A and NIR-R modes themselves must be calibrated. The NIR requires two targets as calibration standards. The first one is an internal reference load at the inner instrument's temperature. The second target is the cold sky. Additionally, a third mode, NIR-AR mode, will be necessary to calibrate NIR-R mode.

The following description is based on the documents [RD 16] and [AD 6].

3.1.8.1. NIR-R mode measurements

3.1.8.1.1. Reference CAS noise temperature

The CAS noise temperature, used in the System Temperatures Computation (Sections 3.1.4.1and 3.1.5), can be computed through Eq. 39, reproduced here with the correct coefficients:

$$T'_{NS,v} = A_{R,v}\eta_v + B_{R,v}$$
$$T'_{NS,h} = A_{R,h}\eta_h + B_{R,h} \quad \textbf{Eq. 71}$$

With A_R defined as

$$A_{R,v} = \frac{T_{NR0,v} + u_{Rv}\left(T_{p1v} - T_{p1v,0}\right)}{L_{Rv}} \frac{L_{DCv}}{L_{DRv}}$$
$$A_{R,h} = \frac{T_{NR0,h} + u_{Rh}\left(T_{p1h} - T_{p1h,0}\right)}{L_{Rh}} \frac{L_{DCh}}{L_{DRh}} \quad \textbf{Eq. 72}$$

where all the coefficients have the same meaning as in Section 3.1.5.3 but are reference values (hence the subscript *R*), T_{NR0} is computed in External Calibration Mode and $T_{p1,0}$ is the value of T_{p1} during on-ground calibration (stored in NIR ADF file).

As for the coefficient B_R it is computed through

$$B_{R,v} = \frac{T_{p3,v}}{L_{Rv}}\frac{L_{DCv}}{L_{DRv}} + T_{t3v}$$
$$B_{R,h} = \frac{T_{p3,h}}{L_{Rh}}\frac{L_{DCh}}{L_{DRh}} + T_{t3h} \qquad \textit{Eq. 73}$$

with

$$T_{t3v} = \left(1 - \frac{1}{L_{Rv}}\right) T_{Cabv}\frac{L_{DCv}}{L_{DRv}} + \left(1 - \frac{L_{DCv}}{L_{DRv}}\right) T_{pUv}$$
$$T_{t3h} = \left(1 - \frac{1}{L_{Rh}}\right) T_{Cabh}\frac{L_{DCh}}{L_{DRh}} + \left(1 - \frac{L_{DCh}}{L_{DRh}}\right) T_{pUh} \qquad \textit{Eq. 74}$$

After applying Eq. 71, the CAS noise temperature is further corrected through the equivalent of Eq. 45:

$$T_{NS,v}^{LV-CIP} = T_{NS,v}^{'} + c_{Rv}\left(T_{NS,v}^{'} - T_{A\_ON0,v}^{CIP}\right) + d_{Rv}\left(T_{NS,v}^{'} - T_{A\_ON0,v}^{CIP}\right)^2$$
$$T_{NS,h}^{LH-CIP} = T_{NS,h}^{'} + c_{Rh}\left(T_{NS,h}^{'} - T_{A\_ON0,h}^{CIP}\right) + d_{Rh}\left(T_{NS,h}^{'} - T_{A\_ON0,h}^{CIP}\right)^2 \qquad \textit{Eq. 75}$$

with $T_{A\_ON0,v,h}^{CIP}$ measured in NIR-A mode during NIR calibration with an external target (see Section 3.1.9.1).

3.1.8.2. Reference receiver noise temperatures

The receiver noise temperatures at CIP planes are computed through the PMS measurements obtained when the instrument is in LICEF-LU mode inside the PMS calibration sequence, by using the following equation:

$$\left.\begin{aligned} T_{rec_k}^{LV-CIP} &= T_{sys_k}^{UC}\frac{\left|S_{LCk}\right|^2}{\left|S_{LVk}\right|^2\eta_{Vk}} - T_{phUk} \\ T_{rec_k}^{LH-CIP} &= T_{sys_k}^{UC}\frac{\left|S_{LCk}\right|^2}{\left|S_{LHk}\right|^2\eta_{Hk}} - T_{phUk} \end{aligned}\right\} \quad where \quad T_{sys_k}^{UC} = \frac{v_k^U - v_{off}}{G_k^{LV,H-CIP}} \qquad \textit{Eq. 76}$$

where v_k^U are the PMS voltages when the instrument is in uncorrelated noise injection mode, but taking care to use the voltage, offsets and gains from the appropriate NIR-LICEF unit, and the rest of the terms are identical to Eq. 26. NIR-LICEF PMS gains and offsets are computed in the following section.

The explanation for this receiver noise temperature estimation can be found in more detail in section 3.1.10.

3.1.8.3. NIR-LICEF Receiver gains and offsets

The NIR-LICEF receiver gain and offsets are also found though the 4-point method. Measurements from NIR modes LICEF-LC and LICEF–LC2 are used in the equivalent of Eq. 14:

$$G_{PMS_k}^{LV-CIP} = \frac{v_{2k} - v_{1k}}{T_{NS2}^{LV-CIP} - T_{NS1}^{LV-CIP}}$$

$$G_{PMS_k}^{LH-CIP} = \frac{v_{2k} - v_{1k}}{T_{NS2}^{LH-CIP} - T_{NS1}^{LH-CIP}} \qquad \textit{Eq. 77}$$

$$v_{off_k h,v} = \frac{v_{2k}v_{3k} - v_{1k}v_{4k}}{(v_{2k} - v_{4k}) - (v_{1k} - v_{3k})}$$

The voltage offsets are computed from noise injection from the ODD Noise Sources configuration.

3.1.9. NIR absolute calibration through external sources

In order to calibrate the remaining parameters of the NIR, the next measurement steps must be made

- Look at a cold scene in NIR-A mode
- Look at a cold scene in NIR-AR mode
- Look at a cold scene in NIR-LA mode

3.1.9.1. NIR-A Calibration

The parameters T'_{A0} and T_{NA0} are calibrated periodically in flight, by measuring a "known" scene. The values $T'_{A0,h}$ and $T'_{A0,v}$ represent the expected NIR measurement from that scene. It must be computed combining the Sky observed Brightness Temperature distribution with the NIR antenna patterns. The observed Sky distribution is computed using PVT and AOCS to obtain the instrument pointing direction, and the Galaxy Map layer with the averaged NIR values.

$$T'_{A0} = \int_{(\xi,\eta)\in UnitCircle} \frac{T^{Galaxy}(\xi,\eta)\left|F_{NIR}(\xi,\eta)\right|^2}{\sqrt{1-\xi^2-\eta^2}} d\xi d\eta \qquad \textit{Eq. 78}$$

The antenna noise injection temperature is computed as:

$$T_{NA0} = \left[L_{NC}L_A L_{DA}(T_U - T_{t2}) - \frac{T'_{A0}}{L_1 L_2} - T_{t1} \right] \frac{1}{\eta} \qquad \textit{Eq. 79}$$

where the attenuation coefficients and physical temperatures are defined as in Section 3.1.5.3.

Additionally, two parameters are computed, to be used in NIR-AR mode. First

$$T_{A0}''' = \frac{T_{A0}'}{L_1 L_2} + \left(1 - \frac{1}{L_1}\right)\frac{T_{p7}}{L_2} + \left(1 - \frac{1}{L_2}\right)T_{p6} \qquad \textit{Eq. 80}$$

This value is then used to compute

$$T_{A\_ON0}^{(6)} = \left(T_U - \frac{T_{A0}'''}{L_{NC}L_A L_{DA}} - T_{t2}\right)\frac{1}{\eta_A} + \frac{T_{A0}'''}{L_{NC}L_A L_{DA}} + T_{t2}$$

and also

$$T_{A\_ON0,v}^{CIP} = T_{A\_ON0,v}^{(6)} L_{DC,v} - \left(L_{DC,v} - 1\right)T_{pU,v} \qquad \textit{Eq. 81}$$

$$T_{A\_ON0,h}^{CIP} = T_{A\_ON0,h}^{(6)} L_{DC,h} - \left(L_{DC,h} - 1\right)T_{pU,h}$$

These last values are stored in the NIR calibration product in the NIR-A Data Set. All the parameters in the previous two Eqs. have the same meaning as in Section 3.1.5.3.1.

3.1.9.2. NIR-AR Calibration

The NIR-AR mode is used to calibrate the NIR-R mode, by computing the noise injection temperature in the reference branch T_{NR0}. This is done by applying

$$T_{NR0} = \frac{L_R L_{DR}}{\eta_{AR}}\left(T_{A\_ON0}^{(6)} - \frac{T_{p3}}{L_R L_{DR}} - T_{t3}\right) \qquad \textit{Eq. 82}$$

where T_{p3} is used instead of T_{ref} (the noise coming to the V,H-OPR planes), since there is no noise injection ([RD 16], Section 4.3). T_{t3} is defined as

$$T_{t3} = \left(1 - \frac{1}{L_R}\right)\frac{T_{Cab}}{L_{DR}} + \left(1 - \frac{1}{L_{DR}}\right)T_{pU} \qquad \textit{Eq. 83}$$

where all the coefficients have the same meaning as in Section 3.1.5.3 but are reference values (hence the subscript *R*).

3.1.9.3. Leakage and cross-coupling calibration

To account for cross-coupling between the different channels of the NIR and leakage from the noise injection channels to the remaining ones, the factors χ (cross-coupling) and ϑ (leakage) must be extracted and used to compute the correction functions f_{ii} and f_{qi} that calibrate the values of the third and fourth Stokes parameters (Section 3.1.5.3.1.2).

Several modes of the instrument are needed to collect all the data necessary for this computation. The denormalised correlations extracted in each mode are listed here:

- V_{LA} are measured in LICEF-LA mode when looking at the cold sky
- V_{NA} are measured in NIR-A mode when looking at the cold sky

- V_{UL} are measured from a uncorrelated load, in LICEF-LU mode (uncorrelated noise injection)

V_{NA} is denormalised as shown in Section 3.1.5.3.1.2. while V_{UL} and V_{LA} denormalized as the LICEFs visibilities.

Then, when the instrument is in LICEF-LA mode, looking at cold sky, this value is used, together with the antenna temperatures, $T'_{A,v}$ (Eq. 39), and V_{LA}, to compute

$$\chi|_{ii} = \frac{1}{T^c_{A,v} + T^c_{A,h}}\left(V_{LA}|_{ii} - V_{UL}|_{ii}\right)$$
$$\chi|_{qi} = \frac{1}{T^c_{A,v} + T^c_{A,h}}\left(V_{LA}|_{qi} - V_{UL}|_{qi}\right) \qquad \textit{Eq. 84}$$

where $T^c_{A,v}$ is computed from the antenna temperature and the temperature of the U-load by

$$T^c_{A,v} = T_{pUv} - T'_{A0,v}$$
$$T^c_{A,h} = T_{pUh} - T'_{A0,h} \qquad \textit{Eq. 85}$$

Using χ during measurement in NIR-A mode, assuming that the cross-coupling between channels is equal, the value V_{UT} (denormalised correlation induced by cross-coupling) is computed by

$$|V_{UT}| = \left(T^c_{A,v} + T^c_{A,h}\right)|\chi| \qquad \textit{Eq. 86}$$

where T^c_A is now computed from T_{pU} and $\hat{T}_A$. Since in NIR-A the antenna is measured only half of the time, we have

$$V^{blind}_{UT} = \frac{V_{UT}}{2} \qquad \textit{Eq. 87}$$

As for the leakage factor, ϑ, it is computed in NIR-A mode, when looking at the cold sky, by

$$\vartheta|_{ii} = \frac{1}{\left(T''_{NA0,v} + T''_{NA0,h}\right)\eta}\left(V_{NA}|_{ii} - V^{blind}_{UT}|_{ii} - V_{UL}|_{ii}\right) \qquad \textit{Eq. 88}$$

and

$$\vartheta|_{qi} = \frac{1}{\left(T''_{NA0,v} + T''_{NA0,h}\right)\eta}\left(V_{NA}|_{qi} - V^{blind}_{UT}|_{qi} - V_{UL}|_{qi}\right) \qquad \textit{Eq. 89}$$

where η is the NIR pulse length, both in NIR-A, when looking at cold sky. T''_{NA0} is the corrected noise injection temperature transferred to the VAP plane through Eq. 50, but using T_{NA0} as it is measured during cold sky calibration.

Using ϑ during measurement in NIR-A mode, the denormalisation factor due to noise leakage is computed by

$$\left|V_{UT}^{noise}\right| = \eta\left(T''_{NA,v} + T''_{NA,h}\right)\left|\vartheta\right| \qquad \textbf{Eq. 90}$$

Where, this time, T''_{NA} is the antenna noise injection temperature and η is the NIR pulse length, both in NIR-A while the instrument is in science measurements.

In conclusion, the correction functions f_{ii} and f_{qi} are computed during measurement by solving V_{UT}^{blind}, V_{UT}^{noise} and V_{UL} and then using

$$\begin{aligned} f_{ii} &= -2\,\mathrm{Re}\left\{V_{UT}^{blind} + V_{UT}^{noise} + V_{UL}\right\} \\ f_{qi} &= -2\,\mathrm{Im}\left\{V_{UT}^{blind} + V_{UT}^{noise} + V_{UL}\right\} \end{aligned} \qquad \textbf{Eq. 91}$$

3.1.10. Receiver Noise Temperature Monitoring

As of September 2006, a new step has been introduced in the PMS calibration sequences. In this step, the instrument is in Uncorrelated Noise Injection configuration, with the NIR-LICEF also in LICEF-LU configuration.

The purpose of this step is to measure the System Temperatures with the switch in U position, at the same time (and temperature) as the rest of PMS calibration is performed, and use it to derive the Receiver Noise Temperature. This way, the Receiver Noise Temperature can be characterised in the same way as the PMS gain and offset are, and be computed during nominal science observations. The objective is to have an independent source for the antenna temperature not related to the NIR measurements.

The basic principle behind this formulation is presented in [RD.28], and is repeated here below.

The System temperature at LIP plane when the switch is in U position is given by the following equation:

$$T_{sysk}^{UL} = \left(T_{phUk} + T_{rec}\right) \qquad \textbf{Eq. 92}$$

Where T_{rec} is receiver temperature at LIP plane and T_{phUk} is the physical temperature of the U-Load (LICEF isolator). However, since the PMS is calibrated at CIP plane, we must write system temperature at this plane:

$$T_{sysk}^{UC} = \frac{1}{\left|S_{LCk}\right|^2}\left(T_{phUk} + T_{rec}\right) \qquad \textbf{Eq. 93}$$

And now, taking into account that this system temperature can be retrieved by the PMS as per Eq. 65, the receiver temperature at LIP plane can be recovered from PMS measurement as

$$T_{rec} = \left|S_{LCk}\right|^2 T_{sysk}^{UC} - T_{phUk} \qquad \textbf{Eq. 94}$$

Note that PMS gain at CIP plane must be temperature corrected to have $G_k^C\left(T_{phUk}\right)$. This is directly achieved, as the U-load is incorporated to the short calibration sequences, where PMS gain is calibrated simultaneously. Now, the magnitude we want to retrieve is receiver temperature at VAP (HAP) plane, when the switch is in A=V,H position. This can be written as:

$$T_{Rk}^A = \frac{1}{\eta_{Ak}\left|S_{LAk}\right|^2}\left[T_{rec} + T_{phUk}\left(1-\eta_{Ak}\left|S_{LAk}\right|^2\right)\right] \qquad \textbf{Eq. 95}$$

If we insert the expression of T_{rec} in the equation above, it yields

$$T_{Rk}^A = \frac{\left|S_{LCk}\right|^2}{\eta_{Ak}\left|S_{LAk}\right|^2}T_{sysk}^{UC} - T_{phUk} \qquad \textbf{Eq. 96}$$

Note that we are retrieving receiver temperature at VAP/HAP plane at the temperature that the short calibration has been performed, $T_{Rk}^A\left(T_{phUk}\right)$, in spite of the fact that the switch has not been connected either to H or V.

During the orbit in calibration mode, long calibration, LICEF_k receiver temperature can be retrieved as a function of temperature. This must be performed at VAP/HAP plane. This allows to compute receiver temperature sensitivity to physical temperature by linear fit, in the same way as performed for PMS gain and offset (A=H,V), using a sensitivity value $S_{\Delta Tphk}^{T_{RA}}$ K/ºC

Now, the receiver noise temperature at any orbit position in measurement mode can be computed by finding the two nearest calibrated receiver temperatures, T_{Rcal1}^A and T_{Rcal2}^A, and applying

$$\begin{aligned} T_{R1}^A &= T_{Rcal1}^A + S_{Tphk}^{T_R}\left(T_{ph1k}\right) \\ T_{R2}^A &= T_{Rcal2}^A + S_{Tphk}^{T_R}\left(T_{ph2k}\right) \\ T_{Rk}^A &= T_{Rcal1}^A\frac{\left(\theta-\theta_{cal1}\right)}{\left(\theta_{cal2}-\theta_{cal1}\right)} + T_{Rcal2}^A\frac{\left(\theta-\theta_{cal2}\right)}{\left(\theta_{cal2}-\theta_{cal1}\right)} \end{aligned} \qquad \textbf{Eq. 97}$$

Where T_{ph1k} and T_{ph2k} are the temperatures at the orbit position in measurement mode and the θ are the arguments of latitude for each position. It must be pointed out that once receiver temperature is known at T_{ph2k}, this gives an estimate of the antenna temperature seen by the LICEF in measurement mode:

$$T_{Ak}\left(T_{ph2k}\right) = T_{sysk}^A\left(T_{ph2k}\right) - T_{Rk}^A\left(T_{ph2k}\right) \qquad \textbf{Eq. 98}$$

Where $T_{sysk}^A\left(T_{ph2k}\right)$ is the system temperature used to denormalize the correlations. Finally, a weighted average is applied taking into account the estimations from the two adjacent calibration point in the orbit.

3.1.11. PMS cold sky calibration

3.1.11.1. PMS characterisation

The CAS calibration procedure can be validated when the instrument is in deep sky measurement, by calibrating the PMS in the same way as the NIR is calibrated, and then comparing both calibration sets of parameters. A calibration sequence has been designed for this process and it will be recognised by the L1PP.

First, we define a method to calibrate the PMS gain in orbit, G_k^{AA}, by using the U-load as WARM noise, v_{U_k}, and the receiver output when looking ate cold sky, v_{SKY_k} as COLD noise:

$$G_k^{AA} = \frac{v_{U_k} - v_{SKY_k}}{T_{U_k} - T_{SKY_k}^A} \qquad \textit{Eq. 99}$$
$$A = H, V$$

where T_{U_k} are the physical temperatures of the receivers when in Uncorrelated noise injection and $T_{SKY_k}^A$ are retrieved from the cold sky map as in Section 3.1.9. The PMS offset and attenuator ratios can also be computed if the PMS 4-point voltages are redefined as

- v_{1_k} - PMS output voltage for deep sky mode with attenuator off (L_{0k})
- v_{2_k} - PMS output voltage for uncorrelated noise injection mode with attenuator off (L_{0k})
- v_{3_k} - PMS output voltage for deep sky mode with attenuator on (L_{1k})
- v_{4_k} - PMS output voltage for uncorrelated noise injection mode with attenuator on (L_{1k})

and by using

$$v_{offk} = \frac{v_{2_k} v_{3_k} - v_{1_k} v_{4_k}}{\left(v_{2_k} - v_{4_k}\right) - \left(v_{1_k} - v_{3_k}\right)} \qquad \textit{Eq. 100}$$
$$\Delta L_k = \frac{L_{1k}}{L_{0k}} = \frac{v_{2_k} - v_{1_k}}{v_{4_k} - v_{3_k}}$$

The PMS gains can be compared to the ones computed in Section 3.1.5.4, G_k^{CC}, by translating the deep-sky calibrated gains to the CIP plane

$$G_k^{AC} = G_k^{AA} \frac{\left|S_{LC_k}\right|^2}{\eta_{Ak}\left|S_{LA_k}\right|^2} \qquad A = H, V \qquad \textbf{Eq. 101}$$

where η_{Ak} are the antenna ohmic efficiencies and the switch S-Parameters are the ones defined in the previous sections. A measure of the relative error is computed as

$$e_G = \frac{G_k^{AC} - G_k^{CC}}{G_k^{AC}} 100 \qquad A = H, V \qquad \textbf{Eq. 102}$$

3.1.11.2. CAS and receiver temperature validation

The cold sky measurements can also be used to validate the CAS plane translation coefficients computed from ground data. The coefficients used for comparison are defined as

$$C_{Nk}^{gnd} = \frac{\left|S_{LA_k}\right|^2 \left|S_{N0}\right|^2}{\left|S_{LC_k}\right|^2 \left|S_{k0}\right|^2} \eta_{Ak} \qquad A = H, V \qquad \textbf{Eq. 103}$$

The equivalent coefficients can be computed from deep sky measurements when, during short calibration, the following values are collected:

- v_{1_k} - PMS voltages for WARM noise injection (even and odd)
- v_{2_k} - PMS voltages for HOT noise injection (even and odd)
- T_{NS1} - WARM temperature measured in NIR-R
- T_{NS2} - HOT temperature measured in NIR-R

After these values are stored, the coefficients must be computed for the hub, in the first place:

$$C_{Nk}^{hub} = \frac{T_{NS2} - T_{NS1}}{v_{2k}^{hub} - v_{1k}^{hub}} G_k^{AA} \qquad \textbf{Eq. 104}$$

where N are the 6 paths from the hub Noise Sources to the NIRs and there are 12 values for k. For the odd noise sources we have,

$$C_{Nk}^{odd} = \frac{T_{NS2} - T_{NS1}}{v_{2k}^{odd} - v_{1k}^{odd}} G_k^{AA} \qquad \textbf{Eq. 105}$$

where N are the 3 paths from the odd Noise Sources to the NIRs and there are 10 values for k.

The CAS differences plane translation coefficients are then compared by

$$eC_{Nk}^{hub} = 20\log_{10}\left[\frac{C_{Nk}^{hub}}{C_{Nk}^{gnd}}\right]dB$$
$$eC_{Nk}^{odd} = 20\log_{10}\left[\frac{C_{Nk}^{odd}}{C_{Nk}^{gnd}}\right]dB \qquad \textit{Eq. 106}$$

As for the case of the receivers that are driven by a Noise Source without a direct path to the NIRs, the coefficients must be computed using as reference the gain of the receiver closest to the hub in each group sharing the same Noise Source. The gain used as reference is the one computed through the 4-point method, G_r^{CC}. The equivalent to the previous equations in this case is

$$C_{rk}^{odd} = \frac{v_{2r}^{odd} - v_{1r}^{odd}}{v_{2k}^{odd} - v_{1k}^{odd}}\frac{G_k^{AA}}{G_r^{CC}}$$
$$C_{rk}^{even} = \frac{v_{2r}^{even} - v_{1r}^{even}}{v_{2k}^{even} - v_{1k}^{even}}\frac{G_k^{AA}}{G_r^{CC}} \qquad \textit{Eq. 107}$$

There will be 3 sets of coefficients C_{rk}^{odd} and 3 sets of C_{rk}^{even}, each with 11 values for k. The comparison between ground and sky coefficients is done as

$$eC_{rk}^{odd} = 20\log_{10}\left[\frac{C_{rk}^{odd}}{C_{rk}^{gnd}}\right]dB$$
$$eC_{rk}^{even} = 20\log_{10}\left[\frac{C_{rk}^{even}}{C_{rk}^{gnd}}\right]dB \qquad \textit{Eq. 108}$$

3.2. Level 1a to Level 1b

This processing level further refines the L1a data by removing influential sources from the calibrated visibilities, and it also performs what has been called the "Image Reconstruction". The first activity consists then in removing external sources (Sky, Sun, Moon, etc) from the calibrated visibilities, while the second one consists simply in reconstructing the Brightness Temperature distribution out of the calibrated visibilities. This latter reconstruction can be performed using two different algorithms, which are also described.

We shall first start with the theoretical definition of the problem, by studying the equation that rules the instrument's output, moving later on the procedures to be used for each Image Reconstruction Algorithm.

3.2.1. System Response Function

The instrument's System Response Function is determined by the following equation, as referenced in [RD.19], but accounting also for the real antenna positions, which may not be on the same plane and so the third cosine director coordinate (w) has to be included:

$$V_{kj}^{pq}(u,v) = \iint_{\xi^2+\eta^2\le 1} \frac{F_{n,k}^{p}(\xi,\eta)\,F_{n,j}^{q^*}(\xi,\eta)}{\sqrt{\Omega_k^p \Omega_j^q}} \frac{T_B^{pq}(\xi,\eta) - T_{rec}\delta^{pq}}{\sqrt{1-\xi^2-\eta^2}} \times \tilde{r}_{kj}\left(-\frac{u\xi+v\eta+w\sqrt{1-\xi^2-\eta^2}}{f_0}\right) e^{-j2\pi\left(u\xi+v\eta+w\sqrt{1-\xi^2-\eta^2}\right)} d\xi d\eta \qquad \textit{Eq. 109}$$

Where the following parameters are presented:

- $F_{n,k}^{p}(\xi,\eta)$ is the normalised antenna radiation pattern of receiver k in polarisation p, expressed in cosine domain coordinates (ξ,η)
- Ω_k^p is the antenna solid angle of receiver k in polarisation p
- T_{rec} is the averaged physical temperature of the receivers, multiplied by the Dirac delta δ^{pq} to represent that it is not applicable when the polarisation indexes p and q are not equal (i.e. cross-polarisation)
- $\tilde{r}_{kj}$ is the Fringe Washing Function term that accounts for decorrelation effects in the path of the correlated signals

This equation relates the calibrated visibilities measured by the instrument, with the Brightness Temperature scene that is being observed. Due to the nature of the double integral, and expressing the visibilities and Brightness Temperatures matrices as vectors, this relationship can be expressed as a matrix-vector multiplication, hereafter referred as G matrix.

$$V(u,v) = G(u,v;\xi,\eta)\,T(\xi,\eta) \qquad \textit{Eq. 110}$$

This G matrix is dependant on the antenna patterns, the fringe washing function, the (u,v) frequency samples of V (w is the out of plane coordinate) and the spatial samples (ξ,η) of BT. In order to obtain the Brightness Temperature distribution that generated a certain measured calibrated visibilities, it is only required to invert G by whatever method is more appropriate.

The first step is to specify the (u,v) frequency samples, and corresponding spatial samples (ξ,η) for the resolution selected, that match the instrument configuration. The (u,v) frequency samples and the off-plane component w are determined by the location of the receivers in the instrument, whereas the spatial samples are simply chosen based on the desired resolution. The preferred option is to work with a minimum resolution of 128x128 or 256x256 spatial samples. If a finer data sampling is desired, an interpolation may be performed after the reconstruction.

The visibilities measurements are taken at specific frequency samples. Being (x_1,y_1) and (x_2,y_2) the XY plane coordinates of two antennas generating the visibility sample V_{12}, the corresponding frequency sample can be computed as:

$$(u_{12}, v_{12}, w_{12}) = \left(\frac{x_2 - x_1}{\lambda_0}, \frac{y_2 - y_1}{\lambda_0}, \frac{z_2 - z_1}{\lambda_0} \right) \qquad \textit{Eq. 111}$$

Where λ_0 is the wavelength value at the central frequency of operation ($\lambda_0 = \frac{c}{f_0}$), for a typical value of f_0 of 1413.5MHz.

Computation of the spatial coordinates is done in a hexagonal grid but put in a rectangular matrix, according to the following formulation for an array steering of 30º. The corresponding frequency coordinates are also shown. Their outputs are 2 matrices with the coordinates of all points in the spatial and frequency domains according to the resolution specified. This ordering was presented in [RD.22]:

$$(u,v) = \left(\frac{d}{2}(k_1 + 2k_2), \frac{\sqrt{3}d}{2} k_1 \right)$$
$$(\xi,\eta) = \left(\frac{1}{N_T d} k_1, \frac{1}{\sqrt{3} N_T d}(k_1 + 2k_2) \right) \qquad \textit{Eq. 112}$$

Where N_T is the resolution required (typically 128), d is the distance between adjacent receivers in wavelengths (typically 0.875), and k_1 and k_2 are the indexes of the matrix from 0 to N_T-1. It must be noticed that the computation has to be performed according to the "hexagonal quadrant" where the indexes are, since the centre baseline is the first element of the matrix; this accounts to subtracting N_T from the indexes depending on the part of the hexagon being retrieved.

The most complete G matrix is built for the full polarisation processing case, as the dual polarisation G matrix is a subset of it. The input data in the case of full polarisation are three vectors of calibrated visibilities: V_H with 2346 complex elements plus 3 real elements from the NIR measurement, V_V with the same amount of values (2346 complex + 3 real) and V_{HV} with 3303 complex elements. The total number of input real valued elements is then (2346*2+3)*2+3303*2=15996.

In order to understand the origin of these numbers, it must be clear that in H or V polarisation, the amount of signals correlated is always 72, but of these only 69 are in either H or V polarisation. The remaining 3 are signals being correlated by the LICEF-NIR receivers in the opposite polarisation, so only 69*68/2 complex correlations are measured, which is the source for 2346. The NIR elements are also measuring the total power of the image, which is the source for the remaining 3 real elements. The case for HV polarisation is fully explained in [RD.10] and shall not be repeated here.

The required output are the Brightness Temperature values in all polarisations. T_H and T_V are real valued, whereas T_{HV} is complex valued. Assuming a default size of 128x128, the total number of output real valued elements is 128*128*4=65536. Of course, the size can be reduced to 64x64, although a bigger sampling grid means that more detail is introduced in the System Response Function by using a finer antenna pattern grid.

Thus, the unique G matrix is composed by 15996 rows and 65536 columns with real valued elements. Using a real valued matrix is preferred as it reduces the size and ensures that the output in Brightness Temperatures for H and V is real valued.

Rows in the G matrix are generated from particularising the general Eq. 109 for a pair of LICEF receivers (*k, j* indexes) and polarisation values of the antenna patterns and Brightness Temperature (*p, q* indexes).

The rows are ordered as follows:

- The first 2346*2+3 rows correspond to H polarisation calibrated visibilities (p and q are H)
- The next 2346*2+3 rows correspond to V polarisation calibrated visibilities (p and q are V)
- The final 3303*2 rows correspond to HV polarisation calibrated visibilities (p is H and q is V)

Going into more detail:

- The first 3 rows correspond to the zero baselines as measured from the NIR for H polarisation. The first row corresponds to the NIR_AB measurement, then NIR_BC and last NIR_CA
- The next 2346 rows correspond to the real values of the H polarisation calibrated visibilities as received from the L1a products, and ordered in the same approach as shown in figure 11 in chapter 4.3.1.3 of [RD.5]. i.e. first element is the calibrated visibility of LICEF_AB_03 against LICEF_AB_01_H, next is LICEF_AB_03 against LICEF_A_01, etc… until the sixty ninth element LICEF_AB_03 against LICEF_C_21. The next element is then LICEF_AB_01_H against LICEF_A_01, and so on until LICEF_AB_01 against LICEF_C_21. The next one is LICEF_A_01 against LICEF_A_02, etc. until LICEF_A_02 against LICEF_C_21. This ordering continues until all LICEF correlations have been inserted, and not including correlations with LICEF_NIR in V polarisation (i.e. correlations with receivers LICEF_AB_01_V, LICEF_BC_01_V and LICEF_CA_01_V)
- The next 2346 rows correspond to the imaginary values of the H polarisation calibrated visibilities, following the same order as above.
- The next 3 rows correspond to the zero baselines as measured from the NIR for V polarisation. The first row corresponds to the NIR_AB measurement, then NIR_BC and last NIR_CA
- The next 2346 rows correspond to the real values of the V polarisation calibrated visibilities as received from the L1a products, and ordered in the same approach as shown in figure 11 of [RD.5]. i.e. first element is the calibrated visibility of LICEF_AB_03 against LICEF_AB_01_V, next is LICEF_AB_03 against LICEF_A_01, etc… until the sixty ninth element LICEF_AB_03 against LICEF_C_21. The next element is then LICEF_AB_01_V against LICEF_A_01, and so on until LICEF_AB_01 against LICEF_C_21. The next one is LICEF_A_01 against LICEF_A_02, etc. until LICEF_A_02 against LICEF_C_21. This ordering continues until all LICEF correlations have been inserted, and not including correlations with LICEF_NIR in H polarisation (i.e. correlations with receivers LICEF_AB_01_H, LICEF_BC_01_H and LICEF_CA_01_H). Please refer to figure 11 of [RD.5] for a visual representation of the order followed.
- The next 2346 rows correspond to the imaginary values of the V polarisation calibrated visibilities, following the same order as above.
- The next 3303 rows correspond to the real values of the HV polarisation calibrated visibilities as received from the L1a products, and ordered in the following approach. Please refer to figures 10 and 11 of [RD.10] (orange cells) for a visual representation of the description:

- First 528 rows with calibrated visibilities of elements in Arm A in H polarisation against elements in Arm B in V polarisation. I.e. first LICEF_AB_03 against LICEF_BC_03, then LICEF_AB_03 against LICEF_BC_01_V, then LICEF_AB_03 against LICEF_B_01, until the 23rd element LICEF_AB_03 against LICEF_B_21. Next is LICEF_AB_01_H against LICEF_BC_03, then LICEF_AB_01_H against LICEF_B_01, and so on until all elements in arm B are correlated with LICEF_AB_01_H (Please note that this row does not include the correlation against LICEF_BC_01_V). This ordering continues until the last element correlated is LICEF_A_21 against LICEF_B_21.
- Next 528 rows with calibrated visibilities of elements in arm A in H polarisation against elements in arm C in V polarisation. Same order as above, i.e. first LICEF_AB_03 against LICEF_CA_03, then LICEF_AB_03 against LICEF_CA_01_V, then LICEF_AB_03 against LICEF_C_01, until the 23rd element LICEF_AB_03 against LICEF_C_21. Next is LICEF_AB_01_H against LICEF_CA_03, then LICEF_AB_01_H against LICEF_C_01, and so on until all elements in arm C are correlated with LICEF_AB_01_H (Please note that this row does not include the correlation against LICEF_CA_01_V). This ordering continues until the last element correlated is LICEF_A_21 against LICEF_C_21.
- Next 528 rows with calibrated visibilities of elements in arm B in H polarisation against elements in arm A in V polarisation. Same order as above, i.e. first LICEF_BC_03 against LICEF_AB_03, then LICEF_BC_03 against LICEF_AB_01_V, then LICEF_BC_03 against LICEF_A_01, until the 23rd element LICEF_BC_03 against LICEF_A_21. Next is LICEF_BC_01_H against LICEF_AB_03, then LICEF_BC_01_H against LICEF_A_01, and so on until all elements in arm A are correlated with LICEF_BC_01_H (Please note that this row does not include the correlation against LICEF_AB_01_V). This ordering continues until the last element correlated is LICEF_B_21 against LICEF_A_21.
- Next 528 rows with calibrated visibilities of elements in arm B in H polarisation against elements in arm C in V polarisation. Same order as above, i.e. first LICEF_BC_03 against LICEF_CA_03, then LICEF_BC_03 against LICEF_CA_01_V, then LICEF_BC_03 against LICEF_C_01, until the 23rd element LICEF_BC_03 against LICEF_C_21. Next is LICEF_BC_01_H against LICEF_CA_03, then LICEF_BC_01_H against LICEF_C_01, and so on until all elements in arm C are correlated with LICEF_BC_01_H (Please note that this row does not include the correlation against LICEF_CA_01_V). This ordering continues until the last element correlated is LICEF_B_21 against LICEF_C_21.
- Next 528 rows with calibrated visibilities of elements in arm C in H polarisation against elements in arm A in V polarisation. Same order as above, i.e. first LICEF_CA_03 against LICEF_AB_03, then LICEF_CA_03 against LICEF_AB_01_V, then LICEF_CA_03 against LICEF_A_01, until the 23rd element LICEF_CA_03 against LICEF_A_21. Next is LICEF_CA_01_H against LICEF_AB_03, then LICEF_CA_01_H against LICEF_A_01, and so on until all elements in arm A are correlated with LICEF_CA_01_H (Please note that this row does not include the correlation against LICEF_AB_01_V). This ordering continues until the last element correlated is LICEF_C_21 against LICEF_A_21.
- Next 528 rows with calibrated visibilities of elements in Arm C in H polarisation against elements in Arm B in V polarisation. Same order as above, i.e. first LICEF_CA_03 against LICEF_BC_03, then LICEF_CA_03 against LICEF_BC_01_V, then LICEF_CA_03 against LICEF_B_01, until the 23rd element LICEF_CA_03 against LICEF_B_21. Next is LICEF_CA_01_H against LICEF_BC_03, then LICEF_CA_01_H against LICEF_B_01, and so

on until all elements in arm B are correlated with LICEF_CA_01_H (Please note that this row does not include the correlation against LICEF_BC_01_V). This ordering continues until the last element correlated is LICEF_C_21 against LICEF_B_21.

- Next 23 rows with calibrated visibilities of LICEF_AB_01_H against all other receivers in arm A in V polarisation. I.e. LICEF_AB_01_H against LICEF_AB_03, LICEF_AB_01_H against LICEF_AB_01_V, LICEF_AB_01_H against LICEF_A_01, etc… until LICEF_AB_01_H against LICEF_A_21
- Next 22 rows with calibrated visibilities of all receivers in arm A in H polarisation against LICEF_AB_01_V, excluding LICEF_AB_01_H against LICEF_AB_01_V, whose equation is presented in the point above. I.e. LICEF_AB_03 against LICEF_AB_01_V, LICEF_A_01 against LICEF_AB_01_V, etc… until LICEF_A_21 against LICEF_AB_01_V
- Next 23 rows with calibrated visibilities of LICEF_BC_01_H against all other receivers in arm B in V polarisation. I.e. LICEF_BC_01_H against LICEF_BC_03, LICEF_BC_01_H against LICEF_BC_01_V, LICEF_BC_01_H against LICEF_B_01, etc… until LICEF_BC_01_H against LICEF_B_21
- Next 22 rows with calibrated visibilities of all receivers in arm B in H polarisation against LICEF_BC_01_V, excluding LICEF_BC_01_H against LICEF_BC_01_V, whose equation is presented in the point above. I.e. LICEF_BC_03 against LICEF_BC_01_V, LICEF_B_01 against LICEF_BC_01_V, etc… until LICEF_B_21 against LICEF_BC_01_V
- Next 23 rows with calibrated visibilities of LICEF_CA_01_H against all other receivers in arm C in V polarisation. I.e. LICEF_CA_01_H against LICEF_CA_03, LICEF_CA_01_H against LICEF_CA_01_V, LICEF_CA_01_H against LICEF_C_01, etc… until LICEF_CA_01_H against LICEF_C_21
- Next 22 rows with calibrated visibilities of all receivers in arm C in H polarisation against LICEF_CA_01_V, excluding LICEF_CA_01_H against LICEF_CA_01_V, whose equation is presented in the point above. I.e. LICEF_CA_03 against LICEF_CA_01_V, LICEF_C_01 against LICEF_CA_01_V, etc… until LICEF_C_21 against LICEF_CA_01_V

❑ The following and last 3303 rows correspond to the imaginary values of the HV polarisation calibrated visibilities as received from the L1a products, and ordered in the approach that has been just described.

Columns in the G matrix are generated from particularising the general Eq. 109 for a certain pair of coordinates in the antenna frame (ξ,η) indexes and polarisation values of the antenna patterns and Brightness Temperature (*p, q* indexes).

The order of the columns is the following:

❑ The first 128x128 columns correspond to H polarisation Brightness Temperatures

❑ The next 128x128 columns correspond to V polarisation Brightness Temperatures

❑ The next 128x128 columns correspond to the real components of the HV polarisation Brightness Temperatures

❑ The final 128x128 columns correspond to the imaginary components of the HV polarisation Brightness Temperatures

Going into more detail, each distribution of 128x128 elements corresponds to the SMOS natural hexagonal grid represented in a rectangular matrix. The centre (0,0) is the first element of the distribution.

The generation of (ξ,η) elements within the matrix is done according to Eq. 112, by moving the two indices k_1 and k_2 from 0 to 127 (or the final resolution desired). Some considerations have to be taken to account for the fact that we are dealing with a hexagonal domain, as depicted in [RD.22].

The following figures show the resulting (ξ,η) distribution of values for a 128x128 Brightness Temperature scene using steering 30º of MIRAS instrument.

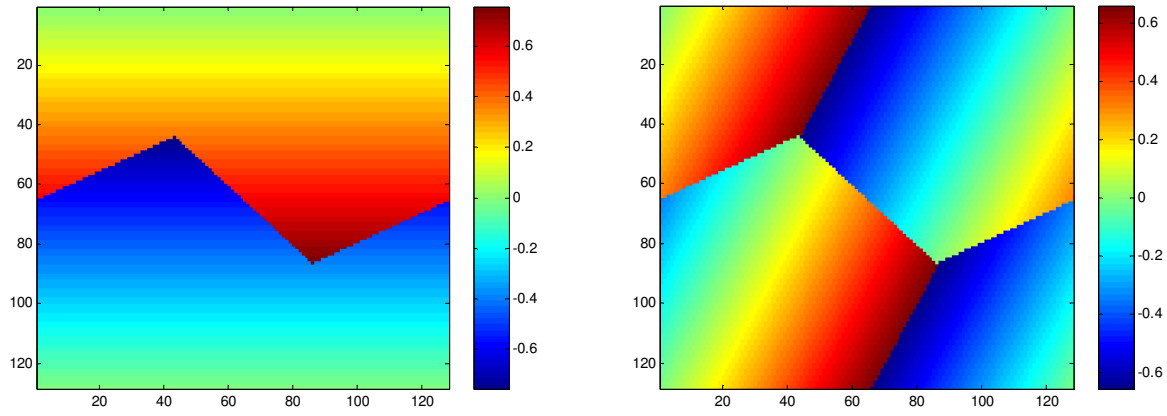

Figure 11: XI (left image) and ETA (right image) coordinates proposed for the G Matrix format

The distribution of 128x128 elements must be arranged in a vector form of 16384 elements, placing elements row after row.

Additionally, the complete size of G is dependant on the level of coupling that exists between polarisations. This coupling is due to the cross-polar antenna patterns of each receiver in each polarisation and finite input switch isolation (included in the antenna pattern measurements through TRF port). The complete G matrix can be expressed as in the following figure, taking all the previous data into account:

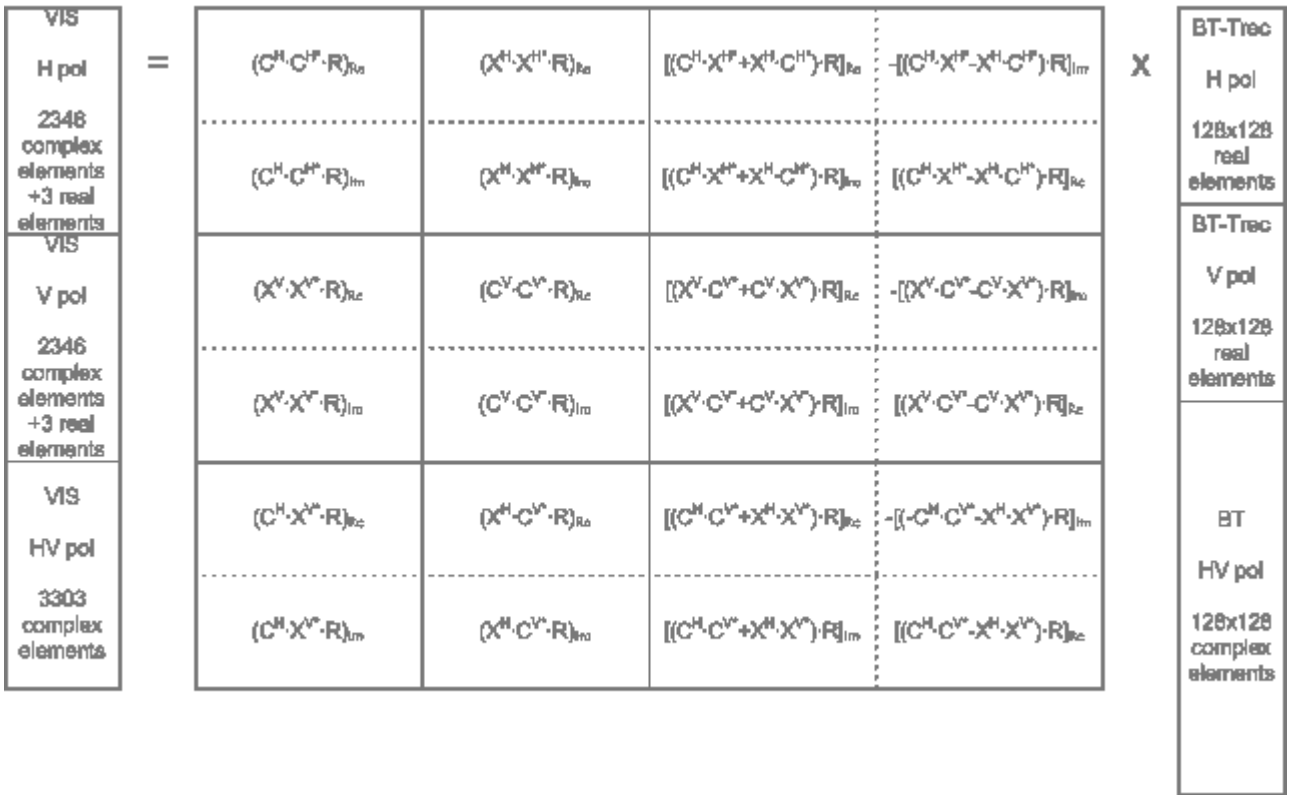

Figure 12: G matrix decomposition. C and X are co- and cross-polar Antenna Patterns and R is the Fringe Wash Function multiplied by the complex exponential term (see Appendix 5)

If the level of the cross-polarisation patterns is negligible when compared to the co-polar patterns (to be addressed in a foreseen study during Phase 4), then the above G matrix may be split into three independent G matrices, each one related to one polarisation only. The format of the H and V polarisation G matrix shall be the same, while the HV G matrix shall be a bit bigger as shown above (see Appendix 5).

The antenna patterns shall be measured on-ground for each receiver, and depending on the image reconstruction method, it shall be possible to calibrate/validate these patterns in-orbit.

The fringe washing function shall be also calibrated in orbit for several baselines (those sharing noise sources), and it shall be estimated for the rest of baselines through the procedure described in the previous chapters. Again, depending on the image reconstruction method, the FWF calibration shall be applied differently.

3.2.2. Foreign Sources Correction

This removal procedure for Foreign Sources has been developed and implemented by A. Camps et al in SEPS, and it is described in [RD.12] and [RD.13].

This procedure starts by subtracting the Earth and Sky contribution from the calibrated visibilities that have been produced as L1a output. Sun and Moon direct and reflected contributions are also removed after following some considerations. Effects from the antenna pattern backlobes and the receiver's physical temperature are also corrected.

This means that the reconstruction process does not work on the calibrated visibilities, but on a "delta" value where the Earth, Sky, Sun and Moon Brightness Temperatures have been removed:

$$\Delta V^{pq}(u,v) = V^{pq}(u,v) - V^{pq}_{Sky}(u,v) - V^{pq}_{Earth}(u,v) - V^{pq}_{Sun,dir/ref}(u,v) - V^{pq}_{Moon,dir/ref}(u,v) - V^{pq}_{Rec}(u,v) - V^{pq}_{Back}(u,v) \quad \textbf{Eq. 113}$$

The indexes p and q represent the polarisation for which the visibilities have been measured. These visibility values are obtained by performing the following integrals. In these equations, the off-plane component entering the Fringe Wash function and the exponential has been simplified to keep each equation in a single line (OF is the Obliquity Factor represented by $\sqrt{1-\xi^2-\eta^2}$:

$$\left(V^{pq}_{kj}\right)_{sky} = \iint_{\xi^2+\eta^2 \subset sky} \frac{T^{pq}_{sky}(\xi,\eta)}{\sqrt{1-\xi^2-\eta^2}} \frac{\hat{F}^{p}_{k}(\xi,\eta)\hat{F}^{q^*}_{j}(\xi,\eta)}{\sqrt{\Omega_k \Omega_j}} \hat{\hat{r}}_{kj}\left(-\frac{u_{kj}\xi + v_{kj}\eta + w_{kj}OF}{f_0}\right) e^{-j2\pi\left(u_{kj}\xi + v_{kj}\eta + w_{kj}OF\right)} d\xi d\eta \quad \textbf{Eq. 114}$$

$$\left(V^{pq}_{kj}\right)_{Earth} = \iint_{\xi^2+\eta^2 \subset Earth} \frac{T^{pq}_{Earth}}{\sqrt{1-\xi^2-\eta^2}} \frac{\hat{F}^{p}_{k}(\xi,\eta)\hat{F}^{q^*}_{j}(\xi,\eta)}{\sqrt{\Omega_k \Omega_j}} \hat{\hat{r}}_{kj}\left(-\frac{u_{kj}\xi + v_{kj}\eta + w_{kj}OF}{f_0}\right) e^{-j2\pi\left(u_{kj}\xi + v_{kj}\eta + w_{kj}OF\right)} d\xi d\eta \quad \textbf{Eq. 115}$$

$$\left(V^{pq}_{kj}\right)_{Sun,dir} = \iint_{\xi^2+\eta^2 \subset Sun,dir} \frac{T^{pq}_{Sun,dir}}{\sqrt{1-\xi^2-\eta^2}} \frac{\hat{F}^{p}_{k}(\xi,\eta)\hat{F}^{q^*}_{j}(\xi,\eta)}{\sqrt{\Omega_k \Omega_j}} \hat{\hat{r}}_{kj}\left(-\frac{u_{kj}\xi + v_{kj}\eta + w_{kj}OF}{f_0}\right) e^{-j2\pi\left(u_{kj}\xi + v_{kj}\eta + w_{kj}OF\right)} d\xi d\eta \quad \textbf{Eq. 116}$$

$$\left(V^{pq}_{kj}\right)_{Sun,ref} = \iint_{\xi^2+\eta^2 \subset Sun,ref} \frac{T^{pq}_{Sun,ref}}{\sqrt{1-\xi^2-\eta^2}} \frac{\hat{F}^{p}_{k}(\xi,\eta)\hat{F}^{q^*}_{j}(\xi,\eta)}{\sqrt{\Omega_k \Omega_j}} \hat{\hat{r}}_{kj}\left(-\frac{u_{kj}\xi + v_{kj}\eta + w_{kj}OF}{f_0}\right) e^{-j2\pi\left(u_{kj}\xi + v_{kj}\eta + w_{kj}OF\right)} d\xi d\eta \quad \textbf{Eq. 117}$$

$$\left(V^{pq}_{kj}\right)_{Moon,dir} = \iint_{\xi^2+\eta^2 \subset Moon,dir} \frac{T^{pq}_{Moon,dir}}{\sqrt{1-\xi^2-\eta^2}} \frac{\hat{F}^{p}_{k}(\xi,\eta)\hat{F}^{q^*}_{j}(\xi,\eta)}{\sqrt{\Omega_k \Omega_j}} \hat{\hat{r}}_{kj}\left(-\frac{u_{kj}\xi + v_{kj}\eta + w_{kj}OF}{f_0}\right) e^{-j2\pi\left(u_{kj}\xi + v_{kj}\eta + w_{kj}OF\right)} d\xi d\eta \quad \textbf{Eq. 118}$$

$$\left(V^{pq}_{kj}\right)_{Moon,ref} = \iint_{\xi^2+\eta^2 \subset Moon,ref} \frac{T^{pq}_{Moon,ref}}{\sqrt{1-\xi^2-\eta^2}} \frac{\hat{F}^{p}_{k}(\xi,\eta)\hat{F}^{q^*}_{j}(\xi,\eta)}{\sqrt{\Omega_k \Omega_j}} \hat{\hat{r}}_{kj}\left(-\frac{u_{kj}\xi + v_{kj}\eta + w_{kj}OF}{f_0}\right) e^{-j2\pi\left(u_{kj}\xi + v_{kj}\eta + w_{kj}OF\right)} d\xi d\eta \quad \textbf{Eq. 119}$$

$$\left(V^{pq}_{kj}\right)_{Back} = \iint_{\xi^2+\eta^2 \le 1} \frac{T^{pq}_{Back}}{\sqrt{1-\xi^2-\eta^2}} \frac{\hat{F}^{p}_{k_{Back}}(\xi,\eta)\hat{F}^{q^*}_{j_{Back}}(\xi,\eta)}{\sqrt{\Omega_k \Omega_j}} \hat{\hat{r}}_{kj}\left(-\frac{u_{kj}\xi + v_{kj}\eta + w_{kj}OF}{f_0}\right) e^{-j2\pi\left(u_{kj}\xi + v_{kj}\eta + w_{kj}OF\right)} d\xi d\eta \quad \textbf{Eq. 120}$$

$$\left(V^{pq}_{kj}\right)_{Rec} = \iint_{\xi^2+\eta^2 \le 1} \frac{-T_{rec}\delta^{pq}}{\sqrt{1-\xi^2-\eta^2}} \frac{\hat{F}^{p}_{k}(\xi,\eta)\hat{F}^{q^*}_{j}(\xi,\eta)}{\sqrt{\Omega_k \Omega_j}} \hat{\hat{r}}_{kj}\left(-\frac{u_{kj}\xi + v_{kj}\eta + w_{kj}OF}{f_0}\right) e^{-j2\pi\left(u_{kj}\xi + v_{kj}\eta + w_{kj}OF\right)} d\xi d\eta \quad \textbf{Eq. 121}$$

In these formulae, taken from [RD.12] and [RD.13], the temperature of the sky has to be retrieved from an auxiliary sky map and the spatial coordinates corresponding to Sky coordinates entering the FOV are

computed with the help of pointing CFI; the temperature of the background Earth is considered constant for each snapshot and computed such that the average Brightness Temperature of the resulting image is zero:

$$T_{Earth}^{pq} = \frac{T_A^{pq} - V_{Sky}^{pq}(0,0) - V_{Sun,dir}^{pq}(0,0) - V_{Sun,ref}^{pq}(0,0) - V_{Moon,dir}^{pq}(0,0) - V_{Moon,ref}^{pq}(0,0) - V_{Back}^{pq}(0,0)}{\bar{V}_{Earth}^{pq}(0,0)} \quad \textbf{Eq. 122}$$

The term T_A^{pq} is the antenna temperature at a given polarisation, which for horizontal and vertical polarisation can be computed from the instrument output (NIR) and for cross-polarisation contribution it is computed from the self-correlations between LICEF_NIR in H and V ports. The term $\bar{V}_{Earth}^{pq}(0,0)$ is the same one as in Eq. 115, but without the term for the Earth constant temperature.

The temperature and position of the Sun and Moon needs to be computed for both Direct and Reflected contributions.

For the Direct Sun contribution, it is treated as a point source, computing the position in the antenna frame using the pointing CFI together with the spacecraft position and attitude. The magnitude of the Sun Brightness Temperature at that position can be retrieved from the measured data itself by doing an FFT on the uncorrected calibrated visibilities and computing the brightness temperatures over that exact position. This FFT is performed assuming ideal FWF, one averaged antenna pattern and perfect positioning of the receivers. In case other methods to obtain the Sun BT are available (like models, external measurements, etc.) they can be used instead of the self-measurement, as the Sun position is known.

For the Reflected Sun contribution, Sun reflection over Oceans shall be modelled through several auxiliary parameters, namely the Sun BT, wind speed and direction, and Sea Surface Salinity and Sea Surface Temperature. As demonstrated in [RD.13], the effect of the Sun BT is dominant in the modelling of the reflected source, and using averaged values for the other variables does not introduce relevant errors. These averaged values are SSS=35psu, SST=15ºC, wind speed=5m/s, wind direction=0º (North). Usage of this model is considered as the baseline for computing the Reflected Sun contribution to be subtracted in visibilities.

For the Direct Moon contribution, it is treated as a point source. Similar to the Sun method, the brightness temperature is self-estimated over the position where the Moon is located (using CFI). The effect of the reflected Moon is negligible.

The equation to be solved is reduced then to the following expression, where the input now is the differential visibilities, and the expected output is the variation of Brightness Temperatures over a constant value:

$$\Delta V_{kj}^{pq} = \iint_{\xi^2+\eta^2 \le 1} \frac{\Delta T_B^{pq}(\xi,\eta)}{\sqrt{1-\xi^2-\eta^2}} \frac{\hat{F}_k^p(\xi,\eta)\hat{F}_j^{q^*}(\xi,\eta)}{\sqrt{\Omega_k \Omega_j}} \hat{\tilde{r}}_{kj}\left(-\frac{u_{kj}\xi + v_{kj}\eta + w_{kj}OF}{f_0}\right) e^{-j2\pi\left(u_{kj}\xi + v_{kj}\eta + w_{kj}OF\right)} d\xi d\eta \quad \textbf{Eq. 123}$$

Or in matrix form:

$$\begin{bmatrix} \Delta V_{kj}^{HH} \\ \Delta V_{kj}^{VV} \\ \Delta V_{kj}^{HV} \end{bmatrix} = \begin{bmatrix} G_{T_{HH}}^{HH} & G_{T_{VV}}^{HH} & G_{T_{HV}}^{HH} \\ G_{T_{HH}}^{VV} & G_{T_{VV}}^{VV} & G_{T_{HV}}^{VV} \\ G_{T_{HH}}^{HV} & G_{T_{VV}}^{HV} & G_{T_{HV}}^{HV} \end{bmatrix} \times \begin{bmatrix} \Delta T_B^{HH}(\xi,\eta) \\ \Delta T_B^{VV}(\xi,\eta) \\ \Delta T_B^{HV}(\xi,\eta) \end{bmatrix} \quad \textit{Eq. 124}$$

The final result of the brightness temperature is obtained from the output of this previous equation plus the constant background Earth temperature contribution that was subtracted earlier. Results are only meaningful in the extended alias free FOV delimited by the Earth replicas, now that the Sky replicas contributions have been eliminated.

$$T_B^{pq}(\xi,\eta) = \Delta T_B^{pq}(\xi,\eta) + T_{Earth}^{pq} \quad \textit{Eq. 125}$$

In full polarisation mode, it must be remarked that the physical temperatures of the receivers is not applicable to HV polarisation, so the corresponding correction term is zero. The Galaxy Map used as baseline contains measurements for HV polarisation, and these shall be used when correcting full pol visibilities. However, there are no sources for Sun or Moon temperatures in HV pol, so they shall be assumed to be zero. New information in this regard may come during commissioning, and never before that

As it can be seen from Eqs. 123-124, the formula can be also expressed as a matrix-vector multiplication, and the only requirement to remove foreign sources is to have the latest G matrix available, and be able to compute the Brightness Temperature distribution of the sources to be removed.

In the case of the Sky, the distribution is taken from the Galaxy map, and set to zero for those spatial coordinates that are not part of the sky area.

In the case of the Earth, the distribution is taken as constant based on Eq. 122, and set to zero for those spatial coordinates that are not part of the Earth area. The distribution may be taken using a model instead of a constant value, to take into account the incidence angle effect.

In the case of the Direct Sun and Moon, the distribution is taken as a point source, setting the computed value over the appropriate spatial coordinates, and zero for the rest.

In the case of the Reflected Sun, it has been mentioned before that it shall use a distribution computed using a reflection model with averaged auxiliary parameters.

The averaged physical temperature of the receivers is taken from the L1a HKTM measurements, and is set as constant in the entire xi-eta integration domain.

The Brightness Temperature distribution entering through the backlobes has an effect that is highly dependant on the level of the backlobes radiating patterns (which are very low). It is most probable that the only worthy contribution will come from the Sun when it is illuminating the back of the instrument. However, in order to take into account the backlobes contribution to the visibilities, the average backlobes antenna patterns are used.

The Flat Target Response measurement is described in the following section.

3.2.2.1. Flat Target Transformation

This process shall compute a transformation similar to the Eq. 113, with the exception that it will only encapsulate the contribution corresponding to the receivers' physical temperature, but at the same time it will make unnecessary the correction for the constant Earth term.

This transformation is first based on the measurement of a set of FTT auxiliary correlations, obtained while the instrument is pointing to the deep sky ($V_{FTT}^{pq}(u,v)$). During these measurements, the Brightness Temperature of the zone being observed shall also be stored (T_p), as well as the average of the physical temperature of the receivers (T'_r).

$$\breve{V}^{pq}(u,v) = V^{pq}(u,v) - \frac{T_B^{pq} - T_r}{T_p - T_r'} V_{FTT}^{pq}\left(u,v;T_p - T_r'\right) \qquad \textit{Eq. 126}$$

In this way, we can write now Eq. 113 as:

$$\Delta V^{pq}(u,v) = \breve{V}^{pq}(u,v) - V_{Sky}^{pq}(u,v) - V_{Sun,dir/ref}^{pq}(u,v) - V_{Moon,dir/ref}^{pq}(u,v) - V_{Back}^{pq}(u,v) \qquad \textit{Eq. 127}$$

~~After reconstruction, the Brightness Temperature Fourier components $\hat{T}(u,v)$ have to be corrected for the subtracted term in the following way:~~

$$\hat{T}_B'^{pq}(u,v) = \hat{T}_B^{pq}(u,v) + \frac{\overline{T}_B^{pq} - T_r}{T_p - T_r'} \hat{T}_{IDEALSky}^{pq}(u,v) + T_r \hat{T}_{IDEAL}^{pq}(u,v;1) \qquad \textit{Eq. 128}$$

~~Where:~~

- ~~$\hat{T}_{IDEALSky}^{pq}(u,v)$ are the Brightness Temperature Fourier components obtained from simulating the observed Sky scene in an ideal instrument. They are obtained by first computing the ideal Sky visibilities, using the G matrix in the complete unit circle and the expected Sky Brightness Temperature (retrieved from the Galaxy Map and the S/C orbital position and attitude). These visibilities are later multiplied by J^+ to retrieve the Brightness Temperature Fourier components.~~
- ~~$\hat{T}_{IDEAL}^{pq}(u,v;1)$ are the Brightness Temperature Fourier components obtained from simulating a uniform 1Kelvin scene in an ideal instrument. They are obtained by first computing the ideal Uniform visibilities, using the G matrix in the complete unit circle and a constant 1K Brightness Temperature in the whole unit circle. These visibilities are later multiplied by J^+ to retrieve the Brightness Temperature Fourier components.~~

3.2.3. Image Reconstruction

This processing step requires two separate functionalities. The first one is to compute the System Response Function, which shall be performed based on a calibration timeline, and the second one is to use that calibrated System Response Function to reconstruct the calibrated visibilities (already corrected for foreign sources). This last step is not reversible, as it shall not be possible to perform corrections once the Brightness Temperature Fourier Components are calculated in case the G matrix changes. It shall be necessary to start over from the calibrated visibilities to obtain new results with the new G matrix.

In the following sections, two algorithms for generating the System Response Function are described (On-ground characterised G Matrix and Parametric G Matrix), which have been selected as baselines. The DLR "Learning Approach", which was also investigated, is not described as it is not part of the baseline, although it has similarities to the Stabilised one.

Inputs to both algorithms are the same, requiring:

- Calibrated visibilities (L1a)
- G Matrix (ADF)

In fact, the only difference between these two methods is the approach in how to compute that G matrix, as the format of the G matrix is shared by both of them.

Once the G matrix is computed and/or calibrated, the inversion method is the same, passing by a mathematical reduction based on a band-limited approach.

3.2.3.1. On-ground characterised G Matrix

This G Matrix is built based solely on input data available, such as calibration data and auxiliary data files. This method has been already implemented in SEPS, and was developed by the *Universitat Politècnica de Catalunya*.

The input data required for the G Matrix are:

- LICEF antenna patterns (Auxiliary Data File)
- Fringe Washing Function shape (L1a Product Data)
- LICEF spatial coordinates (Auxiliary Data File)

Antenna patterns shall be measured once on the ground, and a static Auxiliary Data File shall be generated with the measurements. These measurements shall be done at three different frequencies: the central operation frequency and another two at plus and minus a B bandwidth. Their use in the G Matrix construction is done through a weighted average, as expressed in the next equation, extracted from [RD.20]:

$$\begin{aligned}\hat{F}_k^p(\xi,\eta)\hat{F}_j^{q^*}(\xi,\eta) = &\frac{1}{4}\hat{F}_k^p(\xi,\eta,f_0-\frac{B}{2})\hat{F}_j^{q^*}(\xi,\eta,f_0-\frac{B}{2}) \\ &+\frac{1}{2}\hat{F}_k^p(\xi,\eta,f_0)\hat{F}_j^{q^*}(\xi,\eta,f_0) \\ &+\frac{1}{4}\hat{F}_k^p(\xi,\eta,f_0+\frac{B}{2})\hat{F}_j^{q^*}(\xi,\eta,f_0+\frac{B}{2})\end{aligned} \qquad \textit{Eq. 128}$$

The Fringe Washing Function shape is calibrated/estimated as part of the nominal calibration campaign, by injecting correlated noise and introducing time lags in the correlated signals. An L1a product file is generated every time this type of calibration is performed. This process is described in section 3.1.4.2, and its output is used to compute a set of coefficients for approximating the FWF shape amplitude by a sinc function, and the FWF shape phase by a quadratic function.

$$\hat{\hat{r}}_{kj}(\tau) \approx A \cdot \mathrm{sinc}\left(B \cdot (\tau - C)\right) \cdot e^{i\left(D\tau^2 + E\tau + F\right)} \qquad \textit{Eq. 129}$$

The way to compute the different coefficients is shown in [AD.6]. It consists on using the measurements at time lags $-T_S$, 0 and $+T_S$ from Eq. 19 for estimating the parameters A to F. The equations to be used are:

$$\begin{aligned} \left|g_{kj}(-T_S)\right| &\approx A\cdot\mathrm{sinc}\left(B\cdot(-T_S-C)\right) \\ \left|g_{kj}(0)\right| &\approx A\cdot\mathrm{sinc}\left(B\cdot C\right) \\ \left|g_{kj}(+T_S)\right| &\approx A\cdot\mathrm{sinc}\left(B\cdot(T_S-C)\right) \end{aligned} \qquad \textit{Eq. 130}\sout{131}$$

$$\begin{aligned} D^{H,V} &= \left(\frac{\arg\left(g_{kj}^{H,V}(+T_S)\right)+\arg\left(g_{kj}^{H,V}(-T_S)\right)}{2}-\arg\left(g_{kj}^{H,V}(0)\right)\right)\frac{1}{T_S^2} \\ E^{H,V} &= \frac{\arg\left(g_{kj}^{H,V}(+T_S)\right)-\arg\left(g_{kj}^{H,V}(-T_S)\right)}{2}\frac{1}{T_S} \\ F^{H,V} &= \arg\left(g_{kj}^{H,V}(0)\right) \end{aligned} \qquad \textit{Eq. 131}\sout{132}$$

The FWF is measured independently for H and V polarisation and also for the paths of the in-phase and quadrature signals, meaning that for the same visibility, there are two different values of the FWF. One is applicable to the real part component of the visibility, while the other is applicable to the imaginary part of the component. The following equation shows this behaviour in detail:

$$\begin{matrix}\mathrm{Re}\\ \mathrm{Im}\end{matrix}\left\{V_{kj}^{pq}\right\}=\begin{matrix}\mathrm{Re}\\ \mathrm{Im}\end{matrix}\left\{\iint_{\xi^2+\eta^2\le 1}\frac{T_B^{pq}(\xi,\eta)-T_{rec}\delta^{pq}}{\sqrt{1-\xi^2-\eta^2}}\frac{\hat{F}_k^{p}(\xi,\eta)\hat{F}_j^{q^*}(\xi,\eta)}{\sqrt{\Omega_k\Omega_j}}\left\{\begin{matrix}\hat{\tilde{r}}_{i_k i_j}\left(-\frac{u_{kj}\xi+v_{kj}\eta+w_{kj}OF}{f_0}\right)\\ \hat{\tilde{r}}_{q_k i_j}\left(-\frac{u_{kj}\xi+v_{kj}\eta+w_{kj}OF}{f_0}\right)\end{matrix}\right\}e^{-j2\pi\left(u_{kj}\xi+v_{kj}\eta+w_{kj}OF\right)}d\xi d\eta\right\} \qquad \textit{Eq 132}$$

The LICEF coordinates, which are used to compute the applicable (u,v) baselines as per Eq. 109 can be taken from their initial measured positions in an Auxiliary Data File, or an elastic model may be applied to obtain them as a function of time. Regardless of the approach, UPC has already modelled deviations or errors in the receivers' positions as an error in the retrieved Brightness Temperatures.

3.2.3.2. Parametric G Matrix

The Parametric G Matrix Reconstruction algorithm is based on computing a G matrix based on independent element modelling. Each of the elements used in the G Matrix computation is expressed as a best-fitting formulation based on a set of parameters, and these parameters are later calibrated/validated by observing known Brightness Temperature scenes. This algorithm has been developed by E. Anterrieu from the *Laboratoire d'Astrophysique de l'Observatoire Midi-Pyrénées* [RD.11].

The input data thus required for the G Matrix are:

- LICEF antenna patterns radiative model
- LICEF Filters model (combined in pairs they yield the Fringe Washing Function shape for that baseline)
- MIRAS thermo-elastic model

The models are described in the next paragraphs.

The LICEF patterns are approximated with Spherical Harmonics, using as the first baseline the measurements to be performed by TUD to obtain the initial coefficients. During commissioning and operations, calibration procedures will turn up new values for such coefficients.

Spherical Harmonics are expressions that satisfy the spherical harmonic differential equation, which is given by the angular part of Laplace's equation in spherical coordinates. The spherical harmonic $Y_{lm}(\theta,\phi)$ of degree l and order m, with $-l \leq m \leq l$, is a complex-valued function of the spherical coordinates $\theta \in [0,\pi]$ and $\phi \in [0,2\pi]$. It is related to the associated Legendre's polynomial $P_{lm}(x)$, with $x \in [-1,+1]$, by the relation:

$$Y_{lm}(\theta,\phi) = \sqrt{\frac{2l+1}{4\pi}\frac{(l-m)!}{(l+m)!}} P_{lm}(\cos\theta) e^{im\phi} \qquad \text{Eq. 133~~134~~}$$

Spherical Harmonics provide an orthonormal base for representation that can be used to approximate the LICEF pattern diagram once it has been measured over a discrete grid.

The method for approximation is to express the antenna pattern as a series of Spherical Harmonics:

$$\hat{F}_k^p(\xi,\eta) = \hat{F}_k^p(\theta,\phi) = \sum_{l=0}^{\infty}\sum_{m=-l}^{l} C_{lm} Y_{lm}(\theta,\phi) \qquad \text{Eq. 134~~135~~}$$

With C_{lm} being specific coefficients that are computed doing the scalar product of each Spherical Harmonic base with the discrete LICEF pattern $C_{lm} = \left\langle \hat{F}_k^p(\theta,\phi) \middle| Y_{lm}(\theta,\phi) \right\rangle$

In practice the summation over l cannot be done to infinite, and it must be truncated, typically to a few elements. This means that the C_{lm} coefficients must be optimised to minimise the quadratic error in the approximation, and the retrieval process turns out to be iterative, using the scalar product described above as a first approximation.

This process needs to be performed only once, when all the LICEF antenna patterns are measured on-ground empirically, in order to initialise the model parameters. In-flight there shall not be any more measurements of the antenna patterns, so it is required to validate/calibrate the coefficients using known scenes. This calibration process is still TBD.

The LICEF filters model has been descoped from the parametric G generation, and the L1a calibrated FWF shape shall be used instead.

3.2.3.3. Mathematical inversion (Stabilised approach)

The mathematical inversion of G is a common approach for both algorithms. It is based on a band-limited regularisation, which is equivalent to:

$$\begin{cases} \min_{T\in\square} \|V - GT\|^2 \\ (I - P_H)T = 0 \end{cases} \qquad \text{Eq. 135~~136~~}$$

Where P_H plays the role of a regularisation parameter. This method was proposed by E. Anterrieu in [RD.11] and is applicable to any algorithm based on G Matrix, not only to the Parametric one.

It consists in a reduction of the domain applicability, by creating the J Matrix. The G Matrix operates between Calibrated Visibilities and Brightness Temperatures, whereas the J Matrix operates between Calibrated Visibilities and Brightness Temperature Fourier Components $\hat{T}$.

After being computed, the J Matrix is mathematically inverted using the pseudo-inverse approach (J^+) as described in [RD.25], so that the Brightness Temperature Fourier Components may be obtained after a simple matrix-vector multiplication $\hat{T}$ = (J^+*V)

3.2.3.3.1. J Matrix generation

This method requires to compute the matrix J, whose size is much smaller than G, as it merely relates the calibrated visibilities to the brightness temperatures Fourier components $\hat{T}$. The number of these Fourier components is equal to the number of non-redundant baselines N_f, 1396 for H and V polarisation and 2791 for HV polarisation.

The matrix J is computed by using G to create the expected calibrated visibilities for some specific Brightness Temperatures. These specific Brightness Temperatures are computed by setting to unity each of the non-redundant baselines in the star domain and perform a normal 2D IFFT on the resulting distribution. Each computed set of Brightness Temperatures for each of the non-redundant baselines results in a complete column of the J matrix.

The method can be modelled in the following way:

- Enter a for loop for each of the non-redundant baselines, which correspond to a particular (***U,V***) position (the order to be taken is described in [RD.6])
- Using Eq. 110 an N_TxN_T complex matrix is created for the u,v baselines with zero in all positions except for the (***U,V***) position where the complex number (1+i) is set.
- In H or V polarisation, the complex number (1–i) is also set in the (***-U,-V***) position, and only half of the non-redundant baselines are used (1396)
- In HV polarisation no other value is changed from zero, and all the non-redundant baselines are used (2791)
- A 2D Inverse Fast Fourier Transform is performed on the resulting N_TxN_T complex matrix, which will generate a new N_TxN_T complex matrix. In H or V polarisation, as the input matrix is Hermitian, the output matrix is real valued.
- This new N_TxN_T complex matrix is ordered in vector format, zero-padded to form a 4xN_TxN_T real valued vector and multiplied by G as shown in Figure 12. Notice that depending on the polarisation being used, the zero-padding of the vector in the figure may vary (e.g. if the vector corresponds to H polarisation, the V and HV polarisation components must be filled with zeroes).

- The resulting vector of the matrix vector multiplication is a complete column of the J matrix applicable to the (***U,V***) baseline.
- Continue the loop until all columns of J have been computed

The J matrix contains the same number of rows and ordering than that of the G matrix, which has already been explained in chapter 3.2.1.

However, the number of columns is now dependant on the u,v frequency domain, and is restricted to the number of non-redundant correlations that the instrument shall be measuring. For MIRAS, the number of non-redundant visibilities is 2791, forming a star shape in the u,v plane, and is only dependant on the number of receivers per arm and the Y shape of the instrument.

Thus, the number of columns for this matrix is 11164. This number comes from 1395 complex elements plus one real element that is measured for H or V polarisation, plus 2791 complex elements measured for HV polarisation. Again, the total size of the matrix is dependant on the level of coupling between polarisations through the cross-polarisation antenna patterns. If they can be considered negligible, the J matrix can be split into three separate and independent matrices, one for each polarisation.

For the column elements ordering, it follows the ordering indicated below:

- The first column corresponds to the real component of the zero baseline for the H polarisation Brightness Temperature Fourier Components
- The next 1395 columns correspond to the real components of the H polarisation Brightness Temperature Fourier Components
- The next 1395 columns correspond to the imaginary components of the H polarisation Brightness Temperature Fourier Components
- The next column corresponds to the real component of the zero baseline for the V polarisation Brightness Temperature Fourier Components
- The next 1395 columns correspond to the real components of the V polarisation Brightness Temperature Fourier Components
- The next 1395 columns correspond to the imaginary components of the V polarisation Brightness Temperature Fourier Components
- The next 2791 columns correspond to the real components of the HV polarisation Brightness Temperature Fourier Components, with the zero baseline as the first column
- The next 2791 columns correspond to the imaginary components of the HV polarisation Brightness Temperature Fourier Components, with the zero baseline as the first column

The distribution of elements within each sub-group of 1395 columns follows the order described next. This ordering is based on reporting only the baselines with positive v coordinate and u positive for v=0:

- The v coordinate for the upper half of the baselines goes continuously from 0 to sqrt(3)*NEL*d, where NEL=21 and d=0.875, in incremental steps of sqrt(3)*d/2
- The u coordinate of the upper half of the baselines follows the mathematical rules defined as:
  - If v=0, then u goes from d to 24*d in incremental steps of d
  - If v>0 and v<=sqrt(3)*NEL*d/2, then u goes from –(NEL*d +v/sqrt(3)) to +(NEL*d +v/sqrt(3)) in incremental steps of d

- If *v*=sqrt(3)*(NEL+1)*d/2, then *u* goes from –11*d to +11*d in incremental steps of d
- If *v*=sqrt(3)*(NEL+2)*d/2, then *u* has the values –23*d/2, –19*d/2 to +19*d/2 in incremental steps of d and +23*d/2. Notice that the elements ±21*d/2 are not present.
- If *v*=sqrt(3)*(NEL+3)*d/2, then *u* has the values –12*d, –9*d to +9*d in incremental steps of d and +12*d. Notice that the elements ±11*d and ±10*d are not present.
- Finally, if *v*>sqrt(3)*(NEL+3)*d/2 and *v*<=sqrt(3)*NEL*d, then *u* goes from –(NEL*d – *v*/sqrt(3)) to +(NEL*d –*v*/sqrt(3)) in incremental steps of d

The order followed is shown in the next picture. For the 1395 element vector, the baselines are taken first from left to right, then from bottom to top, starting from the centre of the star (0,0). I.e. the first 24 elements are the ones with v=0 and ordered by increasing u; the next 42 elements are the ones with v=sqrt(3)*d/2 and ordered by increasing u (from negative to positive), and so on until the 1395 elements are covered.

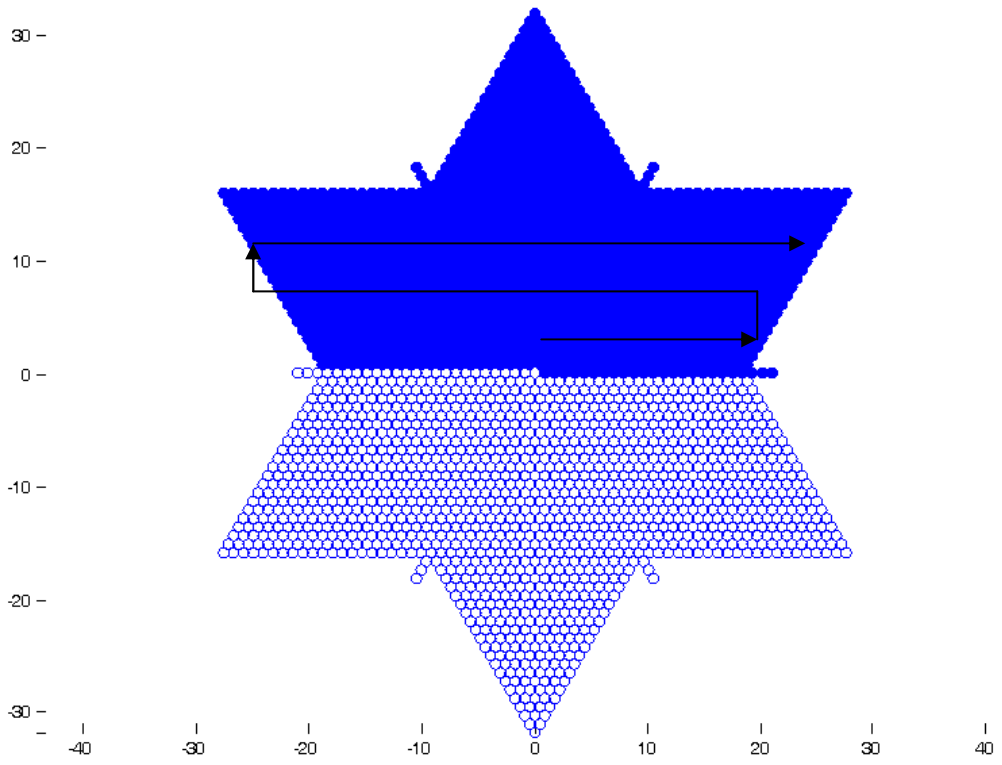

Figure 13: J matrix baselines ordering

For the case of HV polarisation, where the vector is 2791 elements long, the complete star must be covered. In this case, the ordering is similar to the one adopted above. The first element is the zero baseline (u=0, v=0); the next 1395 elements are ordered like it has been described (left to right, then bottom to top); and the remaining 1395 element are ordered in the same way as well, but inverting the sign of the resulting u and v coordinates (i.e. it changes to ordering from right to left, then top to bottom).

It is important to define a common format so that the L1b output is coherent and can be interpreted.

3.2.3.3.2. J Matrix inversion

As the J matrix relates the Brightness Temperature Fourier Components with the Calibrated Visibilities, once it has been generated, the J matrix needs to be inverted in order to obtain $\hat{T}(u,v)$. The inversion is achieved by using the pseudo-inverse:

$$J \cdot \hat{T} = V$$
$$J^* J \cdot \hat{T} = J^* V$$
$$\hat{T} = \left(J^* J\right)^{-1} J^* V \qquad \text{Eq. 136}$$
$$J^+ = \left(J^* J\right)^{-1} J^*$$

3.2.3.3.3. J Matrix application

The result of multiplying J^+ by the calibrated visibilities V is the brightness temperatures Fourier Components $\hat{T}(u,v)$, expressed in the frequency star domain.

The calibrated visibilities must be ordered in a very precise way, in order to match the way in which the J and G matrix were generated. This ordering is described in chapter 3.2.1, as it is equivalent to the rows ordering of the System Response Function. Visibilities for H and V polarisation in two consecutive integration times must be used in dual polarisation mode, while visibilities for H, V and HV polarisation in two consecutive integration times must be used in full polarisation mode. For a comprehensive analysis on the HV visibilities ordering and location, please refer to [RD.10]

In fact, in order to give the user more configuration flexibility to take into account e.g. possible hardware failures, the temperature frequencies are instead obtained by multiplying J^+ by WV ($\hat{T} = J^+ WV$), where W is a diagonal matrix whose entries consist of user configurable weights for each baseline. These baseline weights (whose default value is 1) are obtained from the `SM_xxxx_AUX_BWGHT_<ID>` Auxiliary Data File

3.3. Level 1b to Level 1c

The last steps of the processing consist first on a computation of the Ionospheric data applicable to each snapshot. Afterwards, the Brightness Temperature values are computed, grouping all snapshots into a single swath product. The purpose is to provide for each footprint, an array of Brightness Temperature expressed at Top of Atmosphere values along with their observation angles.

Based on the Spacecraft orbital position and also in the instrument's attitude, it is possible to compute the antenna-frame-to-pixel incidence (θ) and azimuth (ϕ) angles for any pixel on the ground. This computation is shown in the next chapter's equations, although for implementation purposes it shall be better performed with the help of the Earth Explorer CFI functions.

3.3.1. Ionospheric Correction

Ionospheric correction requires the computation of the Faraday rotation angle based on the Total Electron Content (TEC) and the geomagnetic angles at boresight. Later on, the values can be particularised at each pixel by simply using the incidence (θ_g) and azimuth (ϕ_g) angles from the spacecraft to the pixel (shown in Fig. 14).

The geomagnetic angles can be computed using the IGRF 10 model, valid until 2010 and available as an Auxiliary Data File, and the IGRF FORTRAN code available from NSSDC. The required inputs at any time are the S/C geodetic longitude and latitude, the time in decimal years and the altitude. The expected outputs are the magnetic field strength in Tesla (F), as well as the magnetic inclination (I) and declination (D) in degrees.

The TEC can be obtained from several sources, the first one is the IRI2001 model available as well from NSSDC in FORTRAN code, the second one is the IGS combined TEC map produced by UPC and available daily as Auxiliary Data File at ftp://gage152.upc.es/rapid_iono_igs.

The IRI2001 model is based on the 11-year Sun solar cycle, and requires as input the geodetic longitude and latitude, the time and the altitude, as well as several configuration parameters. The altitude to be used in this model shall be 450km, to match the altitude at which the TEC is computed.

The IGS combined TEC map is an ASCII file with TEC values over a Mercator grid at an altitude of 450km and measured every 2 hours. The frequency with which this file is released is every 24 hours. The expected output in both methods is the TEC value for the given spatiotemporal coordinates expressed in TEC Units ($10^{+016}e^{-}/m^2$).

Computation of Faraday rotation (ω), expressed in degrees, for each pixel can be computed using Eqs. 3 and 4b of [RD.8] with the retrieved pixel observation angles (θ_g, ϕ_g), TEC and geomagnetic data (F, I, D).

$$\omega = -6950 \times F \times TEC \times \left[\sin I + \cos I \times \tan \theta_g \times \cos\left(\phi_g - D\right) \right] \qquad \text{Eq. 137}$$

3.3.1.1. Geometrical rotation

The geometrical rotation between the polarisation axes in the antenna frame and the pixel frame can be also computed in this module, by following the next two procedures.

3.3.1.1.1. Waldteufel and Caudal Implementation

The following diagram shows the intended angles for a projection of point P into the antenna frame (SXYZ)

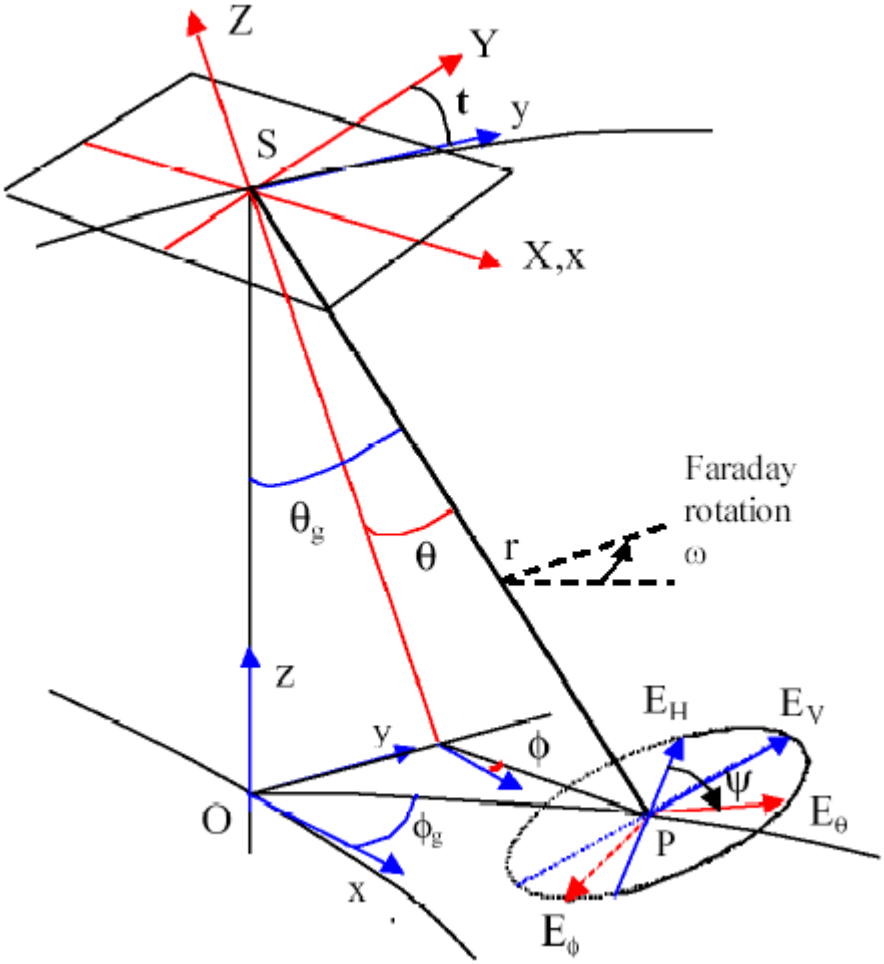

Figure 14: Geolocation and projection angles [RD.14]

Where t is the tilt angle of the instrument (32.5º), X and Y are the polarisation axes in the antenna frame, and E_H and E_V are the polarisation axes in the pixel frame. E_H is orthogonal to the PS and PO directions, and E_V is orthogonal to E_H and PS.

The angles may be computed using the following expressions, as defined in [RD.14]:

$$\theta = \arccos\left[\sin t \sin\theta_g + \cos t \cos\theta_g\right] \qquad \text{Eq. 138~~139~~}$$

$$\phi = \arcsin\left[\frac{-\sin t \cos\theta_g + \cos t \sin\theta_g \sin\phi_g}{\sin\theta}\right] \qquad \text{Eq. 139~~140~~}$$

$$\varphi = \pi - \arcsin\left[\frac{\cos t \sin\theta_g - \sin t \cos\theta_g \sin\phi_g}{\sin\theta}\right] \qquad \text{Eq. 140~~141~~}$$

Where ϕ is measured from the X axis and positive clockwise in the XYZ reference frame, and φ is the in plane geometrical rotation between polarisation frames. The above expressions are valid for the range $\phi_g \in \left[-\frac{\pi}{2}, \frac{\pi}{2}\right]$, for the range $\phi_g \in \left[\frac{\pi}{2}, \frac{3\pi}{2}\right]$, the angles must be simply computed as:

$$\phi = -\pi - \arcsin\left[\frac{-\sin t \cos\theta_g + \cos t \sin\theta_g \sin\phi_g}{\sin\theta}\right] \qquad \text{Eq. 141142}$$

$$\varphi = \arcsin\left[\frac{\cos t \sin\theta_g - \sin t \cos\theta_g \sin\phi_g}{\sin\theta}\right] \qquad \text{Eq. 142143}$$

The final geometrical rotation value from pixel frame to antenna frame is given by $\alpha = \phi - \varphi$

The antenna frame observation angles can also be obtained using the Cartesian coordinates of the S/C and the Cartesian coordinates of the pixel, plus the instrument attitude rotation matrix (and additionally miss-pointing like Best Fit Plane deviation). Using this last method, the pixel coordinates do not need to be restricted to the Reference Ellipsoid, but they can be expanded with the local altitude value using a Data Elevation Model. This process of orthorectification would be done with the help of the EE CFI functions.

This method is no longer used in L1PP v2.0, but its description is kept for historical reasons.

3.3.1.1.2. Duesmann and Zundo Implementation

In [RD.29] an alternative method to compute the geometric rotation angle is proposed. It consists on calculating the emission basis vectors in the Earth's surface and the Ludwig-3 polarization basis vectors on the instrument frame and from them extract the geometrical rotation angle, α. This method is the algorithm baseline for L1PP v2.0 onwards.

The emission basis vectors in the topocentric frame of the pixel are calculated from the observation angles as

$$\begin{aligned} \widehat{Ehe}_{x_{topocentric}} &= -\cos\phi_e \\ \widehat{Ehe}_{y_{topocentric}} &= \sin\phi_e \\ \widehat{Ehe}_{z_{topocentric}} &= 0 \end{aligned} \qquad \text{Eq. 143}$$

$$\begin{aligned} \widehat{Eve}_{x_{topocentric}} &= -\cos\theta_e \sin\phi_e \\ \widehat{Eve}_{y_{topocentric}} &= -\cos\theta_e \cos\phi_e \\ \widehat{Eve}_{z_{topocentric}} &= \sin\theta_e \end{aligned} \qquad \text{Eq. 144}$$

To calculate the Ludwig-3 basis vectors on the satellite one must start by defining the target vector from the satellite to the pixel, $\vec{r}^{MIRAS}$,

$$\vec{r}^{\,MIRAS} = \begin{cases} \cos\theta_s \sin\phi_s \\ \cos\theta_s \cos\phi_s \\ -\sin\theta_s \end{cases} \qquad \textbf{Eq. 145}$$

and with it define two auxiliary vectors, N_x and N_y:

$$v_{aux}^{\ MIRAS} = \vec{r}^{\,MIRAS} - u_z^{\ MIRAS}$$
$$N_x^{\ MIRAS} = \frac{v_{aux}^{\ MIRAS} \times u_x^{\ MIRAS}}{\left\| v_{aux}^{\ MIRAS} \times u_x^{\ MIRAS} \right\|} \qquad \textbf{Eq. 146}$$
$$N_y^{\ MIRAS} = \frac{v_{aux}^{\ MIRAS} \times u_y^{\ MIRAS}}{\left\| v_{aux}^{\ MIRAS} \times u_y^{\ MIRAS} \right\|}$$

These auxiliary vectors are used to calculate the Ludwig-3 vectors

$$L_x^{\ MIRAS} = \frac{N_x^{\ MIRAS} \times \vec{r}^{\,MIRAS}}{\left\| N_x^{\ MIRAS} \times \vec{r}^{\,MIRAS} \right\|} \qquad \textbf{Eq. 147}$$
$$L_y^{\ MIRAS} = \frac{N_y^{\ MIRAS} \times \vec{r}^{\,MIRAS}}{\left\| N_y^{\ MIRAS} \times \vec{r}^{\,MIRAS} \right\|}$$

Having $\hat{Eh}_{topocentric}$, $\hat{Ev}_{topocentric}$, $L_x^{\ MIRAS}$ and $L_y^{\ MIRAS}$ to the same referential, the polarization angle is obtained as shown in the following equation:

$$\alpha' = \arctan\left(\frac{\vec{Eh}_{MIRAS} \cdot \vec{L}_y^{\ MIRAS}}{\vec{Eh}_{MIRAS} \cdot \vec{L}_x^{\ MIRAS}} \right) \qquad \textbf{Eq. 148}$$

For further details, please refer to [RD.29].

3.3.2. Geolocation

This objective of the geolocation requirement is to compute the Brightness Temperature values expressed at Top of Atmosphere over pixels in an Earth fixed grid (ISEA). That the values are expressed at TOA means that the Faraday and geometrical rotations are not corrected in L1c. The pixel coordinates are defined in an Auxiliary Data File using longitude, latitude and altitude.

The objective of the Geolocation process is to compute for each of the pixels observed the corresponding Brightness Temperature and observation angles, the radiometric accuracy, the Faraday and geometric rotation angles, the footprint major and minor semi-axis and a set of quality flags.

The first step is to identify which pixels of the ISEA grid are contained within the extended alias-free FOV (EAF-FOV) for one particular snapshot. This is done by first projecting the EAF-FOV contour onto the ISEA grid and gathering the points falling inside. Once identified, the incidence and azimuth angles in the antenna frame are computed for each of the pixels, which also correspond to the xi-eta coordinates, according to the following equation.

$$\xi = \sin\theta\cos\phi$$
$$\eta = \sin\theta\sin\phi$$

Eq. 149~~144~~

Based on a land-sea mask, the pixels are separated into two different loops: pure sea pixels are flagged for OS L1c processing, land and mixed pixels are flagged for SM L1c processing. Additionally, pixels belonging to the alias-free FOV (not extended) are flagged, as well as pixels near the border or on the diagonals of the antenna frame $(\xi = \pm\eta)$

Once the antenna frame coordinates are known for all the pixels, they shall be used to compute the different values at each pixel specifically.

The output data information is written into the L1c products first starting with a reference to the snapshots in which the measurements were made, which include OBET, UTC, PVT, AOCS, and magnitudes of the removed foreign sources, TEC and geomagnetic angles and the averaged physical temperature of receivers.

Following that, the data is ordered by pixels, where for each pixel it is indicated the numeric identifier to the ISEA grid and the number of BT measurements available. Each of the measurements is composed of the BT component measured (real for H and V, complex for HV), incidence (θ_p) and azimuth (ϕ_p) observation angles, radiometric accuracy, Faraday rotation angle (ω), geometric rotation angle (φ), pixel footprint elliptical major and minor semi-axes and quality flags.

3.3.2.1. Pixel Brightness Temperature computation

The Brightness Temperature computation to be performed for each pixel uses a Discrete Fourier Transform, using as input the brightness temperatures Fourier Components $\hat{T}(u,v)$ produced as L1b output, the *(u,v)* baselines coordinates, the apodisation window coefficients *W(u,v)* and the xi-eta coordinates of that particular point. The equation used is the following:

$$T(\xi,\eta) = \frac{\sqrt{3}}{2} d^2 \sum_m \sum_n \hat{T}(u_{mn}, v_{mn}) \cdot W(u_{mn}, v_{mn}) \cdot e^{j2\pi(u_{mn}\xi + v_{mn}\eta)}$$

Eq. 150~~145~~

In the nominal case, the apodisation window W coefficients are constant regardless of the xi-eta coordinates (e.g. Blackman window). In the case of strip adaptive, the coefficients are also a function of the xi-eta coordinates. The method for W computation is shown in the last chapter of this section.

In case Foreign Sources correction removed a constant Earth Brightness Temperature (Eqs. 115 and 122), the equivalent of Eq.125 has to be applied here, in order to add back the subtracted quantity. This is not applicable to full polarisation scenes, as the Earth is not subtracted for HV pol reconstruction.

3.3.2.2. Pixel Radiometric Accuracy computation

Additionally, the radiometric accuracy is computed for each pixel and polarisation. The equation for doing this is the following:

$$\Delta T^{pq}(\xi,\eta)=\frac{\Omega^{pq}\sqrt{1-\xi^2-\eta^2}}{\bar{G}^{pq}(\xi,\eta)}\frac{\sqrt{3}}{2}d^2\frac{T_{sys}^{pq}}{\sqrt{B\cdot\tau_{eff}}}\alpha_w\alpha_{ol}$$ **Eq. 151~~146~~**

Where the different parameters are:

- Ω^{pq} is the solid angle of the antenna, and can be approximated by $\frac{4\pi}{D}$ for the current LICEFs, where D is the averaged directivity of the LICEFs for the corresponding polarisation. For full polarisation, D^{HV} is computed as $\sqrt{D_H D_V}$.
- $G^{pq}(\xi,\eta)$ is the averaged LICEF receiver directional power Gain function normalised so that it is unity at boresight. This data is retrieved from the antenna patterns ADF for each polarisation. For full polarisation, $\bar{G}^{HV}(\xi,\eta)$ is computed as $\sqrt{G^{HH}G^{VV}}$.
- d is the distance ratio between receivers (0.875)
- T_{sys}^{pq} is the averaged System Temperature measured by the PMS system, which has been used to de-normalise the L1a calibrated visibilities.
- B is the equivalent receiving frequency bandwidth in Hz, currently being 19 MHz
- τ_{eff} is the effective integration time, and is equivalent to τ/c_{eff} where τ is the integration time and c_{eff} is the coefficient that accounts for the 1-bit correlation, oversampling and hermiticity (c_{eff}=1.81) as quoted in [RD.21]. τ is considered as 1.2s for H and V polarisation measurements, and 0.8s for HV polarisation measurements..
- $\alpha_w=\sqrt{\sum_u\sum_v\frac{(W(u,v))^2}{R(u,v)}}$ accounts for the apodisation window and redundancies in the measurements, where W is the apodisation window term for each (u,v) baseline and R is the redundancy level of that same baseline (i.e. number of times that the baseline has been measured, 1 for non-redundant baselines, greater than 1 for the rest)
- $\alpha_{ol}=\sqrt{1+e^{-2\pi\left(\frac{f_0-f_{01}}{B}\right)^2}}$ accounts for the local oscillator factor, where B is the bandwidth mentioned before, f_0 is the central frequency and f_{01} is the low frequency, whose values are 1413 and 1403MHz.

3.3.2.3. Pixel Observation Angles computation

Afterwards, the incidence (θ_p) and azimuth (ϕ_p) observation angles are computed. The incidence angle is the angle between the local normal at each pixel and the pixel-to-satellite direction, whereas the azimuth angle is the angle measured between the pixel-to-satellite direction projected in the local tangent plane and the local North direction. These angles shall be computed with the help of the CFI functions, using the spacecraft position and the latitude, longitude and altitude coordinates of each pixel in the Earth fixed grid.

3.3.2.4. Pixel Footprint Shape Computation

Beyond these computations, the pixel shape is obtained as the projection onto the Earth fixed Grid of the –3dB contour of the Synthetic Antenna Directional Gain. This projection is approximated by an ellipse, in which its major semi-axis is oriented with the azimuth (ϕ_p) observation angle. The Synthetic Antenna Directional Gain (also known as Equivalent Array Factor) may be computed in the antenna frame by following the expression:

$$AF_{eq}(\xi,\xi',\eta,\eta') = \frac{\sqrt{3}}{2} d^2 \sum_m \sum_n W(u_{mn},v_{mn}) \cdot \tilde{r}\left(-\frac{u_{mn}\cdot\xi + v_{mn}\cdot\eta}{f_0}\right) \cdot e^{j2\pi(u_{mn}(\xi-\xi')+v_{mn}(\eta-\eta'))} \quad \textbf{Eq. 152~~147~~}$$

Where:

- $W(u_{mn},v_{mn})$ is the apodisation function computed before
- $\tilde{r}$ is the fringe-washing function which accounts for the spatial decorrelation between antennas. It is calibrated as part of the nominal processing, but it can also be approximated by $\tilde{r} \approx e^{\left[-\pi W_r^2 (u\xi+v\eta)^2\right]}$, where W_r is the relative bandwidth of the filters (i.e. bandwidth divided by the central frequency)
- (u_{mn},v_{mn}) are the baseline coordinates in the frequency domain
- (ξ',η') are the coordinates of the resulting pixel centre (or viewing direction) in the antenna frame
- d is the antenna element spacing (0.875)
- f_0 is the central frequency (1413 MHz)

The resulting distribution over the antenna frame, cut at half of the maximum (–3dB) will yield a contour (circular or elliptical) that must be projected over the Earth. As mentioned, the major semi-axis is oriented along the azimuth (ϕ_p) observation angle, so it is only necessary to project two points to compute the ellipse axes on the ground.

3.3.2.5. Apodisation window computation

In the nominal case (i.e. no strip adaptive), the apodisation window is simply a function of the u,v baseline coordinates.

For the Blackman window, the expression is the following:

$$W(u,v) = 0.42 + 0.5\cdot\cos\left(\pi\frac{\sqrt{u^2+v^2}}{\sqrt{3}N_{EL}d}\right) + 0.08\cdot\cos\left(2\pi\frac{\sqrt{u^2+v^2}}{\sqrt{3}N_{EL}d}\right) \quad \textbf{Eq. 153~~148~~}$$

In which the MIRAS/SMOS case for a Y-shaped array has already been taken into account, and N_{EL}=21 and d=0.875.

This apodisation window, when used in Eq. 150~~145~~, produces a circular footprint in the antenna frame, which is later projected into an elliptical footprint over the Earth's surface.

In order to ensure a circular footprint on the ground, the process must be initiated backwards, i.e. given the Earth pixel; a ground circular footprint is considered and projected onto the antenna frame as an

ellipse. This ellipse is the desired output of the –3dB contour for the Array Factor computed in Eq. 152~~147~~, which will require a specific window for that purpose.

First, we will deal with the computation of the ellipse equation in the antenna frame of a circular ground footprint. The following diagram illustrates some angular relationships like Fig. 14:

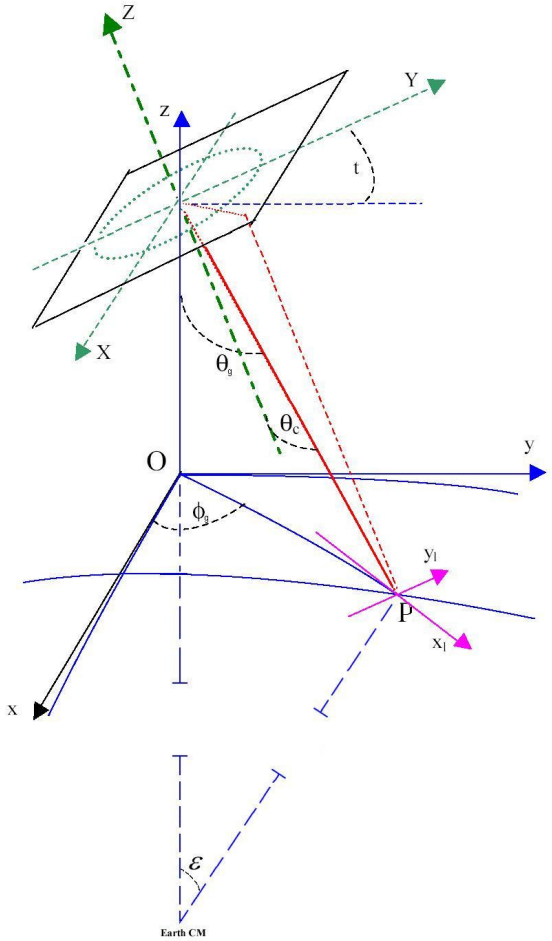

Figure 15: Angular relationships for pixel

The transformation of the coordinates of any vector from the (X, Y, Z) to the (x_l,y_l,z_l) frames must be expressed as a product of the following rotations:

$$\begin{pmatrix} x_l \\ y_l \\ z_l \end{pmatrix} = \begin{pmatrix} \cos\varepsilon & 0 & -\sin\varepsilon \\ 0 & 1 & 0 \\ \sin\varepsilon & 0 & \cos\varepsilon \end{pmatrix} \cdot \begin{pmatrix} \cos\phi_g & \sin\phi_g & 0 \\ -\sin\phi_g & \cos\phi_g & 0 \\ 0 & 0 & 1 \end{pmatrix} \cdot \begin{pmatrix} 1 & 0 & 0 \\ 0 & \cos t & -\sin t \\ 0 & \sin t & \cos t \end{pmatrix} \cdot \begin{pmatrix} X \\ Y \\ Z \end{pmatrix} \quad \textit{Eq. 154~~149~~}$$

where t is the tilt angle of the antenna, $\phi_g = \arctan(y/x)$ is the azimuth angle from the nadir and ε is the arc between the nadir and the point position from the centre of the Earth assumed as spherical. It is obtained solving the following equation:

$$\sin\varepsilon = \tan\theta_g \cdot \left(1 + \frac{H_{Sat}}{R_{Earth}} - \cos\varepsilon\right) \qquad \text{Eq. 155}$$

with R_{Earth} as the Earth radius, H_{Sat} as the orbital height and θ_g as the nadir angle of the considered point.

Expanding the rotation matrix (K), it has the following coefficients:

$$\begin{pmatrix} x_l \\ y_l \\ z_l \end{pmatrix} = \begin{pmatrix} \cos\varepsilon\cos\phi_g & \cos\varepsilon\sin\phi_g\cos t - \sin\varepsilon\sin t & -\cos\varepsilon\sin\phi_g\sin t - \sin\varepsilon\cos t \\ -\sin\phi_g & \cos\phi_g\cos t & -\cos\phi_g\sin t \\ \sin\varepsilon\cos\phi_g & \sin\varepsilon\sin\phi_g\cos t + \cos\varepsilon\sin t & -\sin\varepsilon\sin\phi_g\sin t + \cos\varepsilon\cos t \end{pmatrix} \begin{pmatrix} X \\ Y \\ Z \end{pmatrix} \qquad \text{Eq. 156}$$

In order to calculate the projection of an antenna beam contour on the ground, it is necessary to define a link between the variations of the coordinates in the antenna frame and the coordinate variations in the coordinate frame defined in the plane tangent to the Earth surface in the considered point.

Now expressing the position of point P in the reference system SXYZ can be done using spherical coordinates in the antenna frame, r, θ and ϕ:

$$\begin{aligned} X_P &= r\cdot\sin\theta\cos\phi \\ Y_P &= r\cdot\sin\theta\sin\phi \\ Z_P &= r\cdot\cos\theta \end{aligned} \qquad \text{Eq. 157}$$

The distance r can be computed assuming a spherical Earth by means of the expression:

$$r = \sqrt{R_{Earth}^{\ 2} + (H_{Sat} + R_{Earth})^2 - 2R_{Earth}(H_{Sat} + R_{Earth})\cos\varepsilon} \qquad \text{Eq. 158}$$

Computing the differential on the above equations results in:

$$\begin{aligned} dX_P &= \sin\theta\cos\phi dr + r\cos\theta\cos\phi d\theta - r\sin\theta\sin\phi d\phi \\ dY_P &= \sin\theta\sin\phi dr + r\cos\theta\sin\phi d\theta + r\sin\theta\cos\phi d\phi \\ dZ_P &= \cos\theta dr - r\sin\theta d\theta \end{aligned} \qquad \text{Eq. 159}$$

That can be expressed in form of another rotation matrix (M):

$$\begin{pmatrix} dX_P \\ dY_P \\ dZ_P \end{pmatrix} = \begin{pmatrix} r\cos\theta\cos\phi & -r\sin\theta\sin\phi & \sin\theta\cos\phi \\ r\cos\theta\sin\phi & r\sin\theta\cos\phi & \sin\theta\sin\phi \\ -r\sin\theta & 0 & \cos\theta \end{pmatrix} \cdot \begin{pmatrix} d\theta \\ d\phi \\ dr \end{pmatrix} \qquad \text{Eq. 160}$$

So variations in the coordinates in the pixel reference frame can be related to angular and radial variations in the antenna frame, using the expression:

$$\begin{pmatrix} dx_{lP} \\ dy_{lP} \\ dz_{lP} \end{pmatrix} = \begin{pmatrix} \cos\varepsilon\cos\phi_g & \cos\varepsilon\sin\phi_g\cos t - \sin\varepsilon\sin t & -\cos\varepsilon\sin\phi_g\sin t - \sin\varepsilon\cos t \\ -\sin\phi_g & \cos\phi_g\cos t & -\cos\phi_g\sin t \\ \sin\varepsilon\cos\phi_g & \sin\varepsilon\sin\phi_g\cos t + \cos\varepsilon\sin t & -\sin\varepsilon\sin\phi_g\sin t + \cos\varepsilon\cos t \end{pmatrix} \times$$
$$\times \begin{pmatrix} r\cos\theta\cos\phi & -r\sin\theta\sin\phi & \sin\theta\cos\phi \\ r\cos\theta\sin\phi & r\sin\theta\cos\phi & \sin\theta\sin\phi \\ -r\sin\theta & 0 & \cos\theta \end{pmatrix} \times \begin{pmatrix} d\theta \\ d\phi \\ dr \end{pmatrix} = [L] \times \begin{pmatrix} d\theta \\ d\phi \\ dr \end{pmatrix} \quad \text{Eq. 161156}$$

In which the complete rotation matrix can be called *L*.

Thus, if a circular pixel of radius *R* on the Earth surface is required, and contained in the local tangent plane at the pixel position, the following expression can be imposed.

$$\begin{pmatrix} dx_{lP} & dy_{lP} & dz_{lP} \end{pmatrix} \cdot \begin{pmatrix} 1/R^2 & 0 & 0 \\ 0 & 1/R^2 & 0 \\ 0 & 0 & 0 \end{pmatrix} \cdot \begin{pmatrix} dx_{lP} \\ dy_{lP} \\ dz_{lP} \end{pmatrix} = 1 \quad \text{Eq. 162157}$$

Then, if the dependency calculated above between pixel centred coordinates and antenna frame spherical coordinates is introduced, the following expression is obtained:

$$\begin{pmatrix} d\theta & d\phi & dr \end{pmatrix} \cdot \begin{pmatrix} L_{11} & L_{21} & L_{31} \\ L_{12} & L_{22} & L_{32} \\ L_{13} & L_{23} & L_{33} \end{pmatrix} \begin{pmatrix} 1/R^2 & 0 & 0 \\ 0 & 1/R^2 & 0 \\ 0 & 0 & 0 \end{pmatrix} \begin{pmatrix} L_{11} & L_{12} & L_{13} \\ L_{21} & L_{22} & L_{23} \\ L_{31} & L_{32} & L_{33} \end{pmatrix} \cdot \begin{pmatrix} d\theta \\ d\phi \\ dr \end{pmatrix} = 1 \quad \text{Eq. 163158}$$

It can be easily seen that for negligible variations in the radial direction, the classic equation of an ellipse is obtained in the antenna frame. Of course, this assumption is not valid for high incidence angles, where the radial direction is almost tangent to the Earth:

$$(L_{11}^2 + L_{21}^2)\cdot d\theta^2 + 2\cdot(L_{11}L_{12} + L_{21}L_{22})\cdot d\theta d\phi + (L_{12}^2 + L_{22}^2)\cdot d\phi^2 = R^2 \quad \text{Eq. 164159}$$

Deriving the (ξ,η) coordinates from Eq. 149144, the variations are expressed as:

$$d\theta = \frac{\cos\phi}{\cos\theta}d\xi + \frac{\sin\phi}{\cos\theta}d\eta \quad \text{Eq. 165160}$$

$$d\phi = -\frac{\sin\phi}{\sin\theta}d\xi + \frac{\cos\phi}{\sin\theta}d\eta \quad \text{Eq. 166161}$$

Substituting these expressions and transforming the differential elements into discrete increments the following equation of an ellipse in the antenna frame is defined:

$$A \cdot \Delta \xi^2 + 2 \cdot B \cdot d\,\Delta \xi \cdot \Delta \eta + C \cdot \Delta \eta^2 = 1$$ Eq. 167~~162~~

where the ellipse coefficients are:

$$A = \frac{1}{R^2}\left((L_{11}^2 + L_{21}^2)\frac{\cos^2\phi}{\cos^2\theta} - 2\cdot(L_{11}L_{12} + L_{21}L_{22})\frac{\cos\phi\sin\phi}{\cos\theta\sin\theta} + (L_{12}^2 + L_{22}^2)\frac{\sin^2\phi}{\sin^2\theta}\right)$$ Eq. 168~~163~~

$$B = \frac{1}{R^2}\left((L_{11}L_{12} + L_{21}L_{22})\frac{2\cos^2\phi - 1}{\cos\theta\sin\theta} - (L_{11}^2 + L_{21}^2)\frac{\cos\phi\sin\phi}{\cos^2\theta} - (L_{12}^2 + L_{22}^2)\frac{\cos\phi\sin\phi}{\sin^2\theta}\right)$$ Eq. 169~~164~~

$$C = \frac{1}{R^2}\left((L_{11}^2 + L_{21}^2)\frac{\sin^2\phi}{\cos^2\theta} + 2\cdot(L_{11}L_{12} + L_{21}L_{22})\frac{\cos\phi\sin\phi}{\cos\theta\sin\theta} + (L_{12}^2 + L_{22}^2)\frac{\cos^2\phi}{\sin^2\theta}\right)$$ Eq. 170~~165~~

The angle of the first semi-axis with respect to the axis ξ is:

$$\delta = \arctan\left(\frac{2B}{A - C}\right)$$ Eq. 171~~166~~

and the semi-axis are defined by:

$$E_1 = \sqrt{A\cos^2\delta + 2B\sin\delta\cos\delta + C\sin^2\delta}$$ Eq. 172~~167~~

$$E_2 = \sqrt{A\sin^2\delta - 2B\sin\delta\cos\delta + C\cos^2\delta}$$ Eq. 173~~168~~

Once we have the desired ellipse parameters in the antenna frame, it is required to find a suitable apodisation window whose Equivalent Array Factor –3dB contour fits that ellipse.

For this purpose, a previous study described in [RD.15] shows how to adjust a 2D window based in Kaiser windows. This apodisation window expression is the following:

$$W(u,v) = \frac{I_0\left(\alpha_u\sqrt{1-\left(\frac{u'}{\rho_{\max}}\right)^2}\right)}{I_0(\alpha_u)} \times \frac{I_0\left(\alpha_v\sqrt{1-\left(\frac{v'}{\rho_{\max}}\right)^2}\right)}{I_0(\alpha_v)}$$ Eq. 174~~169~~

Where I_0 is the Modified Bessel Function of the First Kind, and has the following expression:

$$I_0(x) = \sum_{k=0}^{\infty}\frac{(x/2)^{2k}}{(k!)^2}$$ Eq. 175~~170~~

The alpha parameter in each Kaiser window drives the tapering capabilities of the apodisation, meaning that higher values of alpha provide higher tapering. The baselines are normalised with the same maximum value $\rho_{\max} = \sqrt{u_{\max}^2 + v_{\max}^2} = \sqrt{3} N_{EL} d$

Rotation is introduced by making a linear combination of the u and v coordinates and applying the apodisation along those new directions, as it is shown in the following equation:

$$u' = u\cos\delta + v\sin\delta$$
$$v' = -u\sin\delta + v\cos\delta \qquad \text{Eq. 176171}$$

The problem to be solved would be to find the α_u and α_v coefficients by forcing that the Equivalent Array factor as computed in Eq. 152147 particularised at the semi-axes points needs to be half of the maximum (measured at xi=eta=0). The expression has been simplified considering FWF unity on the right side of the equations:

$$\sum_{u'}\sum_{v'} \frac{W(u',v')}{2} = \sum_{u'}\sum_{v'} W(u',v') \times e^{j2\pi u E_1}$$
$$\sum_{u'}\sum_{v'} \frac{W(u',v')}{2} = \sum_{u'}\sum_{v'} W(u',v') \times e^{j2\pi v E_2} \qquad \text{Eq. 177172}$$

Substituting Eqs. 174169 and 176171 in the above one, it results in an equation system with two unknowns:

$$\frac{1}{2}\sum_u\sum_v I_0\left(\alpha_u\sqrt{1-\left(\frac{u\cos\delta+v\sin\delta}{\rho_{\max}}\right)^2}\right)\times I_0\left(\alpha_v\sqrt{1-\left(\frac{-u\sin\delta+v\cos\delta}{\rho_{\max}}\right)^2}\right) =$$
$$= \sum_u\sum_v I_0\left(\alpha_u\sqrt{1-\left(\frac{u\cos\delta+v\sin\delta}{\rho_{\max}}\right)^2}\right)\times I_0\left(\alpha_v\sqrt{1-\left(\frac{-u\sin\delta+v\cos\delta}{\rho_{\max}}\right)^2}\right)\times e^{j2\pi u E_1}$$

$$\frac{1}{2}\sum_u\sum_v I_0\left(\alpha_u\sqrt{1-\left(\frac{u\cos\delta+v\sin\delta}{\rho_{\max}}\right)^2}\right)\times I_0\left(\alpha_v\sqrt{1-\left(\frac{-u\sin\delta+v\cos\delta}{\rho_{\max}}\right)^2}\right) =$$
$$= \sum_u\sum_v I_0\left(\alpha_u\sqrt{1-\left(\frac{u\cos\delta+v\sin\delta}{\rho_{\max}}\right)^2}\right)\times I_0\left(\alpha_v\sqrt{1-\left(\frac{-u\sin\delta+v\cos\delta}{\rho_{\max}}\right)^2}\right)\times e^{j2\pi v E_2} \qquad \text{Eq. 178173}$$

Which unfortunately cannot be solved analytically, so the solution is to tabulate the alpha values for a set of ellipse parameters (E_1, E_2 and δ) and interpolate among them to obtain a fitting window.

This methodology can be seen in the following example, where contour plots are made for equal semi-major and semi-minor axes values against alpha values. This represents the initial tabulation, and it should only be performed once. The way to perform this tabulation is to compute the Equivalent Array Factor according to Eq. 152147 using an array of fixed alpha and δ values. Once the Array Factor is computed, the –3dB contour is fitted with an ellipse, from which the E_1, E_2 parameters can be obtained.

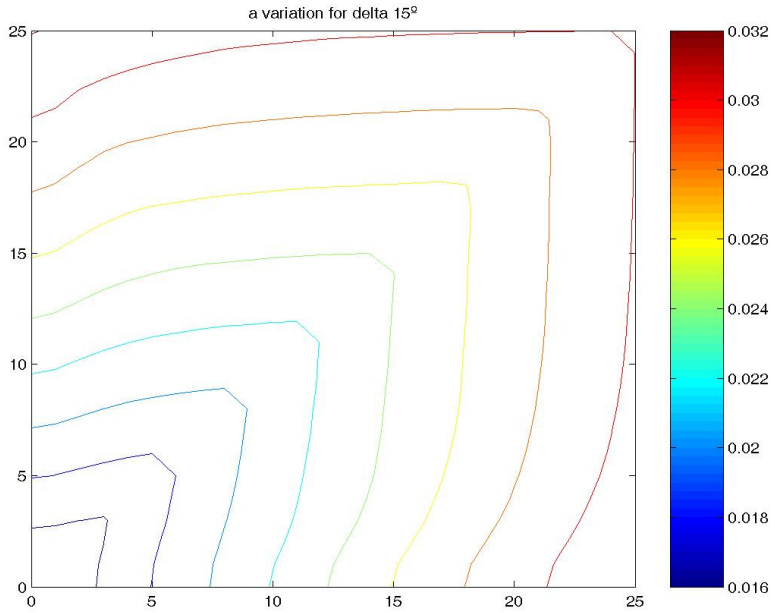

Fig.16: Major semi-axis of elliptical -3dB contour of AF as a function of alphaU (x axis) and alphaV (y axis). Delta is constant at 15º

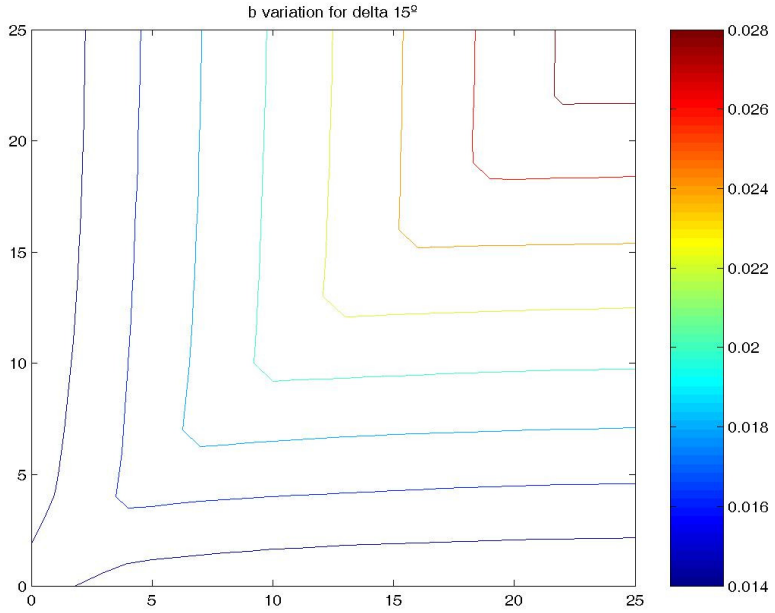

Fig.17: Minor semi-axis of elliptical -3dB contour of AF as a function of alphaU (x axis) and alphaV (y axis). Delta is constant at 15º

Thus, for δ=15º, and for any combination of values of E_1 and E_2, it is possible to obtain the corresponding alpha values which produce such an elliptically distorted Equivalent Array Factor.

The following image shows the graphical method for E_1=0.024 and E_2=0.018, which consists in plotting the curves as a function of the alpha values that produce Array Factors having those E_1 and E_2 values, and finding the intersection of both curves. There shall be two solutions, one indicating that the major semi-axis is oriented along the δ direction, and the other indicating that the minor semi-axis is oriented along the δ direction.

In this image, it is also shown a red line indicating the Beam Efficiency that corresponds to those two alpha values, which in this case is 58%. Please refer to [RD.15] for additional information.

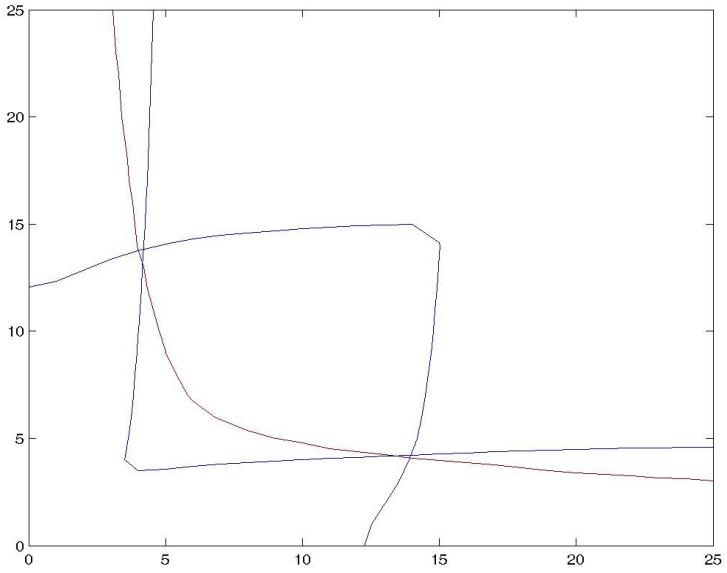

Fig.18: Alpha parameters for E_1=0.024, E_2=0.018. Delta value is 15º.

A system of analytical equations has been derived in [RD.15] by INETI after implementation of the equations above. The system of equations computes the Kaiser parameters (α_u and α_v) out of the relationship between the ellipse semi-axes in the antenna frame. The coefficients used in that system of equations are described in the next equation and have been set as part of the Strip Adaptive ADF (APOD99):

$$\log 10\left(\frac{\alpha_u}{\alpha_v}\right) = -7.2205E^{-8} + 1.9915\log 10\left(\frac{w_1}{w_2}\right) + 1.0776\left[\log 10\left(\frac{w_1}{w_2}\right)\right]^2 + 0.13022\left[\log 10\left(\frac{w_1}{w_2}\right)\right]^3$$

$$\log 10\left(\alpha_u\alpha_v\right) = 8.4703 + 1.5081\log 10\left(w_1w_2\right) - 0.16293\left[\log 10\left(w_1w_2\right)\right]^2 - 0.016226\left[\log 10\left(w_1w_2\right)\right]^3$$

Eq. 179~~174~~

4. OPEN ISSUES

- Modelling of the Parametric G matrix approach is not yet complete~~, although there shall be a dedicated contract with the appropriate parties to finalise it within Phase 4~~.

5. ANNEX: G-MATRIX BLOCKS

In this Appendix the expressions for the elements in each G-matrix block are derived.

Rewriting, Eq. 109, in a slightly different notation, the *System Response Function* is:

$$V_{j\,j'}^{pp'}(u,v)=\iint_{\xi^2+\eta^2\le 1}\frac{\hat{F}_j^{pq}(\xi,\eta)\,\hat{F}_{j'}^{p'q'*}(\xi,\eta)}{\sqrt{\Omega_j^p\Omega_{j'}^{p'}}}\frac{T_{\mathrm{B}}^{qq'}(\xi,\eta)-T_{\mathrm{rec}}\delta_{qq'}}{\zeta(\xi,\eta)}\hat{\tilde{r}}_{j\,j'}\left(-\tau(\xi,\eta;u,v)\right)e^{-2\pi i\tau(\xi,\eta;u,v)f_0}d\xi d\eta\,, \qquad \text{Eq. 180}\sout{175}$$

where:

- $\hat{F}_j^{\,p}(\xi,\eta)$ is the normalised *antenna radiation pattern* of receiver j in polarisation p, expressed in director cosines coordinates (ξ,η);
- Ω_k^p is the *antenna solid angle* of receiver j in polarisation p;
- T_{rec} is the *averaged physical temperature of the receivers*, and is multiplied here by the Dirac delta $\delta^{pp'}$ to represent that it is not applicable when the polarisation indexes p and p' are not equal;
- ζ is the *Obliquity Factor* given by $\sqrt{1-\xi^2-\eta^2}$;
- τ is the *Delay Time* given by $(u\xi+v\eta)/f_0$;
- $\hat{\tilde{r}}_{jj'}$ is the *Fringe Washing Function* term, normalised at the origin, which accounts for decorrelation effects in the path of the correlated signals;

and it is assumed a sum over indices $q,q'=\mathrm{H,V}$.

Here the director cosine coordinates are given by $(\xi,\eta)=\left(X/R,Y/R\right)$ in the instrument's coordinate system and (u,v) are the baseline coordinates.

In matrix form, i.e. discretising the director cosine coordinates[3] as (ξ_k,η_k) this becomes:

$$V_{j\,j'}^{pp'}\approx\sum_{k=1}^{128^2}\hat{F}_j^{pq}\hat{F}_{j'}^{p'q'*}R_{j\,j',k}T_{\mathrm{k}}^{pp'}\,, \qquad \text{Eq. 181}\sout{176}$$

where $T_k^{pp'}:=\dfrac{T_{\mathrm{B}}^{pp'}-T_{\mathrm{rec},k}\delta_{pp'}}{\zeta_k}$, $R_{j\,j',k}:=\dfrac{\hat{\tilde{r}}_{j\,j'}\left(-\tau(\xi,\eta;u,v)\right)}{\sqrt{\Omega_j^p\Omega_{j'}^{p'}}}\exp\left(-2\pi i\tau(\xi,\eta;u,v)\,f_0\right)$ and the sum over index $k=1,\ldots,128^2$ is implicit.

[3] It is assumed a regular discretisation in (ξ_k,η_k), otherwise the discretisation step sizes must be also included.

Making the sum over q and q' explicit, and expanding for the indices $p, p' = H, V$, Eq. 181~~176~~ becomes:

$$V_{j\,j'}^{HH} \approx \hat{F}_j^{HH}\hat{F}_{j'}^{HH*}R_{j\,j',k}T_k^{HH} + \hat{F}_j^{HV}\hat{F}_{j'}^{HV*}R_{j\,j',k}T_k^{VV} + \hat{F}_j^{HH}\hat{F}_{j'}^{HV*}R_{j\,j',k}T_k^{HV} + \hat{F}_j^{HV}\hat{F}_{j'}^{HH*}R_{j\,j',k}T_k^{VH}, \quad \textit{Eq. 182~~177~~}$$

$$V_{j\,j'}^{VV} \approx \hat{F}_j^{VH}\hat{F}_{j'}^{VH*}R_{j\,j',k}T_k^{HH} + \hat{F}_j^{VV}\hat{F}_{j'}^{VV*}R_{j\,j',k}T_k^{VV} + \hat{F}_j^{VH}\hat{F}_{j'}^{VV*}R_{j\,j',k}T_k^{HV} + \hat{F}_j^{VV}\hat{F}_{j'}^{VH*}R_{j\,j',k}T_k^{VH}, \quad \textit{Eq. 183~~178~~}$$

$$V_{j\,j'}^{HV} \approx \hat{F}_j^{HH}\hat{F}_{j'}^{VH*}R_{j\,j',k}T_k^{HH} + \hat{F}_j^{HV}\hat{F}_{j'}^{VV*}R_{j\,j',k}T_k^{VV} + \hat{F}_j^{HH}\hat{F}_{j'}^{VV*}R_{j\,j',k}T_k^{HV} + \hat{F}_j^{HV}\hat{F}_{j'}^{VH*}R_{j\,j',k}T_k^{VH}, \quad \textit{Eq. 184~~179~~}$$

$$V_{j\,j'}^{VH} \approx \hat{F}_j^{VH}\hat{F}_{j'}^{HH*}R_{j\,j',k}T_k^{HH} + \hat{F}_j^{VV}\hat{F}_{j'}^{HV*}R_{j\,j',k}T_k^{VV} + \hat{F}_j^{VH}\hat{F}_{j'}^{HV*}R_{j\,j',k}T_k^{HV} + \hat{F}_j^{VV}\hat{F}_{j'}^{HH*}R_{j\,j',k}T_k^{VH}, \quad \textit{Eq. 185~~180~~}$$

Now, using $T_k^{p'p} = T_k^{pp'*}$ and expanding the complex numbers, we have:

$$\begin{aligned} V_{j\,j',R}^{HH} + iV_{j\,j',I}^{HH} \approx & \left[\left(\hat{F}_j^{HH}\hat{F}_{j'}^{HH*}R_{j\,j',k}\right)_R + i\left(\hat{F}_j^{HH}\hat{F}_{j'}^{HH*}R_{j\,j',k}\right)_I\right]T_k^{HH} \\ & + \left[\left(\hat{F}_j^{HV}\hat{F}_{j'}^{HV*}R_{j\,j',k}\right)_R + i\left(\hat{F}_j^{HV}\hat{F}_{j'}^{HV*}R_{j\,j',k}\right)_I\right]T_k^{VV} \\ & + \left[\left(\hat{F}_j^{HH}\hat{F}_{j'}^{HV*}R_{j\,j',k}\right)_R + i\left(\hat{F}_j^{HH}\hat{F}_{j'}^{HV*}R_{j\,j',k}\right)_I\right]\left(T_{k,R}^{HV} + iT_{k,I}^{HV}\right)' \\ & + \left[\left(\hat{F}_j^{HV}\hat{F}_{j'}^{HH*}R_{j\,j',k}\right)_R + i\left(\hat{F}_j^{HV}\hat{F}_{j'}^{HH*}R_{j\,j',k}\right)_I\right]\left(T_{k,R}^{HV} - iT_{k,I}^{HV}\right) \end{aligned} \quad \textit{Eq. 186~~181~~}$$

$$\begin{aligned} V_{j\,j',R}^{VV} + iV_{j\,j',I}^{VV} \approx & \left[\left(\hat{F}_j^{VH}\hat{F}_{j'}^{VH*}R_{j\,j',k}\right)_R + i\left(\hat{F}_j^{VH}\hat{F}_{j'}^{VH*}R_{j\,j',k}\right)_I\right]T_k^{HH} \\ & + \left[\left(\hat{F}_j^{VV}\hat{F}_{j'}^{VV*}R_{j\,j',k}\right)_R + i\left(\hat{F}_j^{VV}\hat{F}_{j'}^{VV*}R_{j\,j',k}\right)_I\right]T_k^{VV} \\ & + \left[\left(\hat{F}_j^{VH}\hat{F}_{j'}^{VV*}R_{j\,j',k}\right)_R + i\left(\hat{F}_j^{VH}\hat{F}_{j'}^{VV*}R_{j\,j',k}\right)_I\right]\left(T_{k,R}^{HV} + iT_{k,I}^{HV}\right)' \\ & + \left[\left(\hat{F}_j^{VV}\hat{F}_{j'}^{VH*}R_{j\,j',k}\right)_R + i\left(\hat{F}_j^{VV}\hat{F}_{j'}^{VH*}R_{j\,j',k}\right)_I\right]\left(T_{k,R}^{HV} - iT_{k,I}^{HV}\right) \end{aligned} \quad \textit{Eq. 187~~182~~}$$

$$
\begin{aligned}
V_{j\,j',R}^{HV}+iV_{j\,j',I}^{HV} \;\square\; & \sum_{k=1}^{128^2}\left[\left(\hat{F}_j^{HH}\hat{F}_{j'}^{VH*}R_{j\,j',k}\right)_R+i\left(\hat{F}_j^{HH}\hat{F}_{j'}^{VH*}R_{j\,j',k}\right)_I\right]T_k^{HH} \\
& +\sum_{k=1}^{128^2}\left[\left(\hat{F}_j^{HV}\hat{F}_{j'}^{VV*}R_{j\,j',k}\right)_R+i\left(\hat{F}_j^{HV}\hat{F}_{j'}^{VV*}R_{j\,j',k}\right)_I\right]T_k^{VV} \\
& +\sum_{k=1}^{128^2}\left[\left(\hat{F}_j^{HH}\hat{F}_{j'}^{VV*}R_{j\,j',k}\right)_R+i\left(\hat{F}_j^{HH}\hat{F}_{j'}^{VV*}R_{j\,j',k}\right)_I\right]\left(T_{k,R}^{HV}+iT_{k,I}^{HV}\right) \\
& +\sum_{k=1}^{128^2}\left[\left(\hat{F}_j^{HV}\hat{F}_{j'}^{VH*}R_{j\,j',k}\right)_R+i\left(\hat{F}_j^{HV}\hat{F}_{j'}^{VH*}R_{j\,j',k}\right)_I\right]\left(T_{k,R}^{VH}-iT_{k,I}^{HV}\right)
\end{aligned}
\quad , \qquad \textbf{Eq. 188183}
$$

$$
\begin{aligned}
V_{j\,j',R}^{VH}+iV_{j\,j',I}^{VH} \;\square\; & \sum_{k=1}^{128^2}\left[\left(\hat{F}_j^{VH}\hat{F}_{j'}^{HH*}R_{j\,j',k}\right)_R+i\left(\hat{F}_j^{VH}\hat{F}_{j'}^{HH*}R_{j\,j',k}\right)_I\right]T_k^{HH} \\
& +\sum_{k=1}^{128^2}\left[\left(\hat{F}_j^{VV}\hat{F}_{j'}^{HV*}R_{j\,j',k}\right)_R+i\left(\hat{F}_j^{VV}\hat{F}_{j'}^{HV*}R_{j\,j',k}\right)_I\right]T_k^{VV} \\
& +\sum_{k=1}^{128^2}\left[\left(\hat{F}_j^{VH}\hat{F}_{j'}^{HV*}R_{j\,j',k}\right)_R+i\left(\hat{F}_j^{VH}\hat{F}_{j'}^{HV*}R_{j\,j',k}\right)_I\right]\left(T_{k,R}^{HV}+iT_{k,I}^{HV}\right) \\
& +\sum_{k=1}^{128^2}\left[\left(\hat{F}_j^{VV}\hat{F}_{j'}^{HH*}R_{j\,j',k}\right)_R+i\left(\hat{F}_j^{VV}\hat{F}_{j'}^{HH*}R_{j\,j',k}\right)_I\right]\left(T_{k,R}^{HV}-iT_{k,I}^{HV}\right)
\end{aligned}
\quad , \qquad \textbf{Eq. 189184}
$$

From Eqs. 188183 and 189184 it is easily checked that $V_{j\,j'}^{VH}=V_{j'\,j}^{VH*}$, so we only need e.g. Eqs. 186181-188183 which can be rearranged as:

$$
\begin{aligned}
V_{j\,j',R}^{HH} \;\square\; & \left(\hat{F}_j^{HH}\hat{F}_{j'}^{HH*}R_{j\,j',k}\right)_R T_k^{HH} \\
& +\left(\hat{F}_j^{HV}\hat{F}_{j'}^{HV*}R_{j\,j',k}\right)_R T_k^{VV} \\
& +\left[\left(\hat{F}_j^{HH}\hat{F}_{j'}^{HV*}+\hat{F}_j^{HV}\hat{F}_{j'}^{HH*}\right)R_{j\,j',k}\right]_R T_{k,R}^{HV} \\
& +\left[\left(-\hat{F}_j^{HH}\hat{F}_{j'}^{HV*}+\hat{F}_j^{HV}\hat{F}_{j'}^{HH*}\right)R_{j\,j',k}\right]_I T_{k,I}^{HV}
\end{aligned}
\quad , \qquad \textbf{Eq. 190185}
$$

$$
\begin{aligned}
V_{j\,j',I}^{HH} \;\square\; & \left(\hat{F}_j^{HH}\hat{F}_{j'}^{HH*}R_{j\,j',k}\right)_I T_k^{HH} \\
& +\left(\hat{F}_j^{HV}\hat{F}_{j'}^{HV*}R_{j\,j',k}\right)_I T_k^{VV} \\
& +\left[\left(\hat{F}_j^{HH}\hat{F}_{j'}^{HV*}+\hat{F}_j^{HV}\hat{F}_{j'}^{HH*}\right)R_{j\,j',k}\right]_I T_{k,R}^{HV} \\
& +\left[\left(\hat{F}_j^{HH}\hat{F}_{j'}^{HV*}-\hat{F}_j^{HV}\hat{F}_{j'}^{HH*}\right)R_{j\,j',k}\right]_R T_{k,I}^{HV}
\end{aligned}
\quad , \qquad \textbf{Eq. 191186}
$$

$$
\begin{aligned}
V_{j\,j',R}^{VV} \square & \left(\hat{F}_j^{VH}\hat{F}_{j'}^{VH*}R_{j\,j',k}\right)_R T_k^{HH} \\
& +\left(\hat{F}_j^{VV}\hat{F}_{j'}^{VV*}R_{j\,j',k}\right)T_k^{VV}{}_R \\
& +\left[\left(\hat{F}_j^{VH}\hat{F}_{j'}^{VV*}+\hat{F}_j^{VV}\hat{F}_{j'}^{VH*}\right)R_{j\,j',k}\right]_R T_{k,R}^{HV} \\
& +\left[\left(-\hat{F}_j^{VH}\hat{F}_{j'}^{VV*}+\hat{F}_j^{VV}\hat{F}_{j'}^{VH*}\right)R_{j\,j',k}\right]_I T_{k,I}^{HV}
\end{aligned}
\quad \text{Eq. 192 ~~187~~}
$$

$$
\begin{aligned}
V_{j\,j',I}^{VV} \square & \left(\hat{F}_j^{VH}\hat{F}_{j'}^{VH*}R_{j\,j',k}\right)_I T_k^{HH} \\
& +\left(\hat{F}_j^{VV}\hat{F}_{j'}^{VV*}R_{j\,j',k}\right)_I T_k^{VV} \\
& +\left[\left(\hat{F}_j^{VH}\hat{F}_{j'}^{VV*}+\hat{F}_j^{VV}\hat{F}_{j'}^{VH*}\right)R_{j\,j',k}\right]_I T_{k,R}^{HV} \\
& +\left[\left(\hat{F}_j^{VH}\hat{F}_{j'}^{VV*}-\hat{F}_j^{VV}\hat{F}_{j'}^{VH*}\right)R_{j\,j',k}\right]_R T_{k,I}^{HV}
\end{aligned}
\quad \text{Eq. 193 ~~188~~}
$$

$$
\begin{aligned}
V_{j\,j',R}^{HV} \square & \left(\hat{F}_j^{HH}\hat{F}_{j'}^{VH*}R_{j\,j',k}\right)_R T_k^{HH} \\
& +\left(\hat{F}_j^{HV}\hat{F}_{j'}^{VV*}R_{j\,j',k}\right)_R T_k^{VV} \\
& +\left[\left(\hat{F}_j^{HH}\hat{F}_{j'}^{VV*}+\hat{F}_j^{HV}\hat{F}_{j'}^{VH*}\right)R_{j\,j',k}\right]_R T_{k,R}^{HV} \\
& +\left[\left(-\hat{F}_j^{HH}\hat{F}_{j'}^{VV*}+\hat{F}_j^{HV}\hat{F}_{j'}^{VH*}\right)R_{j\,j',k}\right]_I T_{k,I}^{HV}
\end{aligned}
\quad \text{Eq. 194 ~~189~~}
$$

$$
\begin{aligned}
V_{j\,j',I}^{HV} \square & \left(\hat{F}_j^{HH}\hat{F}_{j'}^{VH*}R_{j\,j',k}\right)_I T_k^{HH} \\
& +\left(\hat{F}_j^{HV}\hat{F}_{j'}^{VV*}R_{j\,j',k}\right)_I T_k^{VV} \\
& +\left[\left(\hat{F}_j^{HH}\hat{F}_{j'}^{VV*}+\hat{F}_j^{HV}\hat{F}_{j'}^{VH*}\right)R_{j\,j',k}\right]_I T_{k,R}^{HV} \\
& +\left[\left(\hat{F}_j^{HH}\hat{F}_{j'}^{VV*}-\hat{F}_j^{HV}\hat{F}_{j'}^{VH*}\right)R_{j\,j',k}\right]_R T_{k,I}^{HV}
\end{aligned}
\quad \text{Eq. 195 ~~190~~}
$$

These elements are represented in Figure 12.